Università degli Studi di Pisa
Scuola di dottorato Galileo Galilei
Corso di Dottorato in Fisica Applicata (FIS/07)
(Anno 2003)

Subsystems for High bit-rate Optical Networks

Ph.D. Dissertation of:
Marco Presi

Advisory Committee:

Prof. Ernesto Ciaramella

Prof. Nicolò Beverini

October 2006

Contents

Introduzione

Questa tesi contiene parte del lavoro svolto negli ultimi tre anni presso i laboratori congiunti del CNIT e della la Scuola Superiore Sant'Anna di Pisa, dove ho lavorato nel gruppo di Sistemi Ottici sotto la supervisione del prof. Ernesto Ciaramella, ed in parte presso il Dipartimento di Fisica dell'Università di Pisa, sotto la supervisione del prof. Nicolò Beverini. Durante questi anni ho avuto l'opportunità di lavorare su vari filoni di ricerca (studio di sorgenti laser impulsate, esperimenti di processamento dei segnali tutto ottico, sistemi di protezione dei guasti di rete,...) inquadrati in differenti progetti di ricerca, ed anche in Università straniere (Massachussetts Intitute of Technology MIT di Boston, USA). In questa tesi verrà comunque descritta solo una parte dei risultati sviluppati. In particolare, verrà discussa la ricerca svolta mirata alla realizzazione di sotto-sistemi che possono essere impiegati nei sistemi di comunicazione ottica (o, più in generale nelle Reti Ottiche) basate su trassmissioni di dati alla frequenza di cifra di 40 Gb/s. Ogni sottos-sistema sarà presentato seguendo un ordine che riproduce quello in cui questi sotto-sistemi sono impegati effettivamente: inizierò descrivendo una sorgente di impulsi ottici ad altissimo bit-rate da impiegare nei sistemi ottici multiplati a divisione di tempo (OTDM); si passerà poi alla descrizione di vari convertitori di lunghezza d'onda che sono utilizzati nei nodi di rete; per concludere, verrà discussa una unità tutta ottica per i recupero del sincronisimo, che è tipicamente impiegata alla fine di un sistema di trasmissione ed è usata per affiancare i ricevitori veri e propri.

Tutte queste funzionalità sfruttano le proprietà ottiche non lineari di dispositivi tra i più comunemente usati nei sistemi di comunicazione ottici: le fibre ottiche e gli amplificatori ottici a semiconduttore. Oltre che dalla natura "tutto-ottica", tutti questi dispositivi (o funzionalità) sono accumunati dalla ricerca di semplicità sia realizzativa che progettuale: come verrà mostrato caso per caso, ogni sotto-sistema è stato realizzato cercando di ricorrere al minor numero possibile di dispositivi per ridurre la complessità globale. Questo è un punto fondamentale per dimostrare che le tecnologie "tutto-ottiche" possono rappresentare un'alternativa all'elettronica.

Ogni "sotto-sistema" verrà trattato separatamente in un capitolo. Ogni capitolo contiene una breve discussione sulle novità introdotte, rispetto a soluzioni simili presentate in letteratura o in commercio. Benchè il lavoro riportato in questa tesi è essenzialmente di carattere sperimentale, per migliorarne la comprensione e la completezza ogni capitolo contiene dei paragrafi in cui l'argomento viene illustrato dal punto di vista teorico.

La tesi è divisa in 4 capitoli secondo lo schema seguente:

1. **Introduzione ai sistemi di comunicazione basati su fibra ottica**: un capitolo introduttivo per spiegare l'evoluzione e la struttura e possibili scenari delle Reti Ottiche ed introdurre i motivi fondanti della ricerca riportata nella tesi.

2. **Una sorgente solitonica**, in **chapter 2**
   Questo capitolo contiene una discussione sulla progettazione e la realizzazione di una sorgente laser da impiegare in sistemi OTDM. La sorgente è progetatta per produrre impulsi di durata inferiore al picosecondo ad una frequenza di ripetizione di 40 GHz repetition rate. La sorgente è studiata per essere utilizzata direttamente nei sistemi di comunicazione, senza la necessità di dover ricorrere

a stadi di processamento successivi (come la risagomatura degli impulsi, la loro compressione o la rimozione di piedistallo). Gli impulsi sono generati tramite un fenomeno di propagazione in regime non-lineare controllato in una fibra ottica particolare. Benchè la sorgente sia stata progettata per essere impiegata in sistemi OTDM, dato il suo spettro ottico largo e periodico potrebbe essere utilizzata anche in altri ambiti, come verrà discusso più volte nel corso della tesi.

3. **Esperimenti di conversione di lunghezza d'onda** (includendo anche espeimenti di conversione di lunghezza d'onda multipla), in **chapter 3.**
   In questo capitolo, la conversione di lunghezza d'onda (ovvero il trasferimento della modulazione contenuta su un segnale ottico ad uno su una portante a lughezza d'onda differente) è dimostrata attraverso diverse tecniche, principalmente ricorrendo alle dinamiche veloci non-lineari deli amplificatori a semiconduttore. In tutti questi esperimenti, verrà trattata in dettaglio anche la realizzazione della conversione di lunghezza d'onda simultaneamente su più canali: in particolare questa funzionalità è ritenuta molto importante per le reti di accesso di prossima generazione..

4. **Uno circuito tutto ottico per l'estrazione del segnale di sincronia da un segnale modulato** in **chapter 4**
   Lo schema presentato in questo capitolo per i recupero del sincronismo rappresenta un notevole passo in avanti rispetto ai circuiti presentati precedentemente in letteratura, sia in termini di efficienza che di compattezza. Il dispositivo è basato sull'implementazione tutta-ottico del Tank-Circuit (largamente utilizzato in elettronica). Questo circuito si è dimostrato molto versatile: in particolare è stato dimostrato il suo impiego con diversi formati di modulazione, sia con traffico continuo che a pacchetti. Il circuito inoltre è adatto per un'integrazione fotonica ibrida.

Introduction

This thesis contains part of the work developed over the last three years at Scuola Superiore S.Anna and CNIT joint laboratories (IRCPhonet) in Pisa, where I worked in the Optical System Group under the supervision of prof. Ernesto Ciaramella, and partially at Physics Dept. of Pisa University under the supervision of prof. Niccolò Beverini. During the these years I had the opportunity to work on several different topics (realization of pulsed laser sources, experiments on all-optical signal processing and optical networks failure-protection) and in different research projects. However, here I will describe all the research works aimed to realize subsystems that can be employed in Optical Systems (or, more widely, in Optical Networks) based on 40 Gb/s optical signals. Each subsystem is presented following a logic sense that reproduces the same order in which they can be "implemented" in real systems: I will start describing a pulse source, that represents the first element in every optical communication link; then I will describe the implementation of several kinds of wavelength converters that are employed at networks intermediate nodes; finally I will discuss an all-optical clock recovery unit, that is expected to be placed at links ends, as an helper for receivers apparatus.

All the functionalities are realized exploiting the non-linear optical properties of the most common devices used in Optics Communications, i.e., Optical Fibers and Semiconductor Optical Amplifiers (SOAs). Beside the "all-optical" nature of subsystems, a common feature that characterizes all the reported works is represented by the design and realization simplicity: as it will be shown, each system has been designed in order to reduce the overall complexity and the number of used components; this is a critical factor toward integration of all-optical circuits. This is also a very important point to demonstrate that all-optical technologies can be a reliable alternative to electronics.

Each subsystem will be treated separately in its own chapter; each chapter will include a brief discussion about the novelty of the proposed solution and the improvements in respect to previous published results. Even if the work reported has been developed mainly experimentally, for better clarity and completeness each topic will be accompanied by some theoretical consideration.

The thesis is composed in 4 chapters and structured as follows:

1. **Introduction to Fiber-Optic Communication Systems and Networks**: an introductory chapter to explain Fiber-Optic Communications Systems and Optical Networks. The role of this chapter is to illustrate structures, scenarios and the needing for the various research results (laser sources ans all-optical signal processing functionalities) that are treated in the Thesis.

2. **An optical soliton source**, in **chapter 2**
   This chapter contains the design issues and the realization of laser source for Optical Time Domain Multiplexed (OTDM) systems. The source is designed to produce sub-picosecond pulses at 40 GHz repetition rate (in order to be used in real systems without the needing of further processing, like pulse reshaping, compression or pedestal suppression). Pulses are generated by a carefully optimized and controlled non-linear light propagation phenomenon in a proper Optical Fiber. The pulses quality guarantees the possibility to perform directly OTDM for operations at 160 Gb/s. Although this source was designed mainly for Optics Communication purposes, due to its broad op-

tical spectrum it has a number of other possible applications which will be also discussed through the thesis.

3. **Wavelength conversion experiments** (including also multi-wavelength conversion), in **chapter 3.** Wavelength conversion is demonstrated by means of several techniques, mainly exploiting the fast non-linearities of SOAs. In all these experiments, a particular regard is given to the multi-wavelength (1 to N) conversion that is a key functionality especially in next-generation access networks.

4. **An all-optical clock recovery scheme**, in **chapter 4**
   The scheme presented here represents a net improvement respect to previous circuits previously reported in literature in terms of performances and compactness. It consists in the realization of the well-known Tank Circuit (used in many electrical circuits to implement Optical Clock Recovery) in the Optical Domain.The circuit revealed a good versatility, being able to operate for several different modulation formats, and also with burst traffic. The circuit is suitable for hybrid integration.

1 Introduction to Fiber-Optic Communication Systems and Networks

The (massive) deployment of Fiber-Optics Communication Systems is, interestingly, a three-face phenomenon. First, it involves scientific and technical issues: fundamental physics needed for continuous technology improvements is at the base of the constant evolution of those systems. Second, the development of optics communication systems had an important industrial and economical impact: in every country the major telecom corporations have been involved in this process, realizing a fertile ground for new emerging markets. Not last, the development of Fiber-Optics Communication Systems has been accompanied by the evolution and the spreading of the Internet, that turned out to have a peculiar social importance: Internet generated innovative art forms, new communications styles and novel forms of social organizations.

Fiber-Optics Communication Systems offer the larger transmission capacity ever. In the second half of the twentieth century it was realized that the use of optical waves as the signal carriers (instead of an electrical or a radio signal) had the potential to increase by several orders of magnitude the capacity of communication systems. Until that time Communication Systems were based on electrical cables -telegraph and telephony- or radio links. Since those times a huge effort has been spent to boost Fiber-Optic Communication Systems technology. However, several years were needed before the technology was ready for this new generation systems. Although the main *ingredients* for those systems were discovered quickly (the laser appeared in 1960 and the design of optical fibers in 1966), the *real* revolution took place in 1970, when a compact optical source (a GaAs semiconductor laser) and a low-loss transmission medium (the *optical fiber)* became simultaneously available. Then, accompanied by continuous technology advancements, the transmissive reach and and the capacity of Fiber-Optics Communication Systems have been continuously increased and are still expected to increase.

In the past several issues concerning lightwave systems were addressed: the development of laser operating at 1.5 μm (where optical fibers exhibit the lowest attenuation) and the introduction of optical amplification (lumped or distributed) leaded to very long unrepeated transmissions. All-optical processing techniques which enable the transfer of signal processing capabilities from the electrical to the optical domain are also being developed. Other actual research targets include: system capacity increasing by means of new channel multiplexing (for example sub-carrier modulation); alternative modulation formats that are resilient to transmission impairments; component integration to allow for reduced coupling losses, increased efficiencies, lowered power consumptions, easy mass production.

Interestingly, part of the technology developed to support fiber-optic systems is actually being used also

in other fields: optical sensors technology, as an example, benefits from fiber technology. Another field of application that is taking benefit from Fiber-Communications is the one of the so called Optical Inter Connects, that are expected to replace electrical buses on electrical boards.

Fiber-Optics Communication Systems Building Blocks

Lightwave Systems can be divided in three major classes:

POINT-TO-POINT LINK systems. They are the usual optical communication systems. Depending on their length they are defined as *short, long and ultra-long haul.* Point-to-point links can be employed even in undersea communications, where points that are thousand of kilometers apart are connected. Point-to-point (p-2-p) links exist also for much shorter reaches, e.g. inside a building. P-2-p links are usually installed for telephony and Internet communications.
Fundamental components of a lightwave p-2-p link are: a transmitter (made of an optical source and an electro-optical modulator); a fiber; a receiver (made of a photodiode to convert optical bits in an electrical signal and an electrical receiver). When transmission distances are in the range of $20 \div 100$ m optical amplification is needed. Optical amplification is commonly realized by means of Erbium Doped Fiber Amplifiers (EDFA). In EDFA, optical amplification is obtained by a Stimulated Emission process generated by the amplified signal itself. EDFAs have a gain window that extends all over the range of wavelengths used in Fiber-Optic Communication Systems. Depending on the signal bit-rate and link length, distortions accumulated along the propagation can generate transmission impairments. Those impairments can be due to the linear effects of Chromatic Dispersion (CD) and Polarization Mode Dispersion (PMD). CD is responsible for a linear distortion induced on the propagating signal due to different propagation velocities of the chromatic components contained in the signal itself. PMD is also a dispersion phenomenon, but it is related to the different propagation velocities corresponding to different polarization modes. It is a stochastic effect, and is usually negligible for transmission bit-rate below 40 Gb/s. Transmissions can be impaired also by non-linear propagation effects, which can be observed when signals propagate with a power level above a certain level. In case of multichannel systems, non-linear effects can be responsible for induced cross-talk among the channels. Distortions induced by CD, PMD and non-linearities can be *reduced* by means of dedicated compensators placed periodically along the link, or at the link ends (Figure 1.1). In some cases, depending on various parameters and on the system design, it is useful to insert an ad-hoc pre-compensation stage after the transmitter.

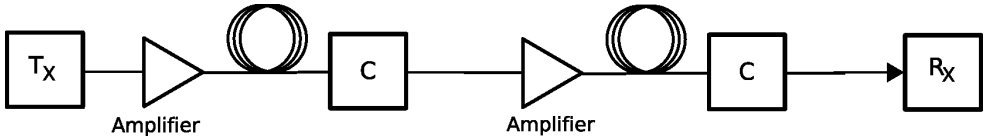

Figure 1.1: Point-to-point fiber links with periodic compensation of losses and accumulated distortions

Longer transmission reaches can be obtained by using regenerators. An optical regenerator is a receiver-transmitter pair that detects the bit stream, converts it to an electrical signal that is regenerated (reshaped,

re timed and re-amplified) and then retransmitted. Regenerators, if placed periodically along the link, cancel the distortions accumulated in each link span. The span length depends on a number of factors (the modulation format used, the bit-rate, dispersion compensation strategy,....). Before the introduction of optical amplifiers, typical span lengths were in the order of about $80 \div 100$ km. To avoid the double electro-optic conversion in each repeater (optical to electrical and then electrical to optical), all-optical regenerators are currently investigated; in some cases (depending on which physical effect they are based) they can be bit-rate and/or modulation format transparent.

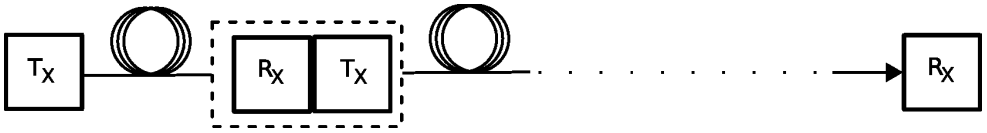

Figure 1.2: Point-to-point link with in line regenerators. Regenerators could be realized also with all-optical technologies.

BROADCAST AND DISTRIBUTION NETWORKS systems are used when information is sent to different subscribers simultaneously. Systems for thi applications are cable television, telephone services, computer data links. In this case the use of the fiber is advantageous: a single fiber allows the distribution of a large number of channels, each one with a huge bandwidth.
Recently, much attention has been dedicated to passive distribution networks, commonly referred to Passive Optical Networks (PON). The passive term indicates that if the network nodes have lengths below 20 km, it is possible to avoid optical amplification. In this case, by using cheap components (power splitters) it is possible to deliver the traffic routed to each subscriber using a simple and effective architecture. In this case star power splitters or cascaded power splitters can be used, each with varying splitting ratio (Figure 1.3).

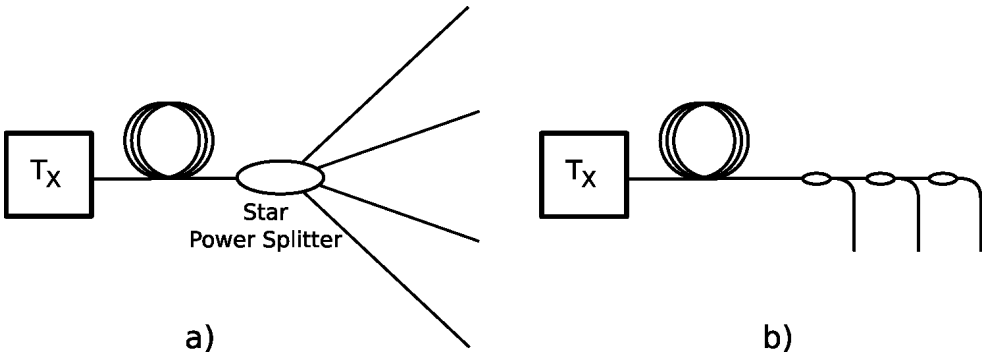

Figure 1.3: Example of a passive broadcast network.

LOCAL-AREA NETWORKS are deployed where a large number of users within a local area (e.g. a small office) are interconnected, and each user can access the network randomly. The random access offered to multiple users is the main distinctive character of this class of networks. To this aim, dedicated protocols have been developed: *Ethernet* is probably the most famous, being at the base of the *Internet*. Ethernet was designed to work initially at 10 Mb/s; later 100Mb/s and 1Gb/s were introduced; today its standardization for 10 Gb/s systems is ready. Common LAN network topologies are the star-coupled and bus networks,

much similar to those employed in Broadcast networks, or ring topology. In small environments, those three configurations are often realized by coaxial, electrical cables or wireless links. In LAN, each node contains a transmitter-receiver pair, that can also act as repeater; data are exchanged in form of packets instead of continuous streams.

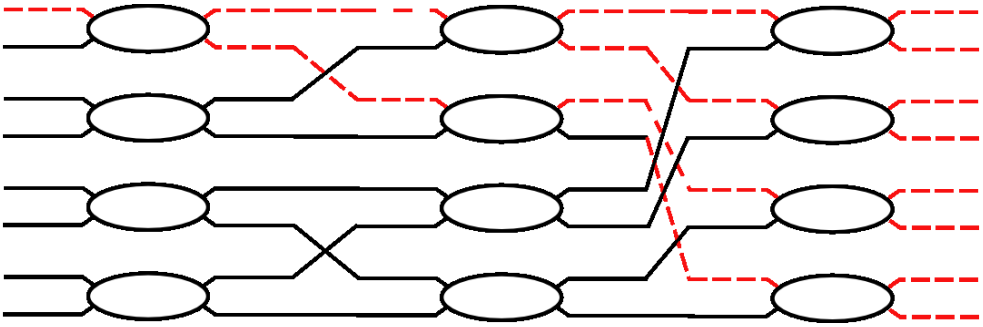

Figure 1.4: Passive 8x8 Star-coupler realized by means of a 12 fused silica directional couplers. Path from upper-left node is evidenced.

Star-couplers can be either *active* or *passive*. In both cases the users are connected by a point-to-point link. Passive star-couplers can be easily realized by means of directional couplers (see Figure 1.4): those kind of couplers are realized in fused silica. With passive star-couplers each destination node receives all the traffic generated by all the other nodes. In this case, each node has to select its own data; this selection is realized by means of the network protocol. Active couplers are able to redirect each packets to only one user (or more than one in case of multicast connections): this is done by a receiver-transmitter pair, and dedicated electrical logic.

Bus topology is less convenient from the power budget point of view. Assuming a constant insertion loss δ at each tap, if C is the fraction of power extracted at each splitter, the power available at $N-$th user is:

$$P_N = P_T C\left[(1-\delta)(1-C)\right]^{N-1} \tag{1.0.1}$$

In a *NxN* star coupler instead, the available power is:

$$P_N = \frac{P_T}{N}(1-\delta)^{log_2 N} \tag{1.0.2}$$

Considering $\delta = 0.05$, $P_T = 1\text{mW}$, $P_N = 0.1\mu\text{W}$, it can be found that N can be as high as 500 in case of star coupled topology and only 60 in case of bus topology.

In LAN networks, the broadcast term is referred to connections established among one node and *all* the LAN node. In some case, it is useful to send the information to a subset of selected networks node. Such connections are defined as *Multicast* connections. Multicast is currently realized with the help of power splitters (either star, bus or ring), and an appropriate protocol; today Multicast connections are possible thanks to active digital routers that perform the appropriate traffic redirection. However, several proposal for the realization of access networks suggested to assign a dedicated wavelength to each node: in this

case, the multicast functionality could be obtained realizing the so-called wavelength multicast: this kind of multicast can be effectuated by transferring the information contained in a channel simultaneously to several channels, each one at its own wavelength. This operation is known as Wavelength Multicasting[1]. This problem will be addressed in chapter 3, where two different schemes to realize this functionality will be presented.

Transmitters and Receivers

Fiber-Optics Communication Systems use mainly digital codings. Each transmitted bit lasts for a certain period of time T_B known as bit period. The number of bit transmitted in the unit time (bits per second) is called bit-rate $B = T_B^{-1}$. In the simplest case, the binary representation, each bit can contain one of two possible symbols, known as *mark* and *space* (or "1" and "0"). There are two major classes in which modulation formats can be divided: *Return-to-Zero (RZ)* and *Non-Return-to-Zero (NRZ)*. In the first case, in each bit slot the symbol "1" is represented by a pulse shorter than the bit slot: its amplitude returns to zero before the time slot ends. In the case of NRZ coding instead, the optical "pulse" remains at an high level and does not drop to zero between two successive "1" symbols. In this case, the pulse duration is not pre-determined. The main difference between those formats, can be found in the bandwidth: at the same signaling rate, the bandwidth of an NRZ signal is about 2 times smaller than the corresponding RZ signal. This can be understood if one thinks that for NRZ transmissions there is a minor number of transitions per bit.

A Continuous Wave (CW) optical carrier before the modulation, can be generally written as:

$$\vec{E}(t) = \vec{u}E_0 cos(\omega_0 t + \phi) \tag{1.0.3}$$

where $\vec{u}$ is a polarization unit vector, E_0 is the amplitude, ω_0 is the frequency and ϕ is the phase. The optical carrier can be modulated in amplitude, phase, frequency or a combination of those quantities. Additionally, it is possible to modulate the signal in polarization. In case of digital modulation, the various schemes are known as *Phase-Shift Keying (PSK), Frequency-Shift Keying (FSK)* and *Polarization-Shift Keying (PolSK)*. Probably the simplest modulation scheme is the so called *On-Off Keying (OOK)* and consists of changing the signal intensity between two levels, of which one is set to zero. This modulation format is the simplest also because it can be received directly by a photodiode, which is able to detect intensity variations. PSK, FSK and PolSK instead have constant intensity (they are often referred as Constant Enveloped (CE) formats): they need a *demodulator* that converts the modulated signal to an OOK signal, in order to be received by a photodiode. However, CE formats have been recently demonstrated to be advantageous for their resilience to CD .

Usually, data to be transmitted are generated in electrical domain, and then transferred to the optical carrier: the modulation can be performed by applying the electrical signal directly on the laser source

[1] In case of a single destination channel, this operation is defined Wavelength Conversion.

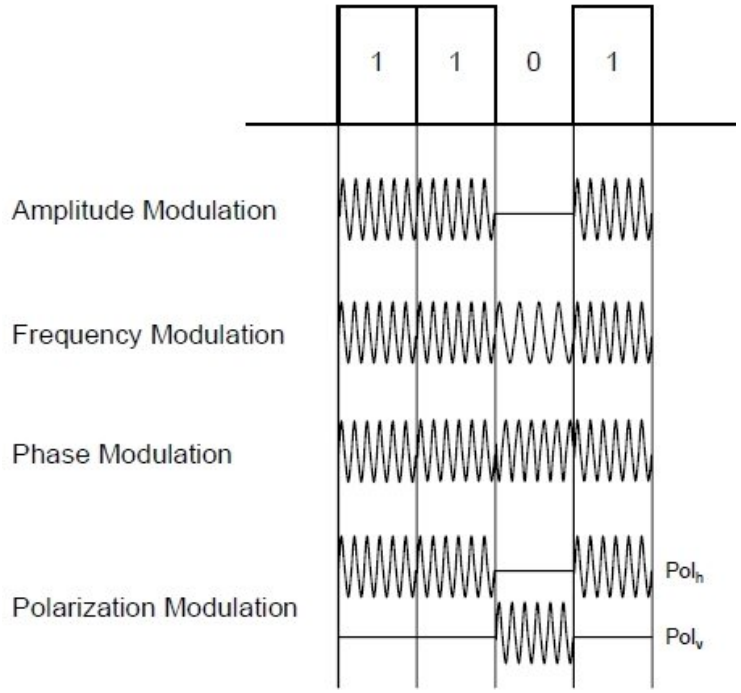

Figure 1.5: Schematic representation of common modulation formats for the NRZ case.

or by external modulation, through an electro-optical modulator. Direct modulation is convenient and useful for signals transmitted at low bit-rates (usually no more than 2.5 Gb/s). Direct laser modulation is accompanied both by intensity and frequency modulation: thus, an OOK modulation performed in this way is always accompanied by a frequency modulation (or chirp) that can increase signal distortions along the fiber.

External modulation can be performed with a variety of electro-optical modulators. Usually, Electro-Absorption (EAM) or Mach-Zender (MZM) based modulators are used in systems implementations. EAM are semiconductor devices that change they absorption coefficient when driven with a current above a determined threshold. For this reason, they are useful to realize OOK transmissions. MZM modulators instead are integrated Mach-Zender interferometers in which the arms relative phase-delay is controlled by an electrical signal. In most cases, electrical signal generator provide NRZ signals. When RZ coding is needed, it is possible to transform the electrical NRZ data stream into an RZ optical signal, by replacing the input CW optical carrier represented in 1.0.3 with a “pulse” train with repetition rate corresponding to the signaling rate, and pulse-width shorter than the bit-time.

PSK and PolSK can be simply realized by launching a CW into an electro-optical crystal; if the input polarization is parallel to one of the crystal principal axes, Phase Modulation is obtained. Otherwise, Polarization Modulation can be performed by entering the modulator with a linear polarization state, with 45° direction, in respect to the crystal contained into the modulator.

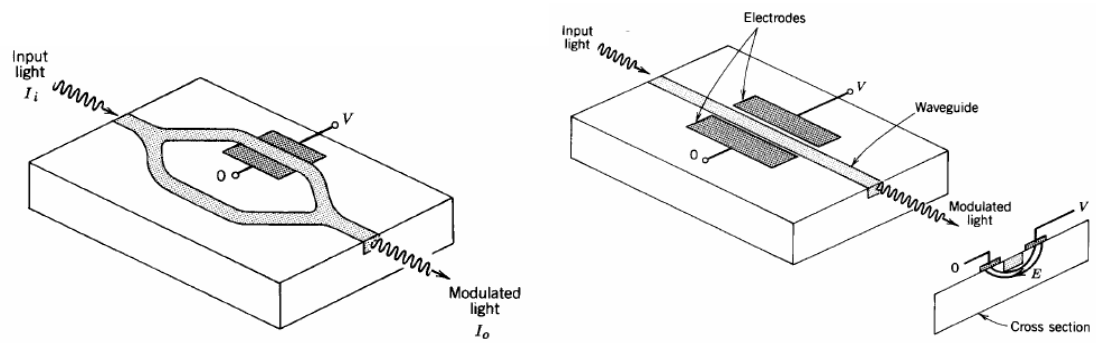

(a) (b)

Figure 1.6: (a) Mach-Zender Modulator: in the picture, only one arm is phase-modulated. (b) A phase modulator. Both modulators are usually realized on $LiNbO_3$ substrates. Polarization modulation can be conveniently realized by using a Phase Modulator in which the input light has a linear polarization state, with 45° direction in respect to crystal axis.

Multiplexing: WDM and OTDM systems

In order to fully exploit the huge bandwidth offered by Optical Fibers it is necessary to transmit many channels simultaneously through multiplexing. It is possible to realize multiplexing in several ways: the most common are wavelength and time division multiplexing. Wavelength Division Multiplexing systems instead are realized by using a dedicated optical carrier wavelength for each channel. Optical Fibers exhibit a 15 THz window in which transmission losses are minimized around the 1500 nm, thus making possible to multiplex a large number of channels (Figure 1.7). At the receiver end, each channel (both in OTDM and in WDM systems) must be demultiplexed and received separately. Several standards have been developed for WDM systems.

WDM systems can be divided in two major categories: Coarse and Dense. Coarse WDM systems are characterized by a large wavelength spacing: originally the term CWDM was meant for systems with channels allocated both in 1300 and 1500 nm windows. Recently WDM have been standardized as systems with 20 nm channel spacing. This large spacing allows to use uncooled lasers: due to large spacing it is possible to avoid laser wavelength stabilization and saving the cost of thermal stabilizers. Dense WDM (DWDM) systems instead are designed to multiplex an higher number of channels. In this case, to obtain the closer wavelength spacing, it is needed to use highly stabilized lasers. However, the lack of spacing DWDM systems are made possible by the use of Erbium Doped Fiber Amplifiers (EDFAs) which guarantee simultaneous amplification of WDM multiplexed channels in the range approximately from1530 to 1560 nm, without introducing significant cross-talk. Grid spacing have been standardized at 200,100, 50 and 25 GHz, leading to systems with more than 160 aggregated channels[2]. The lack of optical amplifiers with larger wavelength operational range limited the realization of CWDM systems to local networks. The typical structure of a point-to-point WDM link is represented in Figure 1.8.

[2]It should be considered that the bit-rate of each channel is limited by the frequency spacing. For example, a 25 GHz grid is not compatible with channels modulated at 40 Gb/s.

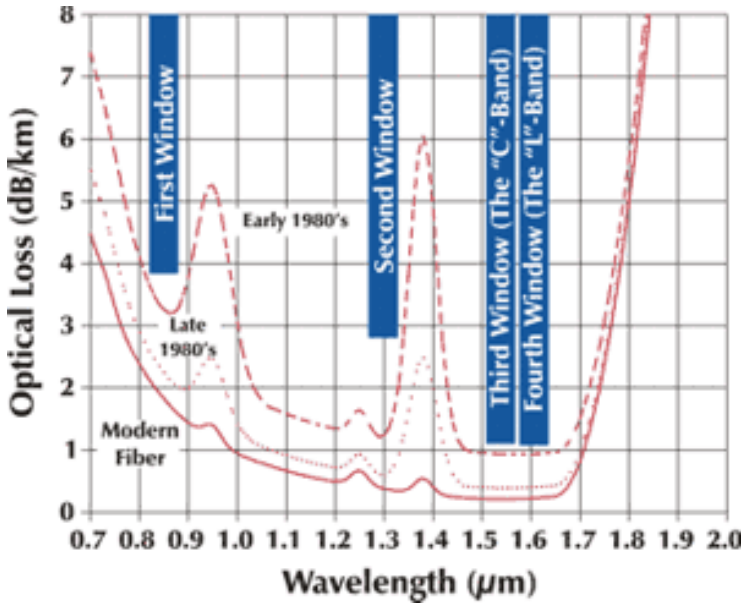

Figure 1.7: Typical optical fiber losses. In correspondence of the region around 1.3 and 1.5μm there are losses minima. Those region are called respectively Second and Third window, and occupy a region of 12 and 15 THz respectively. In those regions it is possible to allocate simultaneously multiple channels, realizing WDM systems.

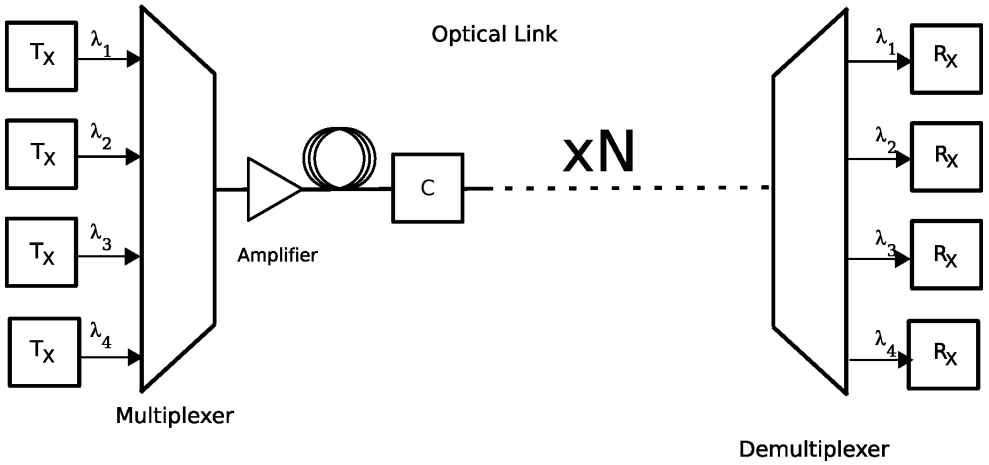

Figure 1.8: Schematic structure of a point to point WDM link. Multiplexing and demultiplexing are realized by means of AWGs. As a common p2p link, it can be composed of several spans.

In point-to-point links, multiplexing and demultiplexing can be realized by Arrayed Waveguide Gratings (AWG). An AWG is a dispersive guided medium such that when a number of WDM channels enter into it, each channel is spatially separated on a dedicated fiber at its exit. At the same time, if used in *reverse* direction, it allows to multiplex signals coming from different emitters (with distinct wavelength on different input fibers) on a single output fiber (Figure 1.9).

Optical Fibers have a linear transfer function that can be expressed as a filter ($e^{i\beta(w)\omega L}$ where ω is the carrier frequency, $\beta(\omega)$ is the parameter accounting for chromatic dispersion and L is the fiber length.

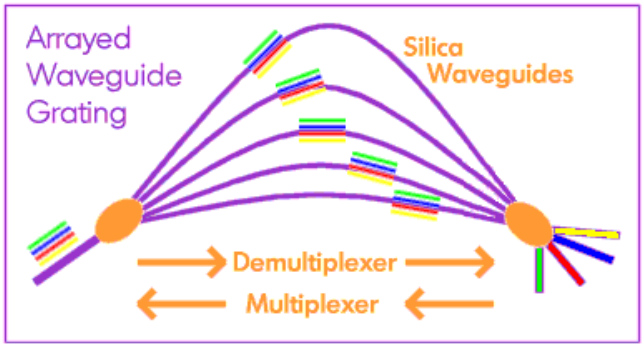

Figure 1.9: Schematic principle of an AWG.

However, above a power threshold, fibers can become a non-linear propagation medium: due to the fiber small sections ($50 \div 100\,\mu m^2$), signals propagate with very high intensities even at low powers. This threshold depends on several fiber design parameters. Fiber non-linearities have been exploited to perform a variety of all-optical processing functions: optical switches, non-linear mixing, optical sampling devices, pulse train generation, ... In WDM transmission, the non-linear fiber response can be really detrimental. Non-linearities generate channels interactions that induce undesired cross-talk among the channels. Such effects are not easy to avoid: long span reaches requires high launch powers. Several solutions have been proposed to mitigate those impairments. The introduction of distributed amplification helped partially to solve this problem: it allows to reduce the launch power and to maintain the average power below the non-linear threshold all along the link.

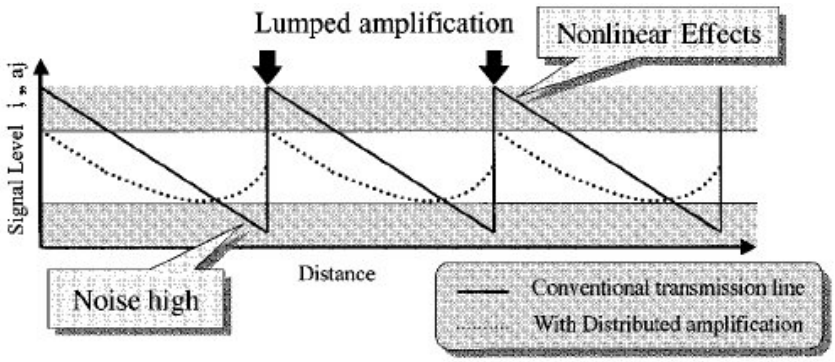

Figure 1.10: The use of distributed Raman allows to avoid propagation regimes in which non-linear effects can impair the signal. With distributed amplification it is also possible to avoid propagation in regimes in which the average power is too low in which noise can be accumulated.

Time Division Multiplexed (TDM) is a type of digital multiplexing in which two or more apparently simultaneous channels are derived from bit stream, by interleaving pulses representing bits from different channels. TDM was first introduced at electrical level to aggregate telephone traffic of different subscribers in a single, larger capacity channel; TDM realizes a single channel at high bit-rate instead of N channels with lower capacity. TDM bit-rates were standardized by ITU consortium. A standard voice signal has a bandwidth of 64 kbit/s, determined using Nyquist's Sampling Criterion. TDM takes frames

of the voice signals and multiplexes them into a TDM frame which runs at a higher bandwidth. So if the TDM frame consists of n voice frames, the bandwidth will be $n * 64$kbits/s. Each individual multiplexed stream is called tributary channel. TDM has been standardized in the SDH protocols, which define multiplexing rates, and operations such frames add and drop. OTDM is an extension of TDM in optical domain. It differs with WDM in two major points: first, all the channel multiplexed with OTDM do not need to be at a distinct frequency; second, OTDM requires RZ coding. WDM instead can be realized with both NRZ and RZ codings. OTDM systems are able to increase the bit-rate of a single optical carrier to values as high as 320 Gb/s. An OTDM transmitter is depicted in Figure 1.11. It requires a pulse source with repetition rate corresponding to the tributary bit-rate. This pulse train is divided in a number of tributary channels that are modulated independently, properly delayed and then coupled together by means of a power splitter. Each branch is delayed by an amount of $(n-1)/NB$ where N is the number of bit streams multiplexed, B is the tributary bit-rate, and $n = 1, ..., N$. In most cases, Mode Locked (ML) lasers are used to this aim. However, it is required that the pulses have a pulse-width $\tau < (NB)^{-1}$in order to fit within the aggregated bit-time. If the source does not fulfills this requirements, a compression stage is needed before performing the multiplexing. In chapter 2 it will be presented an alternative pulse source: it is not based on the common used ML technique, and provides directly short pulses, ready to be multiplexed to an higher bit-rate. Due to its high output power it also eliminates the need of a pre-amplifier, like shown in Figure 1.11.

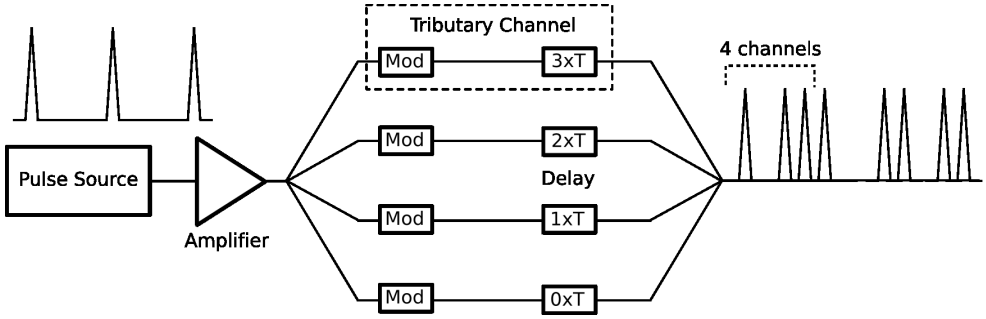

Figure 1.11: Typical OTDM transmitter. A pulsed source is power split. Each branch is modulated, properly delayed and then recombined.

Demultiplexing of OTDM signals is more complex and requires always a clock signal. With clock signal, it is meant a periodic pulse train with a repetition rate that match the bit-rate of the tributary channels. This clock signal is used to *sample* the desired tributary channel. The sampling can be performed with electro-optical or all-optical devices. In general, the latter are preferred because can operate at higher speed. In cases in which an all-optical clock signal is not available at the receiver, an additional unit, a Clock Recovery (CR) circuit is needed. A CR circuit is able to recover the original periodic pulse train from the modulated one. In practice it fills with a pulse the bit-slot in which pulses are not present. This functionality will be discussed in more detail in chapter 4, where a novel and compact all-optical solution to perform this task will be presented.

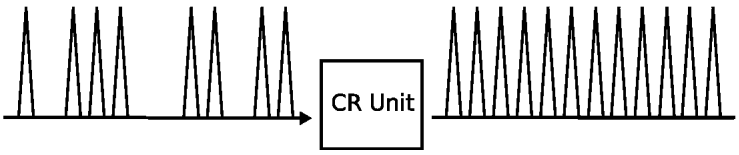

Figure 1.12: Illustration of Clock Recovery functionality: a CR unit removes the modulation from an RZ signal, and extract a produces pulse train.

2 A Soliton Pulse Source for 40 Gb/s systems

2.1 A soliton source based on adiabatic compression in Dispersion Shifted Fiber

In the following section I will describe the realization of a soliton-like pulse source based on the Adiabatic Compression (AC) of a sine-modulated wave by non-linear propagation in a optical fiber. It will be shown that this technique is suitable to produce optical pulse trains to be used in Optical Time Domain Multiplexed (OTDM) Systems. Several kind of sources were demonstrated using this principle in the past. However most of those implementations are based on AC compression of pulses that are already available (i.e. generated by other sources). On the contrary, the source presented here is based on the simultaneous pulse formation and compression in the same non-linear medium. The first part of the chapter provides basic concepts of light propagation in optical fibers and a review of the Adiabatic Compression (AC) of solitons in Optical Fibers; the second part is focused on experimental results.

2.1.1 Theory

2.1.1.1 Pulse propagation in Optical Fiber

Light propagation in Optical Fibers is determined by small number of parameters: the attenuation, the chromatic dispersion and a non-linearity coefficient. All these parameters appear in the wave propagation equation (also known as Non Linear Schroedinger Equation (NLSE) [1]) that in optical fibers assumes the form:

$$i\frac{du}{dz} = -\gamma|u|^2 u + \hat{D}u - i\alpha u \tag{2.1.1}$$

$$\hat{D} = -\sum_{n=2}^{\infty} \frac{i^n \beta_n}{n!}\left(\frac{\partial}{\partial t}\right)^n \tag{2.1.2}$$

Here $u(z,t)$ is the Electric Field complex amplitude at position z and time t. Even if a vectorial representation would provide a complete description the electric field can be treated as a scalar; this approximation is valid for a wide range of scopes (at least for all the ones included in this thesis) and enough to introduce basic concept of light propagation in fibers. In 2.1.1, the time variable t is measured in a reference frame that travels with the light. Attenuations, or losses are most due to Rayleigh scattering and is represented by the parameter α. As a scattering process, the attenuation is a function of the wavelength. However, across

the spectral region of interest for optical communications (the C-band[1]), its value it's almost constant and is equal to 0.2 dB/km (or $0.46 km^{-1}$ linear scale).

Chromatic Dispersion is represented by the operator $\hat{D}$ and accounts for the different propagation velocities of the various chromatic components contained in the field u. This phenomenon is due to the refraction index dependence on the signals wavelength: $n = n(\lambda)$. In the $\hat{D}$ series expansion each term accounts for different order contribution to the chromatic dispersion. Each tern is effective on a determined time scale: The higher is the order, the fastest are the signal dynamics needed to observe the corresponding effects. Typical optical communication signals do not exceed picosecond time scales variations; thus a good representation can be obtained in most cases by retaining only the second order contribution, β_2, while the third order contribution β_3 becomes important to describe propagation of signals with temporal variations on time scales below 1 ps. β_2 is generally not constant vs. the wavelength, even in C-band: its value depends on the material (fused silica) and on the geometrical properties of the fibers (waveguide diameter, for example). For classical optical fibers, in which the propagation is based on total internal reflection, β_2 shows generally a monotone behavior in the region of interest. Typical values range from -1 to $-20\, ps^2/km$ (depending on the fiber and the wavelength). Each type of fibers differ mainly in the slope of this curve. The wavelength at which β_2 cross the zero value, is called *Zero-Dispersion Wavelength*. Most modern fibers, based on light-trapping due to photonic band-gap effects, can be designed instead with almost arbitrary dispersion profile.

Table 2.1: Typical Dispersion Coefficients Values for different Optical Fibers.

Fiber Types	$\beta_2(\frac{ps^2}{km})$	$\beta_3(\frac{ps^3}{km})$
Single Mode (G.652)	-20	0.005
Dispersion Shifted (G.655)	$-3 \div 3$	0.063
Dispersion Compensating	$80 \div 160$	0.02

The non-linear parameter γ accounts for interactions between fields that simultaneously propagate into the fiber, new frequencies generation, self-phase modulation effects. In optical fiber, non-linearities are due to the optical Kerr-effect, that describes the non-linear polarization response of fused silica induced by the traveling waves. Kerr effect [2] is observed in centro-symmetric materials, and it is manifested through a variation of the index ellipsoid of the material when an external electrical field is applied to the material itself. The effect is non-linear because the refraction index modification is proportional to the square of the applied field:

$$\Delta n \propto |E|^2$$

thus, in a Kerr media, the refraction index is usually written as:

[1] The C-band is defined as a wavelength region ranging from 1530 to 1565 nm. The C-band is all contained in the so called *third window*. This "window" corresponds to the the interval with lowest attenuation level in optical fibers.

$$n(\omega,|E|^2) = n_0(\omega) + n_2 \frac{|E|^2}{\varepsilon} \tag{2.1.3}$$

where n_2 is a scalar coefficient if we consider a uni-axial material, and ω is the optical pulsation. When a very intense optical field traverses a Kerr material, Kerr effect can be observed even without applying external bias fields: in this case, it is the electrical field associated to the optical beam itself that generates an refraction index perturbation. This particular effect it is known as Optical Kerr Effect, and it is the one responsible for optical non-linearities in fibers. For Optical Kerr effect, the squared electric field in 2.1.3 is the optical wave intensity I, thus the Optical Kerr effect can be written as

$$n(\omega,I) = n_0(\omega) + n_2 I \tag{2.1.4}$$

The relation between n_2 in 2.1.3 and 2.1.4 and the parameter γ that appears in the propagation equation (eq: 2.1.1),

$$\gamma = \frac{n_2 \omega}{c A_{eff}} \tag{2.1.5}$$

where c is the speed of light, and A_{eff} is the fiber core effective area (strictly related to transverse mode dimensions). As it can be seen from its definition, fixed the optical power, γ contains a dependency on optical intensity (through the effective area A_{eff}). As in optical fibers the core size vary in the range of $2 \div 90\,\mu m$ it is possible to observe the Optical Kerr effect even with relatively small average power levels (tens of mW). To observe the same effects in bulk media, higher power levels would be required.

Standard fused-silica single-mode fibers have non-linear coefficients with a value around $2.2\,\frac{1}{Wkm}$. In more recent fibers, designed with small sized cores or with photonic crystal transverse structure, γ can reach higher values ($10\,\frac{1}{Wkm}$). The highest non-linear coefficient instead has been reached recently by combining a small structure guiding cores (such as $2.2\mu m^2$) and doping techniques. Doping has been tested with chalcogenide [3] or bismuth-oxide [4] compounds. In particular, with this technique it was possible to reach non-linear coefficient values up to $1100\,\frac{1}{Wkm}$ (so 3 orders of magnitude higher respect to the standard fibers). However, those fibers are also characterized by high dispersion values; for example, the bismuth-oxide doped fiber shows a value of $-280\,$ps/nm/km. In this case, the losses are also increased due to the extremely small core sizes.

When considering pulses propagation in fibers it is possible to extract important qualitative information by taking in consideration other few parameters without constraining hypothesis on the pulse temporal shape: those parameters are the peak power P_0 and pulse-width T_0. This is possible by retaining only the second order contribution of $\hat{D}$ operator and introducing a normalized amplitude U as

$$u(\tau,z) = \sqrt{P_0} e^{-\alpha z} U(\tau,z)$$

where $\tau = \frac{t - z/v_g}{T_0}$ is the time variable defined in a reference frame moving with the pulse, and normalized to the pulse-width. The electric field is normalized, by accounting for the losses. After that it is possible

to re-cast the wave propagation equation 2.1.1 in another form, and to define two important length-scales that characterize the pulse evolution:

$$i\frac{\partial U}{\partial z} = \frac{sgn(\beta_2)}{2L_D}\frac{\partial^2 U}{\partial \tau^2} - \frac{e^{-\alpha z}}{L_{NL}}|U|^2 U \tag{2.1.6}$$

$$L_D = \frac{T_0^2}{\beta_2} \quad L_{NL} = \frac{1}{\gamma P_0} \tag{2.1.7}$$

The first length scale, L_D, indicates the length over which it is possible to observe linear propagation (i.e, over which linear effects manifest). A similar meaning can be associated to the length L_{NL} that indicates the length over which non-linear effects can be observed. From their definitions, it is clear that those quantities do not depend on the fiber only (through the parameters γ and β_2), but also on the pulse properties (its width T_0 and the peak power P_0). Once fixed the fiber and the pulse parameters the propagation regime is than regulated by the ratio $\frac{L_D}{L_{NL}}$.

Through the definition of the linear and non-linear scale lengths it is also possible to study the pulse propagation considering separately linear and non-linear regimes and then combining them together to describe the complete pulse evolution.

In linear regime, a pulse-shape is altered by chromatic dispersion: the accumulated distortions can generate pulse broadening or modify the pulse symmetry properties. Broadening effects are related to second order dispersion, while symmetry effects are due to third-order dispersion. Due the low relative magnitude of third-order dispersion compared to the second order dispersion coefficient (more than 2 order of magnitude for the various fibers, cfr. tab. Table 2.1), it is possible to observe the third-order effects only when the second-order dispersion is negligible (i.e., near the zero-dispersion wavelength), or with sub-picosecond pulses. To derive a general description of distortions induced in linear propagation regime for arbitrary pulse shapes let's consider the propagation equation obtained by setting $\gamma = 0$ and $\alpha = 0$ in eq. 2.1.1:

$$i\frac{\partial U}{\partial z} = \hat{D}U \tag{2.1.8}$$

obtained by setting $\gamma = \alpha = 0$ in eq. 2.1.6. If $\hat{D}$ expansion is retained up to the 3^{rd} order, the solution is given by:

$$U(z,t) = \frac{1}{2\pi}\int_{-\infty}^{\infty} \tilde{U}(0,\omega) e^{\left(\frac{i}{2}\beta_2\omega^2 z + \frac{i}{6}\beta_3\omega^3 z - i\omega t\right)} d\omega \tag{2.1.9}$$

where $\tilde{U}(0,\omega)$is the Fourier Transform of the field at $z = 0$.

Even if eq. 2.1.9 furnishes a complete and exact solution, it does not provide directly information about the pulse-width evolution neither about the amount of asymmetry acquired during the propagation. Those information can be obtained by the following argument. The pulse-width can be defined through the Root-Mean-Square width, defined as

$$\sigma = \left[\left\langle t^2\right\rangle - \langle t\rangle^2\right]^{1/2}$$

where the $\langle\rangle$operation indicate the time averaging[2]. Then, its evolution can be described by means of the first and second moments of time variable t, that evolve as (in analogy with the Ehrenfest's theorem for the case for position and momentum observables described by a Schroedinger equation) :

$$\frac{d\langle t\rangle}{dz} = i\left\langle\left[\hat{D},t\right]\right\rangle \tag{2.1.10}$$

$$\frac{d\left\langle t^2\right\rangle}{dz} = -\left\langle\left[\hat{D},\left[\hat{D},t\right]\right]\right\rangle \tag{2.1.11}$$

Here, $\langle t\rangle$ governs the asymmetry of the pulse, while $\left\langle t^2\right\rangle$ is a measure of the pulse broadening. Higher order moments can be calculated, and define the skewness and kurtouis of the pulse (3^{rd} and 4^{th} moments respectively). 2.1.10 and 2.1.11 can be integrated analytically, and their solution is given by:

$$\langle t\rangle = a_0 + a_1 z$$

$$\left\langle t^2\right\rangle = b_0 + b_1 z + b_2 z^2$$

where the coefficient depend only on the initial field shape $U(z=0,t)$ and are given by:

$$a_0 = \int_{-\infty}^{\infty} U_0^*(t)\, t U_0(t)\, dt$$

$$a_1 = i\int_{-\infty}^{\infty} U_0^*(t)\left[\hat{H},t\right] U_o(t)\, dt$$

$$b_0 = \int_{-\infty}^{\infty} U_0^*(t)^2 U_0(t)\, dt$$

$$b_1 = i\int_{-\infty}^{\infty} U_0^*(t)\left[\hat{H},t^2\right] U_0(t)\, dt$$

$$b_2 = -\frac{1}{2}\int_{-\infty}^{\infty} U_0^*(t)\left[\hat{H},\left[\hat{H},t^2\right]\right] U_0(t)\, dt$$

In non linear propagation regime, (discarding the linear effects) the pulse evolution is affected mainly by a phenomenon known as Self Phase Modulation (SPM). This effect describes a dephasing effect among the

[2]the average is defined as$\langle t^p\rangle = \frac{\int t^p |U(z,\tau)|^2 d\tau}{\int |U(z,\tau)|^2 d\tau}$

chromatic components inside a pulse. The dephasing depends on instantaneous power: each chromatic component in the pulse exhibits a nonlinear phase rotation. SPM is evident analytically from the NLSE (eq. 2.1.1), once the non linear propagation effects are isolated (i.e. by putting $\hat{D} = \hat{0}$):

$$\frac{\partial U}{\partial z} = \frac{ie^{-\alpha z}}{L_{NL}} |U|^2 U \tag{2.1.12}$$

By direct integration, the pulse evolution is given by:

$$U(z,\tau) = U(0,\tau) e^{i\phi_{NL}(z,\tau)} \tag{2.1.13}$$

where

$$\phi_{NL} = |U(0,t)|^2 \frac{1-e^{-\alpha z}}{\alpha L_{nl}} \tag{2.1.14}$$

While a dephasing effect is observed also in the linear regime, here the dephasing is such that pulse intensity shape is unaffected (eq. 2.1.13): this means that the pulse acquire a chirp. Due to the losses, this effect is not observed for every propagation length. For this reason, it is convenient to introduce another length (known as Effective Length) defined as:

$$L_{eff} = \frac{1-e^{1-\alpha L}}{\alpha}$$

as the fraction of the fiber length in which the non-linearity can be considered effective.

The dephasing effect in non-linear propagation regime is accompanied by the generation of new frequencies. This can be evinced by analyzing 2.1.14. The phase variation implies an instantaneous optical frequency difference across the pulse, from its carrier frequency ω_0 (a chirp). This frequency difference can be expressed as

$$\delta\omega(t) = -\frac{\partial \phi_{NL}}{\partial t} = -\frac{1-e^{1-\alpha z}}{\alpha L_{NL}} \frac{\partial}{\partial t} |U(0,t)|^2 \tag{2.1.15}$$

The chirp increases with the propagating distance. Thus new frequency components are continuously created while pulse propagate down the fiber.

In real systems, it is not possible to separate linear and non-linear effects; this is particularly true in fibers with high non-linear coefficients: in those fibers the enhanced non-linearity is obtained by reducing the effective area; at the same time, this increases the losses and changes the dispersion properties (that are tightly related to the waveguide dimensions). As result, the linear and non-linear lengths overlap.

If proper boundary conditions are matched, it is possible to observe a mutual cancellation of non-linear and linear propagation effect: this leads (if losses are neglected) to the formation of solitons. Phenomenologically, a soliton is a pulse that propagates indefinitely without changing its electric field.

2.1.1.2 Adiabatic Compression of Solitons in Optical Fibers

Adiabatic Compression of solitons in optical fiber has been extensively studied in the past years [5], [6], [7], [8]: it is based on the intrinsic soliton stability against small energy perturbations that can be observed in anomalous dispersion regime [9]. Using the standard terminology, this stability can be expressed by means of the conservation of the soliton order N. For the fundamental solitons (defined by N = 1) this is expressed by the conservation law $\frac{\gamma T_0^2 P_0}{\beta_2} = 1$. This condition is equivalent to

$$\frac{L_D}{L_{NL}} = 1 \tag{2.1.16}$$

In such conditions the soliton envelope is found to be an hyperbolic secant function, defined as:

$$U(z,\tau) = P_0 sech(\tau) e^{i\frac{z}{2}} \tag{2.1.17}$$

When stability conditions apply, optical solitons react to an energy perturbation (amplification or attenuation, depending on the perturbation sign) by reshaping themselves adjusting their width in order to maintain the soliton order unaltered. Of course this stability it is not achieved for every energy perturbation. For example, in a uniform and lossy fiber, this process can observed on small propagation distances (where the attenuation losses are negligible and thus can be treated like a perturbation); in this case, it is found that the soliton increases its pulse-width (to keep constant the product $T_0 \times P_0$). For longer propagation distances, when the propagation became essentially linear, some chromatic components can escape from the soliton envelope and radiate away, thus destroying the soliton [10]. A simple evaluation of the pulse-width evolution of a soliton in presence of small energy perturbation can be derived as follow. A first order soliton (hyperbolic secant envelope, eq. 2.1.17) carries an energy E equal to:

$$E = 2P_0 \frac{T_{FHWM}}{1.763} = \frac{3.525\,|\beta_2|}{\gamma T_{FWHM}}$$

After perturbing soliton energy by a factor G (over a propagation length z), the following relations hold:

$$\frac{E(z)}{E(0)} = G = \frac{\beta_2(z)\gamma(0)T_{FWHM}(0)}{\beta_2(0)\gamma(z)T_{FWHM}(z)}$$

This means that the pulse-width scales as:

$$T_{FWHM}(z) = \frac{\beta_2(z)\,\gamma(0)\,T_{FWHM}(0)}{\beta_2(0)\,\gamma(z)\,G} \tag{2.1.18}$$

In the case of uniform fibers (such that dispersion and non-linearity do not change along z, $\beta_2(z) = \beta_2(0)$ and $\gamma(z) = \gamma(0)$) with constant losses ($G = e^{-\alpha z}$), the pulse-width increases exponentially with the distance:

$$T_{FWHM}(z) = T_{FWHM}(0)\, e^{\alpha z}$$

As stated before, this is only valid for small energy perturbation (i.e., for propagation lengths in which the relation 2.1.16 holds).

Eq. 2.1.18 states that the pulse-width is not affected only by the gain: choosing a fiber with appropriate dispersion or non-linearity coefficient that vary along the longitudinal dimension, it is possible to control the pulse-width and to compensate for the perturbation effects. Thus, with a proper non-uniform fiber it is possible to maintain the same soliton profile, compress or stretch the pulse. For example, by choosing a dispersion profile such that $\beta_2(z) = \beta_2(0)\, e^{-\alpha z}$ (with α equal to the attenuation coefficient of the fiber) it is possible to compensate exactly the effect of attenuation along the propagation; in this regime, even if constantly loosing power, the soliton maintains its proportions (the product $T_0 \times P_0$). In this sense, it could be said that using dispersion tailoring techniques, it is possible to obtain an *effective amplification*. The same balance could be in principle obtained by using a fiber with increasing non-linear coefficient.

From an experimental point of view, it is not simple nor practical to realize optical fibers with the desired non-uniform parameters. Experiments were carried out by using cascade fibers with decreasing zero-dispersion wavelength, so that the soliton experience a *step* dispersion profile. Of course, with this kind of solutions, it is not possible to design arbitrary shaped dispersion (or non-linearity) profiles.

Even if from a theoretical point of view, dispersion tailoring is equivalent to an *active* amplification, Adiabatic Compression obtained with dispersion tailoring is less effective. In fact, the compression ratio that can be achieved is given by $\beta_2(0)/\beta_2(z)$ (assuming a monotone dispersion profile). This means that the compression ratio is limited by the initial value of the dispersion (as negative dispersion values are not acceptable for soliton propagation); in literature, compression factors near by 20 were reported.

Higher order solitons support higher compression ratios [11], but their temporal shapes are not always compatible with the requirements of Optical Systems.

A trade-off between compression performance and soliton characteristics, has been shown by Pelusi and Liu [11]. They reported that compression ratio can be improved using solitons of order 1<N<2. In their work, they analyze this phenomenon studying several different dispersion profiles. They shown compression factors up to 50: the price to pay in this case, is to handle with pulses that present small chirp and/or pedestal. Chirp and pedestal can be detrimental for pulse transmissions.

Eq. 2.1.18 shows that also distributed amplification (i.e. a fiber in which the gain parameter is a function of the propagation distance, $G = G(z)$) can be useful to the aim of pulse compression.

Distributed amplification, offers a number of advantages and it is easier to implement. The most simple distributed amplification scheme is achieved with Raman amplification [12]. Raman amplification exploits the Raman Scattering that can be observed in molecular media. In Raman Scattering a photon of an incident field (called the pump) is annihilated to create a photon at lower frequency (known as *Stokes wave*), shifted by the vibrational modes of the molecules in the medium. At the same time, another photon is created in order to conserve the energy and the momentum. In this process the incident light

acts as a pump for generating the Stokes waves. If photons at Stokes wave energy are already present in the medium, they experience amplification at pump expenses.

It is also possible to combine together both distributed amplification and dispersion decreasing fibers.

Distributed amplification can be useful to obtain higher compression ratios. An advantage offered by the distributed amplification is that imposing proper boundary conditions, it is possible to obtain almost arbitrary gain profiles in the same fiber (by changing for example pumps power and insertion points). For example, it was shown by [13] that using a configuration with double Raman pumping (both co-propagating and counter propagating) it is possible to realize quasi-loss-less links. Quasi loss-less links are characterized by a gain parameter such that $|G|$ is almost equal to 1 all over the fiber. In this way soliton propagation over distances up to 50 km has been demonstrated. However this solution is not free of limitations; high power levels can generate other undesired non-linear effects (as Stimulated Brilloiun Scattering). Compression of soliton in presence of amplification was studied by Blow, Doran and Wood [14]. They studied soliton dynamics related to amplification processes. They derived that solitons are compressed and that the propagation lead to a stable solution (depending on initial soliton order). Their work also shown that the compression is characterized by a pulse-width oscillating behavior (with decreasing oscillation depth along the propagation) around the final stable solution. Another important conclusion was that a pulse traveling in a amplified fiber tends to converge to a soliton order that depends on the accumulated gain. As it will be shown shortly, this is also important for the realization of the source described in this chapter. Blow et al. paper was limited to the case of constant gain but it is easy to extend their result to the more general case in which $G = G(z)$.

This is possible by solving numerically the standard pulse propagation equation (eq. 2.1.1) in which the loss coefficient is replaced by a distributed gain $G(z)$:

$$i\frac{du}{dz} = -\gamma|u|^2 u + \frac{1}{2}\beta_2\frac{\partial^2 u}{\partial t^2} - iG(z)\,u \tag{2.1.19}$$

In 2.1.19, the loss coefficient has been replaced by the quantity $G(z)$ which represents the amplification (or attenuation) along the fiber. The gain/loss profile $G(z)$ can be determined by first calculating the power profile $P(z)$ of a continuous wave propagating into the amplified fiber. Then, the gain coefficient is given by the relation:

instantaneous

$$G(z) = \frac{1}{P(z)}\frac{dP}{dz}$$

This approximation is valid if the amplification process does not depend on the instantaneous signal shape. Once $G(z)$ has been determined, 2.1.19 can be solved with standard numerical integration method. In particular, 2.1.19 can be solved by the Split Step Fourier Method [1]. An implementation of such algorithm will be included in Appendix A.

2.1.2 Source design

As already mentioned, the pulse source was realized exploiting the AC phenomenon. The main novelty introduced with this scheme, in respect to the previous published works in this area, is that this source combines the processes of pulse generation and compression in the same non-linear medium (the optical fiber). The pulses formation stage, is obtained by launching a sine-modulated wave into a Dispersion Shifted Fiber. It was previously demonstrated by Ciaramella and Artiglia [15] that launching a sine-modulated wave into a fiber with proper dispersion can lead to soliton train formation. This phenomenon is strictly related to the modulation instability. In optical fibers, Modulation Instability is a phenomenon observed when a CW light is let propagate over long distances [16]: if the CW (carrying a power P_0) light is affected by a small amplitude modulation (from noise, for example), such modulation is amplified over the propagation. This phenomenon however can be only observed if the propagation occurs in anomalous dispersion regime. The amplification process is governed both by the non-linear and dispersion coefficients of the fiber. The gain experienced by the noise at various frequencies detuned of an amount Ω from the CW light carrier frequency ω_0 is given by

$$g(\Omega) = |\beta_2 \Omega| \sqrt{\Omega_c^2 - \Omega^2} \tag{2.1.20}$$

where Ω_c is a characteristic frequency determined by the fiber parameters and is given by $\Omega_c = \frac{4\gamma P_0}{\beta_2}$. In particular, the non-linear coefficient governs the frequency of the amplitude modulation at which amplification reach the maximum value at a frequency Ω_{max}, given by $\Omega_{max} = \mp \frac{\Omega_c}{\sqrt{2}} = \mp \sqrt{\frac{2\gamma P_0}{\beta_2}}$.

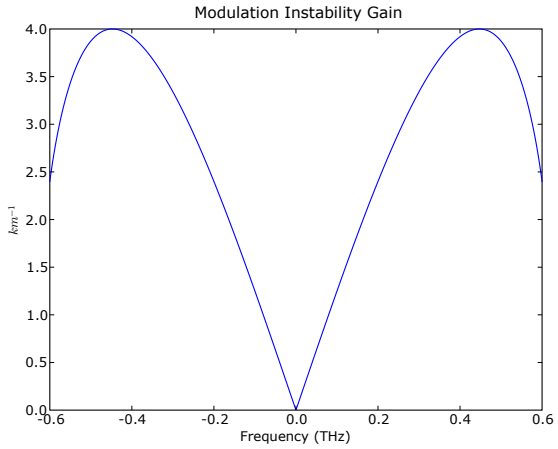

Figure 2.1: Modulation Instability Gain Curve in Optical Fibers ($\beta_2 = -20\, ps^2/km$, $\gamma = 2\,(W km)^{-1}$, $P_0 = 1\,\mathrm{W}$).

This phenomenon is strictly related to the Four Wave Mixing (FWM) process [17], that will be treated in next chapter chapter 3. In our case the initial instability is represented by sine-like wave, that evolves into a pulses train. Adding a distributed amplification stage in the same fiber can improve the soliton formation, leading to narrower pulses. To obtain distributed amplification, we used a counter-propagating Raman laser. The counter propagating configuration, was used mainly for two reason:

1. The counter propagating Raman amplification is characterized by a lower noise contribution in respect to the co-propagating configuration. Raman amplification is characterized by fast response times (about $80fs$) [18], so that, power fluctuations on pump wave, can be reflected in power fluctuation of the amplified signal. However in counter-propagating configuration the noise of the Raman pump is averaged over the amplifier transit time, with a net effect of a low-pass filter [19]

2. By adjusting the power levels of input sine-like wave and the counter-propagating pump it is possible to adjust the gain/loss curve profile $G(z)$ as it will be discussed more in detail later in this chapter. This allows to achieve the optimal compression factor compatible with the required soliton order. The possibility to adjust the gain/loss profile it is also an important advantage from the experimental point of view, because it provides an easy and quick way to tune not only the output pulse-width but also other pulses properties (mainly the chirp and the pedestal residual), in order to obtain the desired quality pulses.

The source can be described by a very simple block diagram (Figure 2.2).

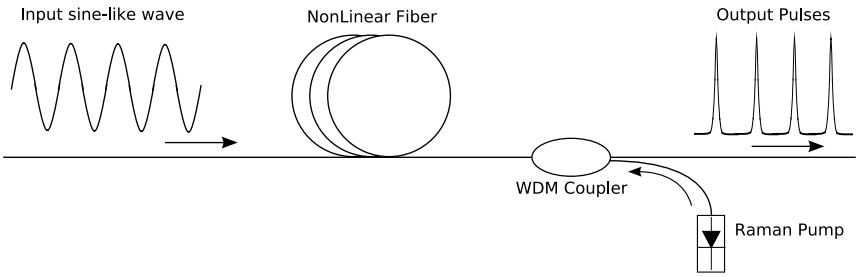

Figure 2.2: Source block diagram: a sine-modulated wave is compressed into a fiber by means of non-linear effects enhanced with distributed parametric amplification.

In this block diagram, an input sine-like wave is launched into a non -linear fiber, where it is adiabatically compressed to form a pulse train. Adiabatic compression is enhanced by inserting a counter-propagating Raman pump into the other end of the fiber, as discussed before.

All the details about the methods that can be used to experimentally realize this block diagram and the choice and characteristics of the single needed components will be discussed in subsection 2.1.3.

In the simplified model represented in Figure 2.2, three main parameters determine the pulses formation and compression:

1. The signal input power (determined by the lumped amplification stage).

2. The Raman diode laser power (or, equivalently the Raman amplification factor).

3. Fiber dispersion

The first two parameters are important because they set the gain/losses profile defined above, through the coupled equations that describe the counter-propagating Raman amplification [1]:

$$\frac{dI_s}{dz} = g_R I_s I_p - \alpha_s I_s$$

$$\frac{dI_p}{dz} = g_R \frac{\lambda_s}{\lambda_p} I_s I_p + \alpha_p I_p$$

In these equations, $\alpha_{s,p}$ represent the fiber attenuation coefficients for the signal and the Raman pump (they are slightly different, due to the different wavelengths[3]), $I_{s,p}$ are the signal and pump intensities, $\lambda_{s,p}$ are the wavelengths of signal and pump waves, and finally g_R represent the Raman gain coupling coefficient, indicating the energy exchange between the pump and the signal (Stokes wave). For the sake of the simplicity we can choose the maximum Raman gain condition ($\lambda_s - \lambda_p \simeq 100\,\text{nm}$ in silica) so that the Raman gain tilt can be neglected. Typical values are chosen for loss coefficient (respectively 0.2 and 0.35 dB/km for signal and pump).

Those equations were solved numerically by setting the signal and pump intensities at the opposite fiber ends as initial conditions. In Figure 2.3 it is shown a typical signal power profile along the fiber. In this case, it is reported the result of a simulation over a 20 km long fiber. It can be seen how in the first half of the fiber, the signal experiences attenuation, while the Raman amplification becomes dominant in the second half, where the pump is more intense. It is also interesting to see that in the reported condition, the pump shows a little depletion. The ratio between the signal power level at the output of the fiber in presence of and without the Raman amplification is defined as Raman on-off gain G_{on-off}.

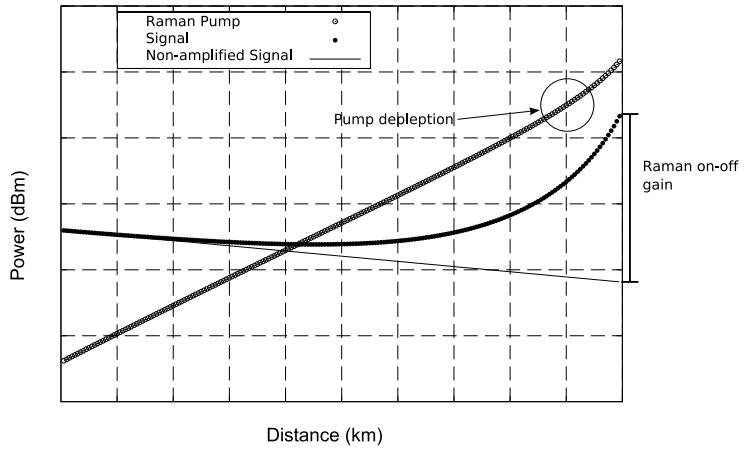

Figure 2.3: Raman gain profile in counter propagating configuration. It can be seen that for high Raman pumping power levels, the pump is affected by slight depletion near the insertion point. For comparison, it is also plotted the loss curve for the signal, indicating the power profile along z when amplification is not supplied. The Raman on-off gain is defined as the power difference between the cases in which the amplification is supplied or not.

[3] We remember that the Raman laser is down-shifted by100 nm respect to the signal

The third parameter taken in consideration here is represented by the chromatic dispersion of the fiber, that determines the pulse evolution in the initial section of the fiber (where propagation is not significantly affected by the amplification, see Figure 2.3), as well as the pulse compression in the second fiber half, where the amplification is dominant. To better understand the role of each parameter simulations are run for an input 40 GHz sine-wave (matching the desired pulse train repetition rate) and considering a fixed signal power at the DSF input (30 mW) for a wide variety of combinations of the two most critical parameters, i.e. the dispersion and the Raman gain. For simplicity, in the following we use D (fiber chromatic dispersion coefficient given in ps/nm/km) and G_{on-off} to account for the two effects. The obtained results significantly depend on these two parameters, as indeed only a proper combination gives the desired soliton-like condition (chirp free and 1 ps pulse-width).

As far as the chromatic dispersion is concerned, the optimum value resulted to be $D \simeq 2$ ps/nm/km, significantly lower compared to values used in [20], [21] and higher than for fibers with no Raman gain [15] (in the last case, 40 GHz solitons require $D \geq 1$ ps/nm/km). Moreover the D value is not as critical as in [15]. Indeed simulations indicate that there is a quite wide range of acceptable D, so that in a practical source λ_s could be tuned with no critical limitations due to the dispersion slope of the DSF. It should be said, however that choosing dispersion values outside this range pulse generation is sub-optimal. For example, lowering the dispersion (for example to $D = 0.5\,ps/nm/km$, as in Figure 2.5-a) the pulses are generated with pedestal. On the contrary, choosing dispersion values that too high from the optimum value, it is possible to obtain always good pulses, but with non-optimal compression factor (output pulse-width up to 5 ps) . This is shown in Figure 2.5-b where output traces of pulses obtained with numerical simulation with fiber dispersion equal to $D = 10\,ps/nm/km$ are reported.

G_{on-off} instead should be between $11 \div 14$ dB. Lower Raman gain gives broader pulses, while excess gain typically results into higher order solitons: indeed, close to the best operating conditions, the source pulse-width can be slightly tuned by changing G_{on-off}. This can be seen from simulation results shown in Figure 2.4 in which two different results are reported, for G_{on-off} set to 8 and 20 dB respectively.

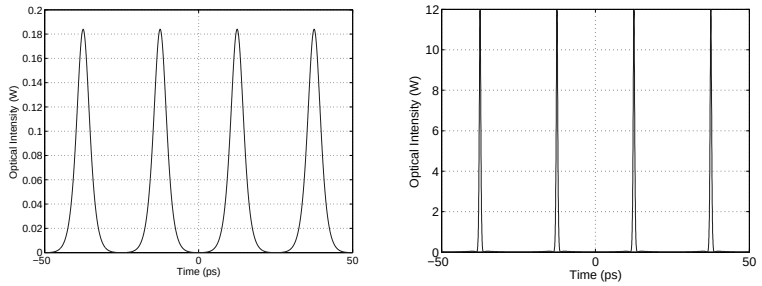

(a) $G_{on-off} = 8$dB (b) $G_{on-off} = 20$dB

Figure 2.4: Impact of G_{on-off} parameter on pulses formation. The figure reports two results of numerical simulations, ran with $D = 2\,ps/nm/km$ and launch power set to $20\,mW$. The main effect of the Raman gain is to affect pulses compression. In the case in which the amplification is maximized, it is possible to obtain very short pulses ($0.5\,ps$) but with a small pedestal.

The launch power, has also a major impact on the pedestal formation under the pulses. An example of what

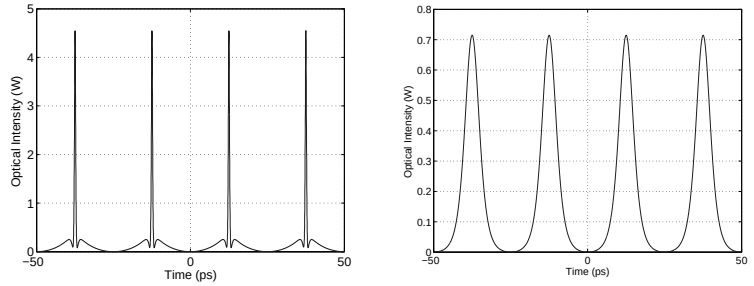

(a) $D = 0.5\,\text{ps/nm/km}$ (b) $D = 10\,\text{ps/nm/km}$

Figure 2.5: Impact of Chromatic Dispersion on pulses formation. Those figures represent the pulses formation obtained with a numerical simulation. In this case, launch power was set to $20\,mW$ while Raman Gain G_{on-off} was set to 13 dB. CD is responsible for pedestal formation at extremely low values (a), while it lowers the compression factor for higher values.

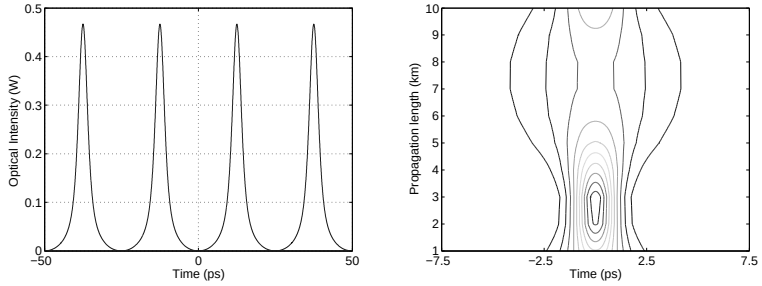

(a) (b)

Figure 2.6: Impact of launch Power. Those figure represent the result of a numerical simulation obtained for $D = 2\,ps/nm/km$, $G_{on-off} = 13\,\text{dB}$ and launch power set to $10mW$. As it can be seen in (a), pulses are formed, but they are not solitons. This it is remarked in (b) where it is reported the simulated result of the propagation of the produced pulses over $10\,km$of fiber with same D parameter: the pulse clearly do not maintain their shape along the propagation.

it is obtained with low launch power (10 mW)is reported in Figure 2.6. This set of simulation has been ran with $D = 2\,ps/nm/km$ and $G_{on-off} = 13\,dB$. Also in this case it is obtained a pulses formation, but there is not enough separation between adjacent pulses. In Figure 2.6-b it is also reported the propagation over $10\,km$ long fiber of the pulse generated with $10\,mW$: it is almost clear that we not have a soliton pulse, as the pulse-width varies along the propagation.

When the sine-modulated wave is launched with higher power into the fiber, we obtain very short pulses, but again with pedestal formation: still this is not good for time domain multiplexing. The numerical simulation results of this case, are shown in Figure 2.7.

In the same figure, it is also possible to observe that propagating that pulses, those are affected by self-frequency shift (due to the high peak power and the short duration). This latter effect is evidenced by the increase of propagation speed (that, in the case of solitons, it is determined by the pulse carrier frequency). Always in b) it is possible to notice that the pedestal varies along the propagation.

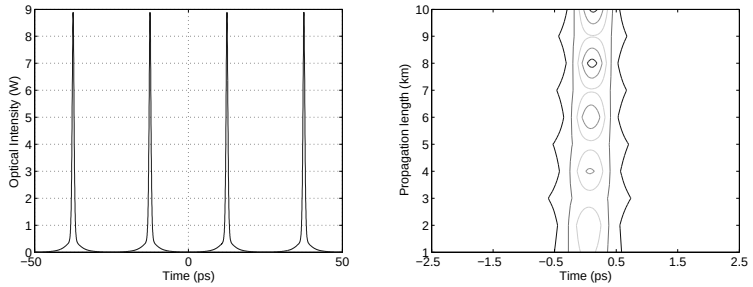

(a) (b)

Figure 2.7: Impact of launch power. Launch power is set to $70\,mW$. The other simulation parameters are the same of Figure 2.6. In b) it is possible to observe the self-frequency shift effect due to the high peak power of the obtained pulse.

Optimal values for pulses generation with pulse-width around $1\,ps$ and pedestal free, can be found tuning the 3parameters inside the range shown up to know.

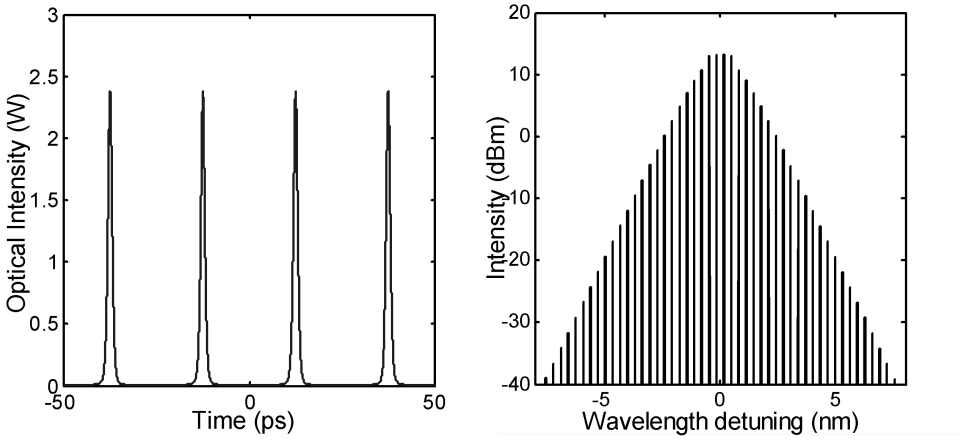

Figure 2.8: Simulation results of pulses produced with optimal parameters. Both time and optical spectrum traces are reported.

In Figure 2.8 two typical optimal results are shown. They are obtained for $D = 2\,\text{ps/nm/km}$ and $g_R = 13\,\text{dB}$. As D and g_R are optimized, the output pulses are very similar to fundamental solitons. On the left we report the output pulse train and on the right we show the optical spectrum. The output intensity profile is well matched with a $sech^2$ fitting and, for each pulse the product $\gamma P_0 T_0^2/\beta_2$ is very close to 1, i.e. the theoretical value for fundamental solitons. Furthermore, the simulated propagation of the obtained pulses along a loss-less uniform fiber (with same γ and D) shows no appreciable distortion.

These results suggest that the fiber output is very close to a regular soliton train.

2.1.3 Experimental Realization

The source was experimentally realized in a number of successive revisions that lead us to a final engineered configuration in a closed box, ready to use. All those variations differ mainly in the choice of the single components, but always around the model treated in the previous sections.

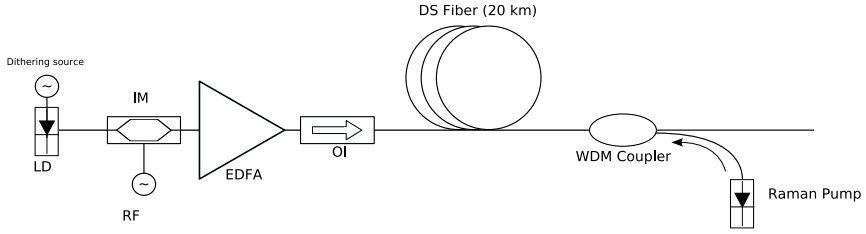

Figure 2.9: Source Experimental Setup. LD: Laser Diode; RF: Radio Frequency generator; EDFA: Erbium Doped Fiber Amplifier; DS: Dispersion Shifted Fiber; WDM: Wavelength Division Multiplexing Coupler; OI: Optical Isolator

The experimental setup is reported in Figure 2.9. It will be illustrated here discussing the various experimental aspects. Results from previous section can be summarized by saying that the optimal model parameters can be represented as follows:

Table 2.3: Summary of optimal values (as resulting from numerical simulations) for the modeling parameters that have been individuated.

Intensity Modulator ext. ratio	>20dB
EDFA output power	14dBm
Fiber Length	20 km
Group Velocity Dispersion	2 ps/nm/km
Raman Gain	13 dB

The first requirement, cannot be satisfied experimentally, because typical $40\,Gb/s$ modulators cannot offer extinction ratio values beyond $12\,dB$. The other parameters, instead, can be fully satisfied with commercially available components. The fiber dispersion of $2\,ps/nm/km$ was matched by using a DSF with $\lambda_0 = 1535\,\text{nm}$ and a CW source emitting around 1560 nm. From an experimental point of view, the dispersion value (fixed the zero-dispersion length of the fiber) can be tuned by adjusting the CW carrier wavelength. To this aim, the first experiments in which we tested the feasibility of the source and make a comparison with the numerical modeling, have been realized by using a tunable CW laser source. Moreover, as deducted from the simulations, the dispersion value it is not critical: little variations still give good solitons at the output. This property, turned out to be interesting, because the tunability of CW initial signal, results also in a tunability of the source itself, giving to it an important added value. Other tests however were carried out using commercial Distributed Feedback Lasers. DFB lasers of course offer a number of advantages in term of compactness, low power consumption (typical operating current around $100\,mA$) and *integrability*.

Another scheme that was used to realize the source, consists in the replacement of all the sine-like generation stage (including the IM), as sketched in Figure 2.10: it requires two CW sources with the proper

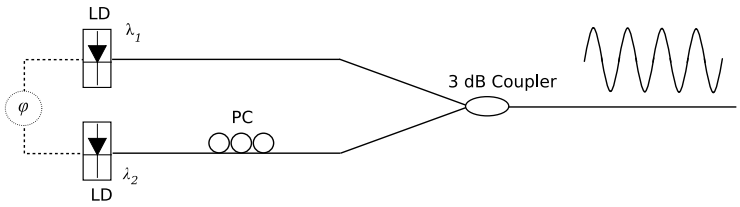

Figure 2.10: Two LDs emitting at frequency f_1 and f_2 coupled with the same polarization states, produce an intensity modulation that behaves like a sine wave at frequency $f = |f_1 - f_2|$. Moreover, if the lasers are phase-locked each other, it is possible to control the phase of the intensity modulated signal.

frequency spacing, a polarization controller and a 3 dB coupler. This scheme limits the possibilities to use the source in telecom applications (due the lack of an interfacing with an external clock); but it can help to reach very high degree of stability if the two CW sources are frequency locked.

Having tested the source in all those configurations, we can affirm that the pulses generation can be obtained with any sine-like wave in the input with a sufficient modulation depth (corresponding to amplitude extinction ratios greater than 12 dB). In an Optical Network environment, this is important because it means that the source can be realized using as input signal a waveform obtained from any proper source available in the Network, for example a signal extracted from an optical clock recovery circuit (see chapter 4).

From Table 2.3 we see that the optimal launch power level into the DSF fiber is quite high ($\simeq 30$ mW): unfortunately at those values Brillouin Scattering is stimulated. It causes the light to be retro-reflected and inhibits the soliton formation.

Stimulated Brillouin Scattering is a threshold effect: it is observed when an optical signal with adequate average power propagates into an optical fiber. Above the threshold an acoustic wave is excited into the fiber, modifying the optical fiber properties, in particular, its index of refraction.A significant fraction of the signal power is then transferred to a back-reflected wave that propagates in the opposite direction. In this process, the signal wave, exciting the acoustic mode into the fiber is referred as a *pump signal* while the back-reflected wave is known as *Stokes wave.* The threshold is determined by several parameters fixed by the fiber (length, geometry and material) but also on the signal spectrum. The threshold is expressed as:

$$P_{th} \simeq \frac{21 A_{eff}}{g_B L_{eff}} \left(1 + \frac{\Delta\nu_s}{\Delta\nu_B}\right) \tag{2.1.21}$$

where A_{eff} denotes the fiber effective area, L_{eff} the fiber effective length (considering the losses), g_B is the Brillouin gain coefficient (around $4 \times 10^{-11} m/W$), $\Delta\nu_B$ is the SBS interaction bandwidth (approx. $20 MHz$ at 1550 nm) and finally $\Delta\nu_s$ represents the signal bandwidth.

SBS is a detrimental effect for our purposes. In fact, for the fiber used in the experiments, the threshold power P_{th} is very low, less than 20 mW, thus below the needed power of 30 mW that is required to produce the desired AC. This limits the amount of light that can propagate into the fiber to generate the pulses as discussed in the previous section, and it has to be suppressed.

Looking at eq. 2.1.21, and taking in account the typical value of SBS interaction bandwidth $\Delta\nu_B$, it can be seen that SBS threshold can be increased by increasing the signal carrier spectral line-width of few tens of MHz: to this aim, both external and direct frequency modulations can be effective.

Direct frequency modulation is achieved by direct modulation of the laser pump current (because for a DFB laser the emission wavelength is directly proportional to the intensity of pump current). Such current modulation will produce a laser line-width broadening related to the modulation depth: if a proper modulation depth is chosen, it is possible to achieve optical line broadening in the region of MHz, even modulating the pump current at lower frequencies (kHz). The required direct modulation depth depends on the λ vs. current characteristic function of the laser. For commercially available DFB lasers typical modulation depth values needed to suppress SBS are below 5%.

External frequency modulation, being obtained with the help of an external frequency modulator, has to be performed at the same frequency of the desired broadening. External frequency modulation should be in theory preferable to amplitude modulation: in fact, even if this kind of modulation reduce the power on the optical carrier, it offers the advantage of keeping the signal with a constant envelope (before the RF modulation). Current modulation instead, is transformed directly in low-frequency amplitude modulation (due to the dependency of the laser power on the pump current intensity). In turn, this low frequency amplitude modulation can be transformed in timing-jitter, especially if they are transmitted over long distances. On the other end, timing-jitter would be also induced by frequency modulation itself (as soliton speed depends on carrier frequency). Moreover, a frequency modulation requires an additional modulator increasing the source complexity. We decided finally to apply a low-frequency direct current modulation to the DFB used to extract the initial CW signal; direct current modulation reflect both in a weak wavelength and power modulation of the CW. As it will be seen later, the use of direct modulation has a very low impact on the source timing-jitter.

In the preliminary tests, the pump signal bandwidth was increased both using an internal function of the employed tunable laser, that enables it to lase in a multi-mode configuration, and with an external phase modulator driven by an arbitrary waveform generator at the proper frequency (tens of MHz).

In the final implementation we realized a simple electrical tunable oscillator that has been integrated into the DFB power supply board, in order to supply the required current modulation at few kHz.

The following figures show the setup used to verify the SBS suppression obtained by modulating directly the DFB laser current. The measurements are taken by measuring the back-reflected power from the fiber, following the scheme illustrated in Figure 2.11.

Figure 2.12 shows the reduction of SBS obtained with direct laser modulation (current dithering). When dithering is applied the SBS threshold is increased from 12 dBm to a value beyond 18 dBm. We tested several modulation patterns at different frequencies, and with different modulation depths. Several combinations of modulation frequency and modulation depth ensure the SBS suppression. Among them, we have chose the one that need the to lowest modulation depth, in order to minimize the possible impairment that can derive from it. We found that in our case, the best performance are obtained dithering the diode current with a sinusoidal waveform at $300kHz$, with a modulation depth of 3%.

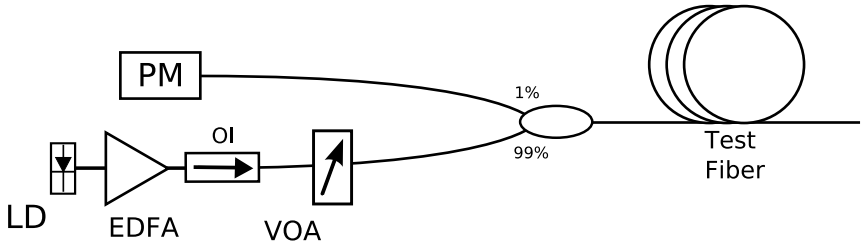

Figure 2.11: Setup used to test SBS suppression. An EDFA in conjunction with a Variable Optical Attenuator (VOA) is used to set the signal launch power level. The VOA was used because it allows a finer control over the signal power. An Optical Isolator (OI) avoids that back-reflected light hits the Laser Diode (LD). The back-reflected power is measured with a Power Meter (PM), after it is separated by a 1-99% coupler.

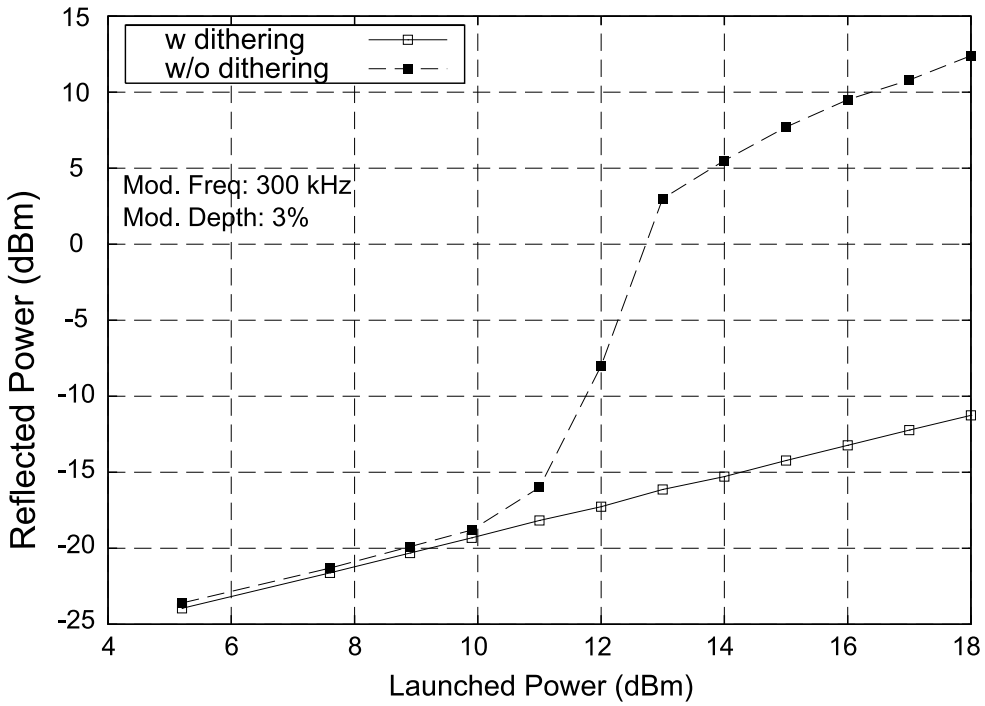

Figure 2.12: Effect of SBS suppression by direct modulation of laser pump current. Without laser dithering light is back-reflected from the fiber by SBS with a threshold power level that is around 12 dBm; after direct current modulation the threshold is increased to higher values (that cannot be reached with the available EDFA).

The 40GHz sine-like modulation was finally impressed by using a tunable Radio Frequency (RF) generator: in preliminary experiments, due to the lack of a 40GHz RF generator, we also used a commercial 40GHz $LiNbO_3$ based Intensity Modulator (IM) driven at 20 GHz and biased at null-point, in order to obtain a modulation at the double frequency. This experimental trick, proposed first in [22] has the disadvantage of a low initial extinction-ratio (around 8dB). Another important difference with the case of modulation directly at 40GHz is the spectrum shape: in the doubling case, the carrier frequency is suppressed. In later experiments we used both RF tunable generator and a small integrated 40GHz oscillator, with fine-tuning option only.

The EDFA used to set the proper launch power into the non-linear finer, is also a commercial component. No special requirements are requested here (apart from the high power output). In the *integrated* version of the source, we used a fixed gain EDFA, using at its output a Variable Optical Attenuator to control the power that it launched into the fiber

We used two configurations to achieve Raman amplification. First we used a commercial system, made by 3 single diodes emitting at distinct wavelengths around 1460 nm to achieve amplification around 1560 nm. Those pumps were coupled together and sent into the fiber by using a multi-wavelength coupler. The system provided a control over the power level of each diode: this control was used both to adjust the gain profile curve and to move the gain peak, that was found to have a width of about 10 nm. In practice, we found no significant difference in pulses compression for different gain profiles, until the amplified signal is close to the Raman gain peak. In a later setup we replaced this source with a couple of Fabry-Perot (FP) diodes emitting around 1480 nm. The two pumps were coupled together by means of a Polarizing Beam Splitter: this ensure that Raman amplification is distributed over all the polarization axes in the fiber; in fact, being the DS fiber non polarization maintaining, the signal polarization changes in random way along the fiber. Those FP diodes can be controlled both with working temperature and injection current. Although they are not stable at all in wavelength they furnish a flat gain profile around the desired region (1560 nm). Both Raman diodes, had typical relative intensity noise (RIN) around 110dB/Hz. From indications taken by [19] we estimated a -50 dB power fluctuation transferred to the amplified signal. The Raman pump (whatever the diode used) is removed by using an Optical Isolator at the input end of the fiber in order to avoid that it enter the EDFA damaging it (Figure 2.9).

Typical pulses produced by the source are reported in Figure 2.13, where it is possible to observe a typical time domain trace (obtained with an high-bandwidth optical sampling oscilloscope that was available at the time by courtesy of Agilent Technologies Italia) and a spectrum image.

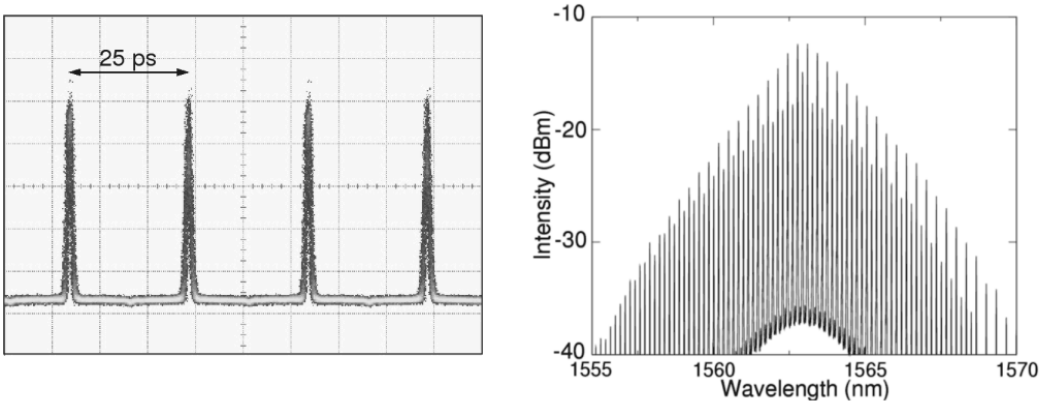

Figure 2.13: Left: Optical Sampling Oscilloscope (by courtesy of Agilent Technology Italia) image of the pulse train at 40 GHz. Right: experimental measure of the Optical Spectrum. In the spectrum it is possible to note residual 20 GHz tones from the initial impressed modulation (see in the text)

The Optical Sampling Oscilloscope used to observe the pulse quality, is based on asynchronous sampling in a Periodically Poled Magnesium doped lithium niobate (PPMgLN) crystal. The sampler is claimed to

have $1THz$ bandwidth, and allows to observe the very fast dynamics of sub-picosecond pulses without introducing distortions [23]. The optical sampled traces provide information on the pulse intensity only; it is impossible to extract information about the optical phase across the pulse.

Those figures refer to the case in which the modulation is achieved by doubling a 20 GHz RF tone as explained above. Such tones are present (even if at quite lower intensity) in the spectrum because we cannot bias the IM exactly at null point. This is due to a non ideal behavior of the available Mach-Zender. As a consequence, there is a residual trace of the original 20 GHz RF tone. As the input lightwave, the generated sequence is Carried Suppressed (i.e. made of pulses with alternating phase): this feature may have positive applications, however it is avoided in the configuration that uses a conventional 40 GHz modulation scheme. Beside this, it is possible to observe the triangular shape of the spectrum envelope. This is a direct consequence of the $sech^2$ shape that characterizes both the time and spectrum profiles (*sech* is a function that is invariant respect to the Fourier transform operation); $sech^2$ has a triangular shape in logarithmic scale.

Autocorrelation and optical spectrum traces recorded with direct 40 GHz modulation can be observed in Figure 2.14-Figure 2.15.

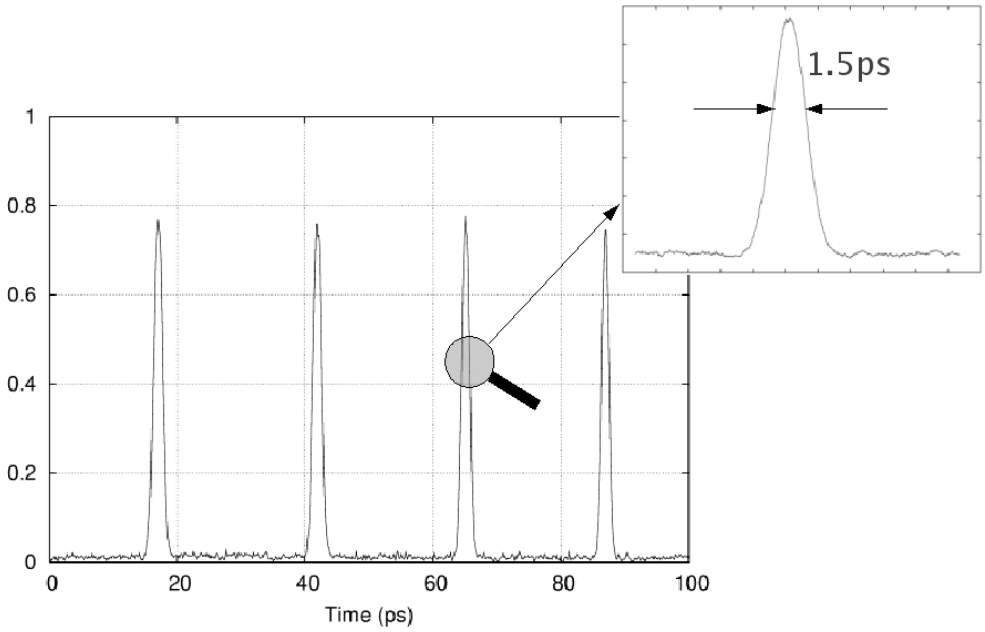

Figure 2.14: Auto-correlation trace of the produced solitons. In this case, the Raman gain is adjusted in order to achieve 1.5 *ps*pulses.

In this case, the Raman gain was set in order to achieve 1.5 ps pulses. Autocorrelation gives nor direct information about the pulse intensity, nor phase information. Those information could be retrieved by means of Frequency Resolved Optical Gating (FROG) measurement apparatus, which was not available (and, however, its realization was far beyond the scope of this thesis work). Phase and amplitude information would be required to affirm the soliton character of the produced pulses. However, a combined reading of intensity and optical spectrum traces together with numerical modeling results lead us to affirm

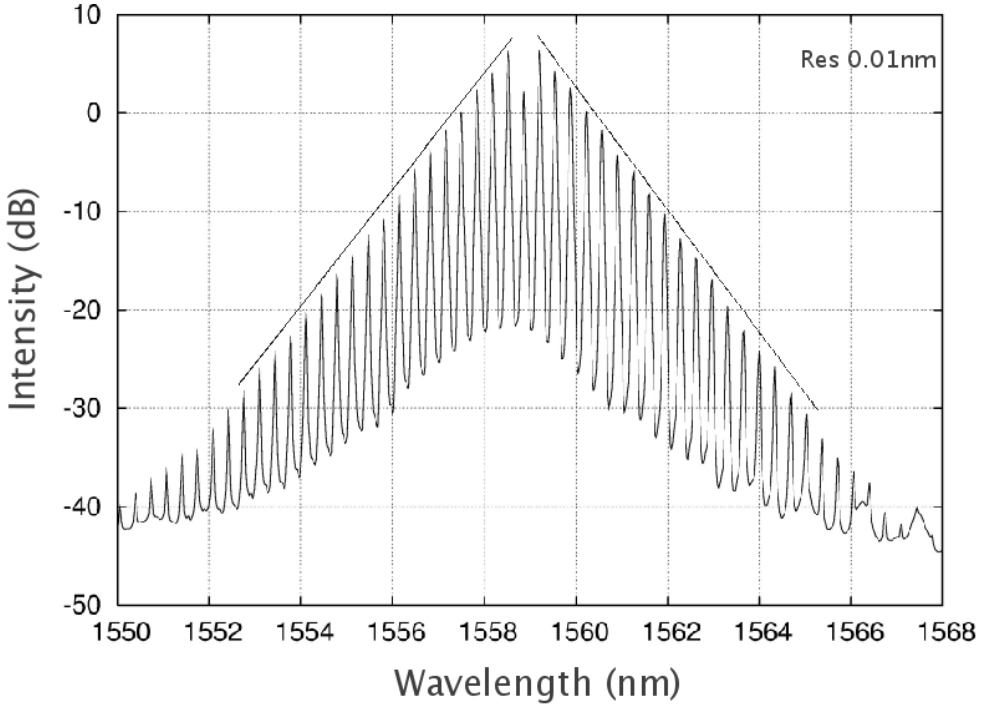

Figure 2.15: Experimental Optical Spectrum trace of a pulse train produced with direct 40 GHz modulation. The spectrum envelope triangular shape is marked in the figure.

that the produced pulses are very close to be fundamental solitons.

This can be evinced first of all by fitting the intensity profiles with the $sech^2$ profile. Looking at the spectrum, it can be easily recognized that its envelope it is characterized by a triangular shape (in logarithm scale representation) indicating an hyperbolic secant profile. The absence of chirp (phase modulation along the pulse) can be verified by evaluating the time-bandwidth product: its value is always estimated to be around 0.316, value that characterizes transform-limited hyperbolic secant pulses.

In the previous section, it was underlined that the main parameters that should be taken in consideration for this kind of source are:

- Fiber Dispersion
- Signal power level at DSF input
- Raman induced gain (parametrized as on-off Raman gain)

It is pretty simple to vary all those parameters in numerical simulations: but it is also possible from an experimental point of view. The signal power level at the input of the fiber can be easily done with the help of a variable attenuator. We noticed that this has a major influence on the pedestal that can be observed in the produced pulses. The dispersion parameter instead, can be *effectively varied* by tuning the wavelength of the CW signal launched into the fiber: this is true because the fiber dispersion profile is not constant. As result, by tuning the CW signal it is possible to experimentally measure the compression behavior for

various dispersion values (just as it has been done with numerical simulations); at the same time it allows to characterize the source tunability: it is important to know this parameter to understand the applications in which the source can be employed. It should be noted that varying the signal wavelength would require to adjust correspondingly the wavelength of the Raman pump, in order to maintain the Raman amplifying condition ($\lambda_s - \lambda_p \simeq 100\,\text{nm}$) and to avoid to change the Raman on-off gain G_{on-off} together with the chromatic dispersion. In other words, it not possible to vary experimentally dispersion and Raman gain independently as it has been done with simulations, so that in this case simulations and experimental observation cannot be compared directly.

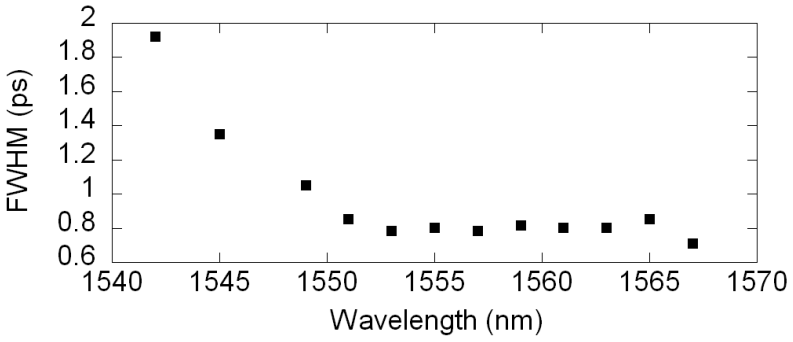

Figure 2.16: Source tunability measurement: good pulses, pedestal free and with pulse-width $< 1.5\,\text{ps}$can be obtained over a 20 nm range, by tuning the initial wavelength.

With the help of a tunable laser, we performed the measurement of pulses Full Width Half Maximum (FWHM) for a wavelength range between 1540 and 1565 *nm*. The FWHM as been evaluated from autocorrelation traces. The results are plotted in Figure 2.16. As it can be seen, the pulse-width is almost unchanged over an interval of 15 nm, then it increase versus lower wavelengths. Outside this range, the compression scheme is not working as desired: pedestal arises and the pulses become distorted; at lower wavelengths the Raman amplification is less effective (we exit from the amplification condition), while for higher wavelengths the EDFA is not capable to sustain the required power (around 30 mW) to start non-linear propagation into the fiber.

The effect of a wrong value of the launch power, is evidenced in Figure 2.17: the image represents an autocorrelation trace of a pulse train obtained with the launch power set to 17 dBm (about 50 *mW*). As expected, and in agreement with numeric simulation (see Figure 2.7) a pedestal arises.

The other parameter that can be varied experimentally is the Raman gain: this can be simply done by changing the power level of the Raman pump. The increase of Raman amplification causes further compression of the pulses. However, the output pulses are no more fundamental soliton-like, as denoted by the formation of pedestal. Strictly speaking, it is not easy to decide whether or not they are higher order solitons. In any case, compression in time domain gives raise to larger spectrum: while on one side this produces worst quality pulses, on the other side it allows to produce a signal with a wide spectrum made of periodical spaced lines (known as a *comb spectrum*). Increasing the Raman gain (beside to an increased output power) results into a great increased spectrum width. Such spectrum can find application in sev-

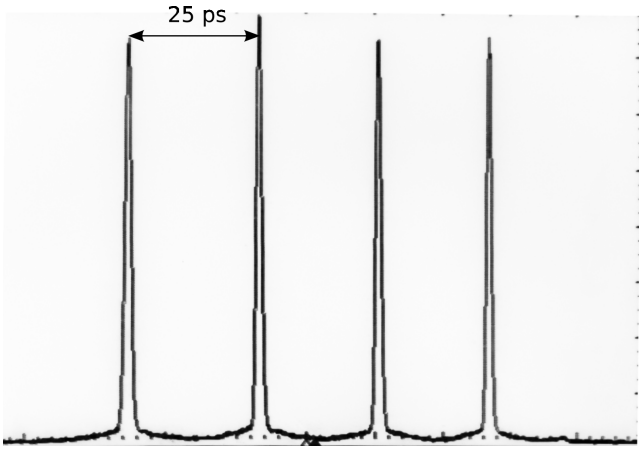

Figure 2.17: Autocorrelation trace of pulse produced with a non-optimal input power level. As predicted by numerical simulations, the pulses are affected by pedestal.

eral non-linear optics experiments, serving as optical reference in mixing experiments. In others possible application, it can also be used as Multi-Wavelength source. Retaining the same experimental setup, and strongly increasing the Raman gain, it is possible to frequency filter the enlarged spectrum obtained at the output to carve pulses in different spectral windows, thus obtaining in each one a pulse train with the carrier set around the filter position. With this parameters, the overall output power is also increased. For example, rising the Raman pump power in order to achieve an on-off gain equal to $20\,dB$, it is possible to obtain an average output power of 150 mW. This process is illustrated in Figure 2.18, where are reported the full-spectrum –inset (a) and two filtered output around 1543 and 1564 nm - inset (b) and (c). In this case, the filter bandwidth is around 2 nm. The spectra are shifted vertically for a better clarity.

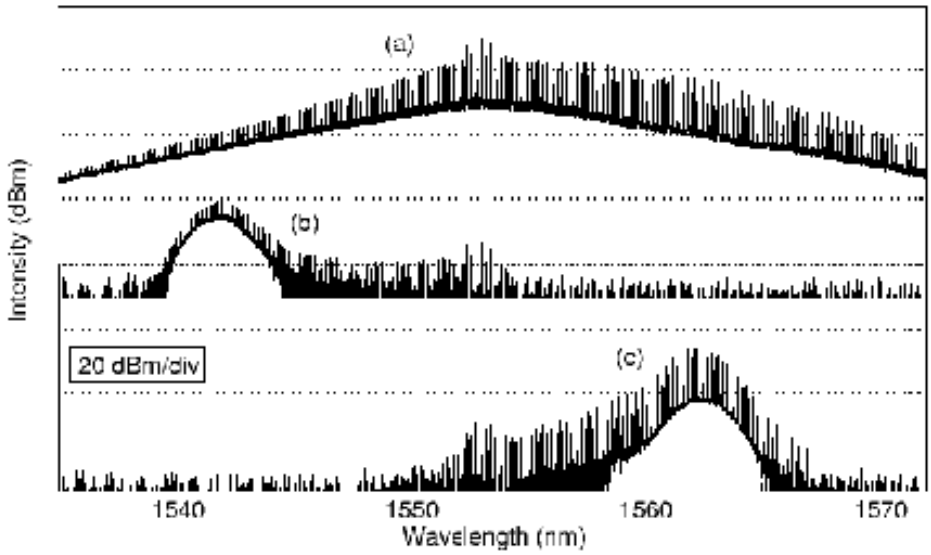

Figure 2.18: By setting the source parameters to produce an ultra-broad spectrum, it is possible to obtain pulses at different wavelength by using proper filtering. a) The full spectrum obtained by increasing Raman gain into the source. b) and c) Filtering effect at two different wavelengths.

In the time domain the pulses are not solitons, and their pulse-width is limited by the filter bandwidth. The pulse-width is not constant at various filter positions: this is due to the fact that the spectrum it is not perfectly symmetrical. Also the power varies along the spectrum: this is more obvious, as the main contribute to the total power is given by the region around the carrier wavelength. Those variations are reported in Figure 2.20. The pulse-width (estimated by the autocorrelation traces assuming a Gaussian pulse) is always less than 3 ps. The pulse quality is not optimal as in the previous case, but still good shaped, with no pedestal and with an high extinction ratio between adjacent pulses. Typical traces are reported in **??** for pulses filtered at 1540 nm and 1560 nm. These characteristics make this kind of source suitable for higher bit-rate multiplexing (for example to 80 GHz).

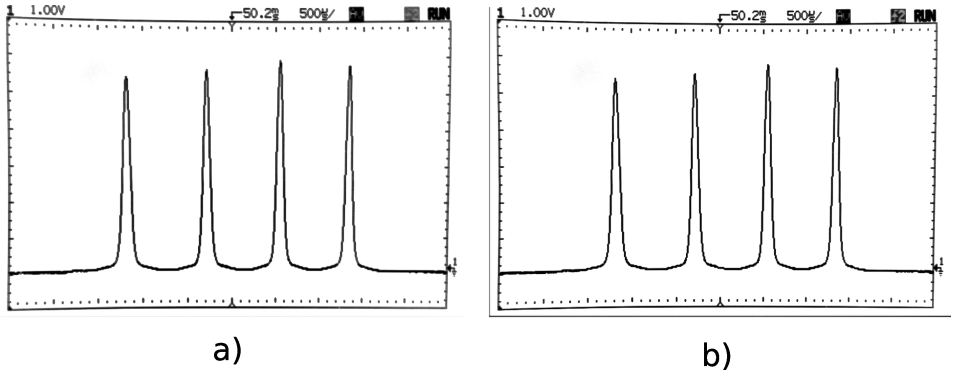

Figure 2.19: Autocorrelation trace of pulses obtained by filtering the output signal at a) 1540 *nm* and b) 1560 *nm*. As it can be seen the pulses show a minimal pedestal; pulses obtained by filtering the spectrum are not suitable to be multiplexed to higher bit-rates.

This kind of tunability is really different from the one shown before. In the first case, we tuned the input CW wavelength; in this case the tunability is obtained by we spectral filtering the source output port.

While the first method offers the possibility to have higher quality pulses and with homogeneous characteristics (pulse-width and power) all over the tunability range, with the second technique it is possible to power split the source output and then filter simultaneously each derived stream: in this case, it could be possible to use the source in a hybrid WDM/OTDM system. In this case, the pulse-width fluctuations can be compensated by a proper choice of dedicated filter on each stream while the power variations can be flattened by using dedicated lumped amplification stages (that do not alter the pulses shape, if provide chromatic dispersion compensation) or attenuators.

2.1.4 Source engineering

Putting together all the considerations illustrated above, we realized a engineered version of the source with the purpose to realize an *instrument* ready to be used. To this aim, some components have been realized ad-hoc, while others were commercially available. Most of the components used to assembly the source in the various versions presented in the previous sections are *space invasive*: power supplies, laser controllers, amplifiers, etc, usually require a whole lab bench. So, the engineering required to choose smaller components, in order to fit everything into a box. The first problem we found is that in

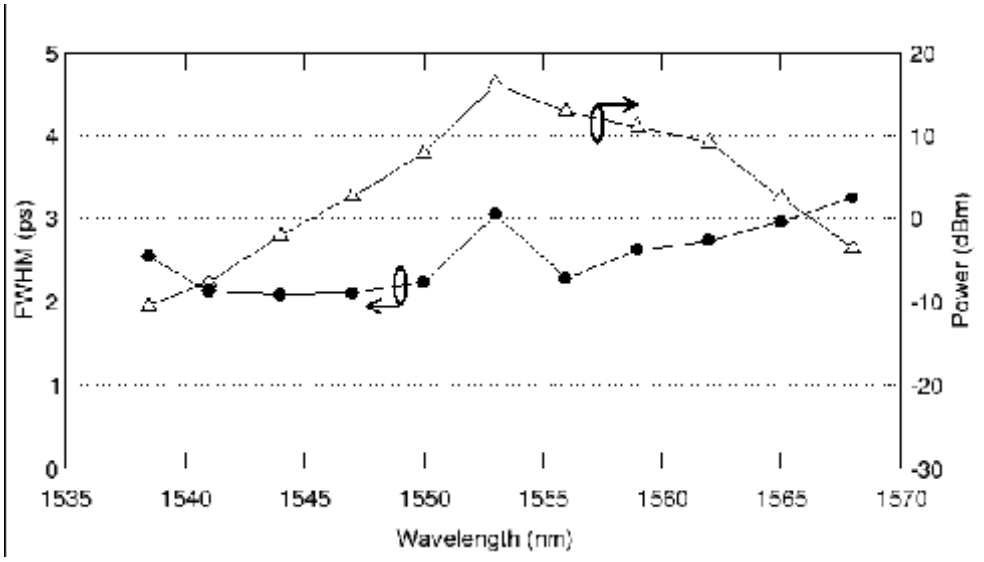

Figure 2.20: Power and pulse-width (FWHM) excursion of the pulses, moving a 2 nmfilter along the broad spectrum produced by the source.

several cases it was difficult to find integrated components with specifications comparable to the ones offered by laboratory instrumentation. For example, it is impossible to find a small laser diode in standard butterfly package tunable over the range shown in Figure 2.16. Hence in some cases, we choose a trade-off between compactness of the components and their performance, taking care that the overall result was still acceptable. To cope with this problem we designed the source in order that all the components that could limit the sources performance can be *by-passed* with external instrumentation.

In this way, the source can operate by itself, as a stand-alone piece of equipment, but there is also the possibility to *improve* its performance if needed by recurring to external devices.

Beside the lack of tunability of DFB laser (that show only a limited tunability range), the other critical component was the RF clock used to generate the 40 GHz modulation. We choose a compact and integrated voltage controlled oscillator, with a line-width of the order of few kHz. RF oscillator, however, provides a tunability range of $10 MHz$.

To solve those problems, we provided two inputs on the box front panel: one for an external laser source (a tunable laser, or a DFB emitting on another wavelength), and one for an external RF generator. This can be used when the source has to be triggered to an external data stream, or when the source has to be used in application where higher stability is required.

The box has been divided in two layers. In the lower one we inserted most of the electronic parts: the Raman pumps, one EDFA and the DFB used as initial CW wave. All these components were inserted into a $19''$rack that has been realized ad-hoc for this purpose. Each element has been mounted over a board that can be removed (each one separately): in this way all the module can be easily replaced in case of a break. The controls of each module are available on the module front panel and each module can be turned on/off separately. The DFB current control is blocked in order to emit on the desired wavelength

(1559.8 nm), while the dithering current is always applied through a simple oscillator circuits that can be frequency tuned between 250 and 400kHz. The EDFA module provides only a control on the current of its internal pumps: changing the pump currents correspond to a change also the in the Raman gain profile. In this case, we decided to set the pump current in order to get an optimal gain profile (with the maximum gain); we also control the power at the output of the EDFA with a Variable Optical Attenuator that can be operated by a knob on the front panel.

The Raman diodes are two Fabry-Peròt cavity lasers, with a nominal emission power equal to 400 mW. Those diodes, have an emission wavelength that has a strong dependency on the temperature (because the FP cavity length that fixes the emission wavelength depends on it). For this reason, it is very important to set their temperature to match the required wavelength (to match the Raman amplification condition) and then using the current control to set the emission power. Strictly speaking, those diodes, do not have a single wavelength spectrum: they emit over a range of wavelength fixed by the internal FP Free Spectral Range. Diodes temperature is controlled by Peltièr cells. At working conditions, the diodes operate at high temperature ($\sim 40°C$) and they can be damaged if over-driven. For this reason, they are controlled by an external PC via a standard RS232 interface that allows their monitoring. However, the external computer it is not needed to operating the source, because the values of current and temperature of each pump are stored into an on-board memory. The pump fiber pig-tails are polarization maintaining and were fusion spliced to a polarization beam splitter: this allows to achieve distribute amplification over all the polarization states inside the DS fiber.

The box contains 3 different power supplies. The first one is dedicated to the DFB laser, the EDFA amplifier and the Raman pumps. It is capable to furnish a total current of 5 A. While the DFB laser operates at very low current levels ($100mA$) the EDFA requires about 1 A while the Raman pumps need a current of 1.3 A each. In this way, there is more than 1 A as safety margin. The power supplies for all the remaining parts hosted in the upper level (electric modules, RF generator, Intensity Modulator,..) are in the rear section of the lower layer.

In the upper layer, we inserted the DSF spool, the Intensity Modulator, and the RF generator. The RF generator signal is split in two arms (by means of an electrical splitter): one arm is connected to the front of the panel, and can be used to extract a clock signal. The other arm drives the Intensity Modulator through the help of a narrow-band electrical amplifier. The amplifier guarantees a $V_\pi = 5V$ that is needed to operate correctly the Intensity Modulator. The modulator needs a bias voltage, supplied by one of the power supply located in the lower layer. This bias can be regulated by a knob on the front panel: this parameter cannot be fixed, because the bias point of the crystal contained into the modulator depends on temperature fluctuations. It was impossible (and, in any case beyond our control) to keep the box at a fixed temperature (also because the Raman pumps produce a lot of heating inside the box itself), so we decide to leave the control on the panel, in order that the bias voltage can be set in every moment the best value. To help air flowing into the box, we used a holed metal plane to divide the two layers.

The external box (60x40x30 cm) cover is reported in Figure 2.23

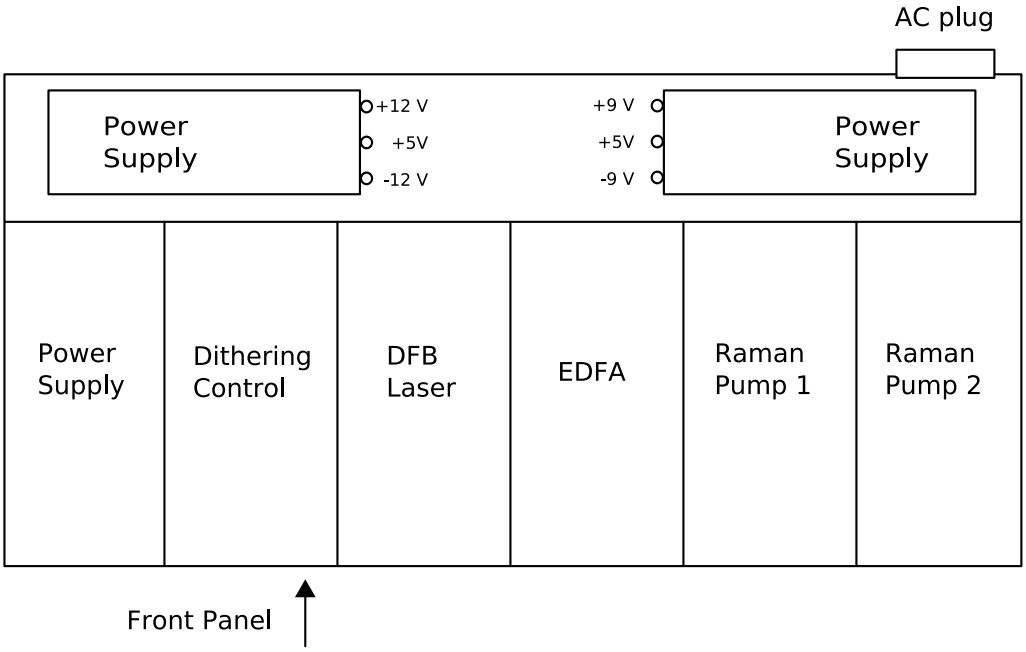

Figure 2.21: Section (Upper View) of the lower layer of the box containing the source.

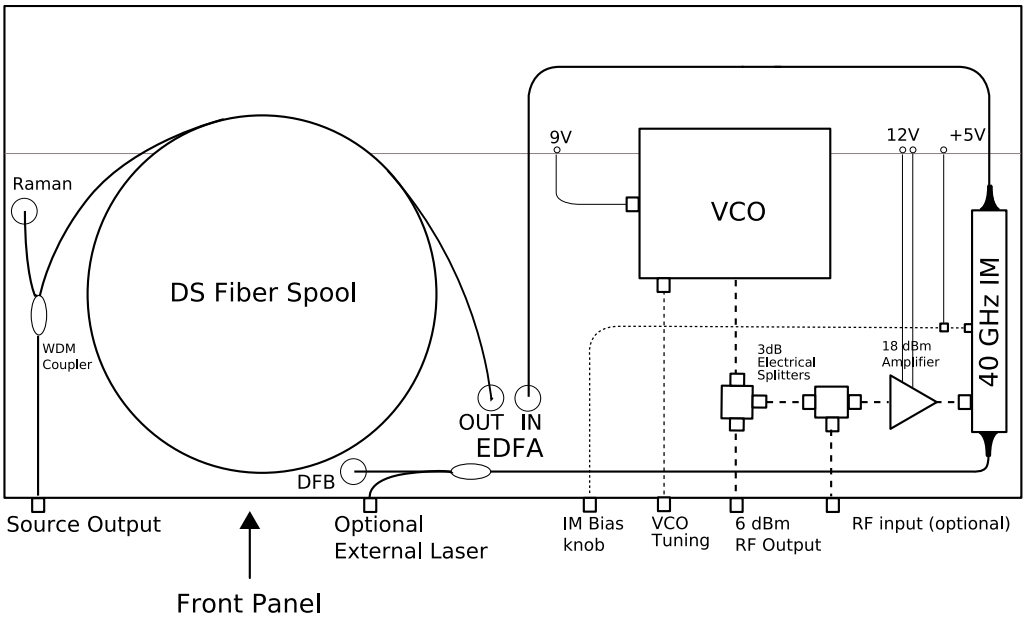

Figure 2.22: Section (Upper View)of top layer. In this figure the elements are not reproduced in-scale but the components displacement is respected. Solid lines indicate optical fibers, while dashed lines indicates electrical wires. The passages that allow fiber pig-tails from parts in the lower layer (EDFA, Raman pump and DFB laser) are also shown.

2.1.5 Time Domain Multiplexing to 160Gb/s

As mentioned previously, one of the main principle on which this source is designed around, is the possibility to implement direct optical time domain multiplexing to higher bit-rate. In particular, this has been

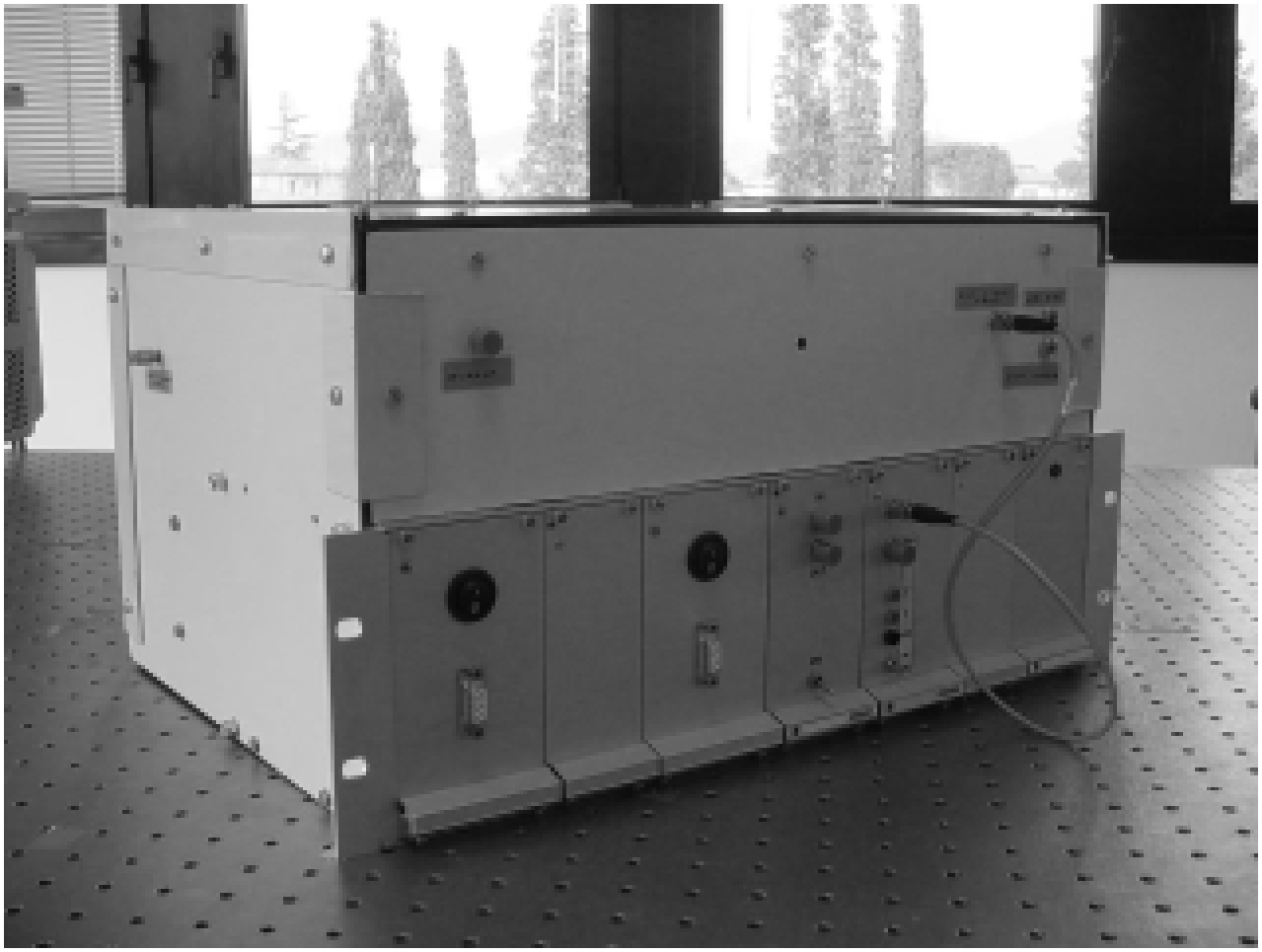

Figure 2.23: Source cover.

done upgrading the source repetition rate to 160 GHz. This has been done by means of a time interleaver OTDM multiplexer. In the Multiplexer, each stage is composed by a splitter in which the incoming flux is divided in two separate fluxes with equal power; then on one of the arm the signal is delayed (of half-bit time) and then aggregated again with the remaining one . In each stage, the delay line contains a polarization controller, to ensure that the aggregate flux is all on the same polarization state. Moreover, each stage is realized with DS fiber, in order to reduce the effects due to chromatic dispersion. The Multiplexer we used was a commercial device, and it was designed to multiply repetition rate by a factor 16, thus passing from a fundamental repetition rate of 10 GHz to an aggregated flux at 160 GHz. Summing all the splitter losses, the total losses are around 15 dB (being composed of 5 3 dB couplers that cannot be by-passed). Thus, in this case, even if the produced pulses are solitons, they loose their solitary behavior after entering the multiplexer, because of the strong losses, and the soliton relation $\frac{\gamma T_0^2 P_0}{\beta_2} = 1$ is not verified anymore. This means that into the multiplexer, dispersive effects are dominant. The multiplexer contained around 10 m of fiber. With picosecond pulses, this means that (supposing a $sech^2$shape) their are not significantly affected by chromatic dispersion broadening. Thus, it is only sufficient to amplify them in order to set the optimal value of peak power in order to acquire the solitary nature again in the fiber where they will be let

propagate.

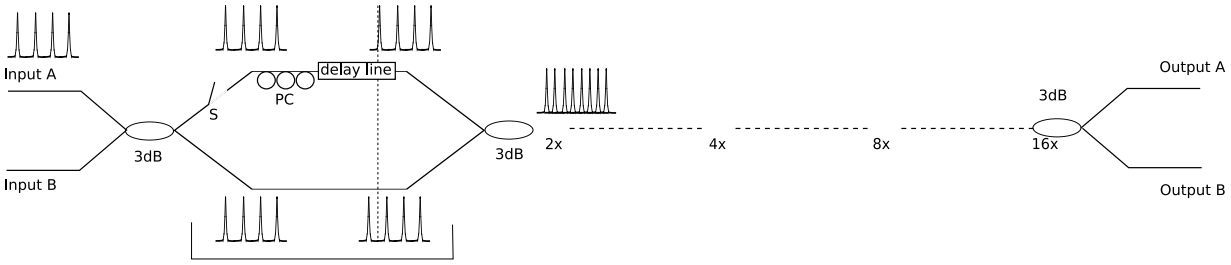

Figure 2.24: Structure of multiplexer used to obtain a 160 GHz pulses stream. The Multiplexer is composed of 4 stages in which the incoming flux is divided, relatively delayed and then aggregated again. In each stage the repetition rate is doubled, and a polarization controller (PC) allows to set the final stream on the same input polarization state. In each state the delay line can be by-passed by means of a mechanical switch (S). To pass from 40 to 160 GHz repetition rate only 2 stages are required. Total loss is 15 dB, independently on the number of stages used.

A typical trace of a 160 GHz pulse train is reported in Figure 2.25. In this case, it is possible to observe a non-optimal amplitude equalization, due to a non-perfect losses equalization in each stage of the multiplexer that was used.

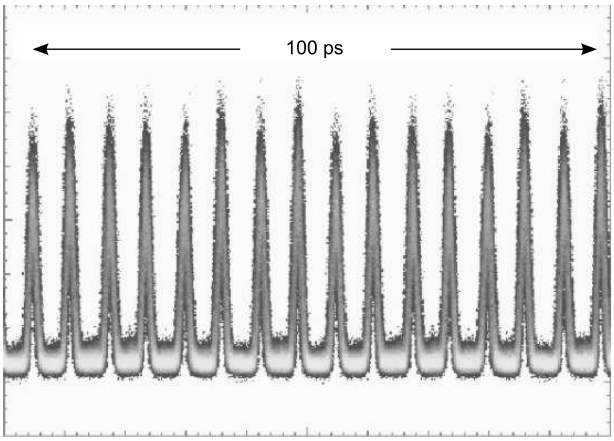

Figure 2.25: Optical Time Domain Multiplexing from 40 to 160 GHz repetition rate. The image has been recorded with an Optical Sampling Oscilloscope (courtesy of Agilent Technologies Italia)

As it can be seen from the picture, the absence of pedestal is very important to realize this multiplexing operation. As a further step, we created a modulated sequence at 160 GHz, using a modulated signal at the input of the multiplexer. The signal is modulated with a Pseudo Random Bit Sequence with $2^{31}-1$ bits. The output extinction ratio is of about 13 dB, as indicated in Figure 2.26. The quality of the aggregated frame can be observed in a *wider* view (Figure 2.26 on the left).

This modulated sequence, has been transmitted over a DS fiber spool 10 km long. Due to the lack of an additional amplifier needed to amplify the pulses in order to sustain fundamental soliton propagation, we choose a fiber with the minimum available dispersion. The fiber had the zero-dispersion wavelength $\lambda_0 = 1555$ nm. With this dispersion value (practically zero, as we tuned the source wavelength to match the fiber zero-dispersion wavelength), the signal can travel without significant broadening for all the fiber

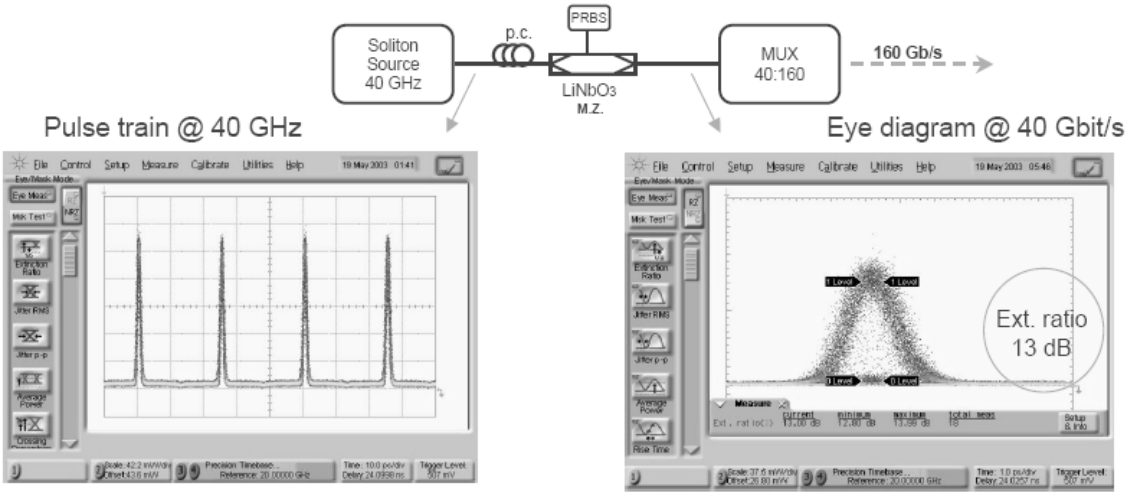

Figure 2.26: Creation of a modulated sequence at $160\,Gb/s$. As it can be seen from the eye diagram shown in the left, the output sequence has an extinction ratio of 13 dB.

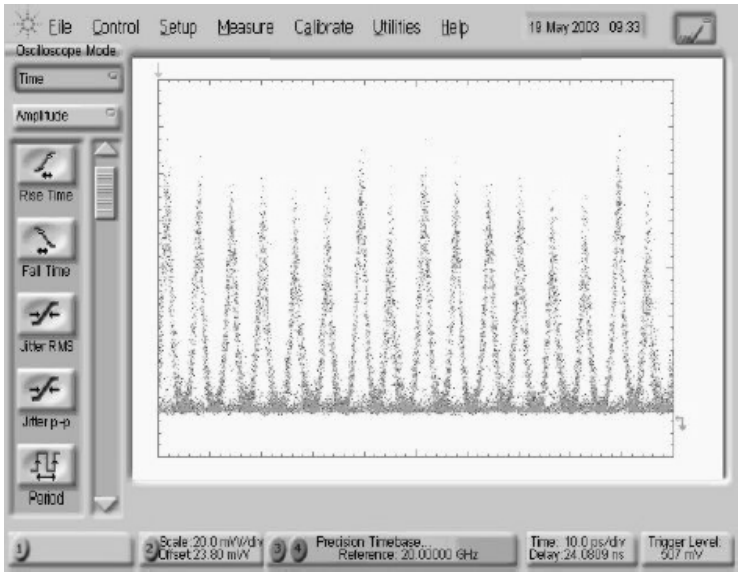

Figure 2.27: Eye diagram of a 160 Gb/s sequence. This picture has been recorded with an Optical Sampling Oscilloscope (by courtesy of Agilent Technologies Italia), after multiplexing the 40 Gb/s modulated signal shown in Figure 2.26 (right)

length. On the other hand, the chromatic dispersion is still present via the 3^{rd} order contribution which impresses a small amount of asymmetry over the pulses.

2.2 Conclusions

In conclusion, we have shown the design and the realization of a soliton source for 40 Gb/s optical systems that is tunable over a range of more than 20 nm. The source is able to produce sub-picosecond pulses that

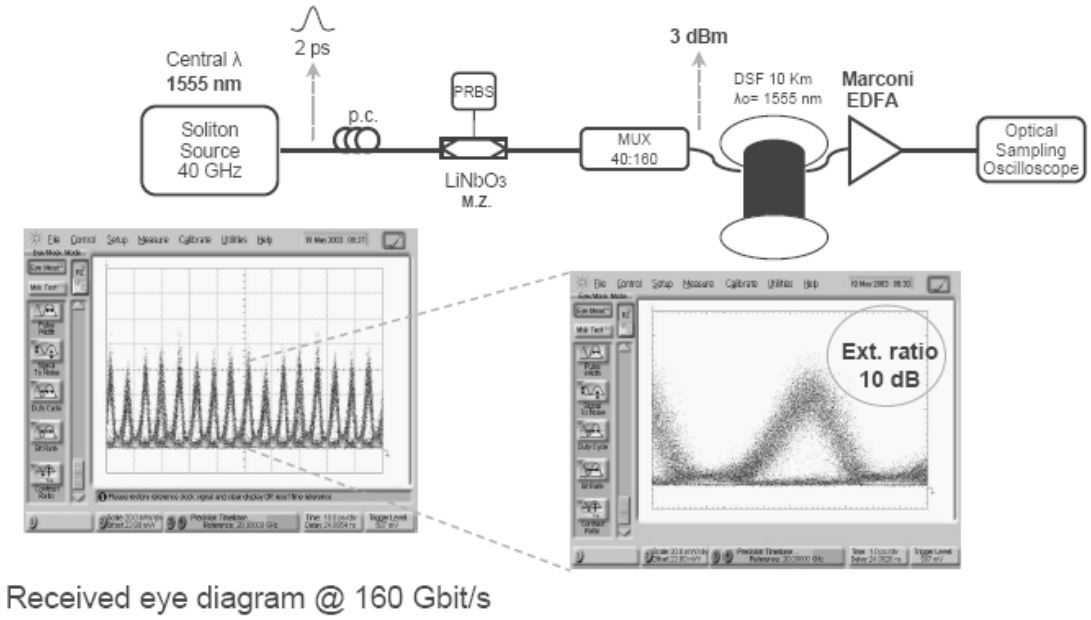

Figure 2.28: Transmission of an OTDM frame at 160 Gb/s aggregate bit-rate. The received eye diagram is still open. Due to some experimental constraints, it was not possible to re-amplify the signal after the multiplexing stage, so this is not a *proper* soliton transmission. Asymmetry acquired by the pulses (Figure 2.26 and Figure 2.27) is attributed to 3^{rd} order dispersion.

are pedestal free, in order to be ready for time-multiplexing to higher bit-rates. From a theoretical analysis it can be inferred the soliton nature of the produced pulses. By slightly tuning the *on-off* Raman gain, it is possible to adjust the pulse-width to various experimental needs, without changing significantly the pulse pedestal in a range of $0.8 \div 3$ ps. On the contrary, doubling the optimal *on-off* Raman gain it is possible to use the source in another regime, in which it can be used as a multiwavelength pulse source, useful, for example in hybrid WDM/OTDM systems. Those features, show an high degree of flexibility of the sources, making possible to use it in a variety of experiment.

As discussed in the chapter, the source is realized from an input sine-like wave. We stressed the fact that, whatever the sine-like modulation is produced, it is possible to transform it into a regular, high quality, pulse train. This feature makes the source a good candidate to operate in Optical Networks. For example, it could be possible to use a signal from an All-Optical-Clock-Recovery circuit (see chapter 4) as starting signal to produce a pulse train (for example in a all-optical RZ regenerator).

While the source engineering has been completed, there is still some theoretical investigation that can be done. By design, the repetition rate stability of the source is directly related to the repetition rate of the RF signal that impress the initial modulation (the two stability values should be coincident). Unfortunately it was not possible to experimentally measure this stability, but there is an ongoing effort to make this measurement in the near future (this point will be treated with more details in section 4.3). However it could be certainly interesting to study from a theoretical point of view, if the adiabatic compression with distributed amplification can add significant timing jitter . This information is extremely important to

understand if the source can be used (and under which limitations) as an optical reference for frequencies multiple of 40 GHz [24].

3 Wavelength Conversion and Optical Broadcasting

Broadcasting and Multicasting are two concepts derived from IP networks; they refer to particular Internet connections established from one single host to multiple destinations. Broadcast and Multicast concepts differ mainly in the number of hosts participating in the connection: while the term *Broadcast* refers to a connection between one host and *all* the network nodes, the term *Multicast* refers to connections realized between one source node and *selected* network nodes. As a consequence of this, Broadcast connections are limited only to a single network[1], while Multicast connections can be realized across several different networks, even if not directly connected. Broadcast and Multicast are used for different purposes. In IPA networks, Broadcast is generally used by single hosts to send a query to all the hosts in a subnet, to gather and exchange service information (for example when a computers joins or leaves the network). Multicast instead is widely used to realize different applications: video conferencing, video distribution, distance learning and so on.

In Ethernet networks each host receives all packets traveling in its network but selects only the packets directed to him, or, more in general, packets related to connections established by the host itself. This simplify the realization of Broadcast and Multicast connections. In case of a single (sub)network, Multicast or Broadcast are realized by simply sending the stream on reserved addresses on which each host is listening; then, each host that doesn't want to be part of the Multi/Broad-cast connection will discard the stream. In this case, there is no need to replicate the information for each host. In more complex cases, in which the stream source and the group of receivers are located on different physical networks, the stream needs to be replicated at each network crossing: digital routers take care of this operation through a variety of network protocols.

In future transparent optical networks, however, this kind of operations should be carried out in the optical domain to fully benefit the capabilities offered by the all-optical processing techniques. Several architecture are being proposed to this aim. Some of them (especially for the access networks) propose to *label* connections between the various hosts with a specific wavelength. In this case, to realize a multicast operation, the data stream from the source host, needs to be replicated for *each* wavelength corresponding to the hosts interested in receiving it. In this case, the network needs a wavelength multicast, i.e. the information carried by a signal at a wavelength λ_0 must be transferred simultaneously to different set of wavelengths $\lambda_1, \ldots, \lambda_N$ each one corresponding to a unique connection with one network host. The trans-

[1] Broadcast connections are limited to sub-networks only also for practical reason: a broadcast connection over the entire Internet (i.e. a connection between one host and ALL the Internet host) would imply a planetary congestion.

fer process is known in literature as "wavelength conversion". In this sense the terms *"multicast"* and *"broadcast"* can be considered synonymous.[2]

This chapter is dedicated to the description of two different wavelength multicast implementations. In one case the multicast is realized at a bit-rate equal to10 Gb/s by means of a Four Wave Mixing (FWM) process: from the *system design* point of view this means that the destination wavelengths must be not present *before* the conversion process. The primary benefit of this feature is found in the cost saving and architecture simplicity. Another benefit of this solution consists in the transparency to the modulation format deriving from the FWM properties.

In the second case, the multicast is performed at 40 Gb/s and the information is transferred to a set of wavelengths that are locally generated. This solution is realized through a non-linear induced polarization switching in a semiconductor optical amplifier, and it is not transparent to the modulation format, but it requires lower operation power levels, and enables operations at higher bit-rates.

3.1 Multi-pump FWM configuration for multicast operation

The first scheme to realize multi-wavelength conversion is based on a particular multi-pump Four Wave Mixing configuration. It is a variation of a scheme proposed in [25]. Here this technique is demonstrated for 10 Gb/s On-Off-Keyed modulated signals, but, due to the coherency of the process, it is expected to work with any modulation format. The scheme has been realized exploiting the FWM in two different media: a Semiconductor Optical Amplifier (SOA) and an optical fiber. Optical response of the two media is driven by fundamentally different processes (non-linear polarization response in the fiber, and gain dynamics in the SOA) but the FWM process shows some common characteristics. In the following, we first review the FWM process in SOAs and Fibers; then we detail the experimental setup used to test the proposed solution, discussing the results obtained using an SOA or a Fiber as a NL medium and the potential improvements that could be achieved with ad-hoc realized components.

3.1.1 Four-Wave Mixing in Optical Fibers and Semiconductor Optical Amplifiers

The non-linear polarization response of an optical medium is described by the relation:

$$P = \varepsilon_0(\chi^{(1)}E + \chi^{(2)} : EE + \chi^{(3)} : EEE + ...) \tag{3.1.1}$$

Here, with standard notation, ε_0 is the vacuum permittivity and $\chi^{(i)}$ is the $i-$order susceptibility. The relative weight of second and third order contributions depends on the particular medium through its symmetry properties. We already seen in chapter 2 how the third-order susceptibility it is responsible for the Kerr effect (as stated in the NLSE, 2.1.1) in fibers; it is also responsible for waves interaction, and

[2] In the following the term multicast and broadcast we will be used as synonymous of "wavelength multicast".

thus for waves mixing. This can be qualitatively explained considering an optical field composed of four waves oscillating at frequencies $\omega_j (j = 1,..,4)$ traveling in the same medium:

$$E = \frac{1}{2}\sum_{j=1}^{4} A_j(z) e^{i(k_j z - \omega_j t)} + c.c \tag{3.1.2}$$

where $k_j = \frac{n_j \omega_j}{c}$ is the propagation constant and $n_j$is the refraction index of the wave j. Both in fibers and semiconductor, the waves are collinear. While evaluating 3.1.1 with 3.1.2 as input field, several terms arises at frequencies that are linear combinations of the input ones. Limiting the nonlinear polarization response analysis to $\chi^{(3)}$ we obtain:

$$P = \frac{1}{2}\left[\Sigma_{j=1}^{4} P_j e^{i(k_j z - \omega_j t)}\right] + c.c$$

where, for example

$$P_1 = \frac{3\varepsilon_0}{4}\chi^{(3)}\left[|A_1|^2 A_1 + 2\left(|A_2|^2 + |A_3|^2 + |A_4|^2\right)A_1 + 2A_2^* A_3 A_4 e^{i\theta_+} + 2A_2 A_3 A_4 e^{i\theta_-} + ...\right] \tag{3.1.3}$$

In 3.1.3 $\theta_+$and $\theta_-$are defined as:

$$\theta_+ = (k_1 - k_2 - k_3 - k_4)z - (\omega_1 - \omega_2 - \omega_3 - \omega_4)t$$

$$\theta_+ = (k_1 + k_2 - k_3 - k_4)z - (\omega_1 + \omega_2 - \omega_3 - \omega_4)t$$

Each term in 3.1.3 represents a different non-linear effect: the first one represents the so called Self Phase Modulation (SPM) and accounts for non-linear phase shifts induced by the field at ω_1 itself; the second term represents the Cross Phase Modulation (XPM) and accounts for non-linear phase shifts induced by the other fields (ω_2, ω_3, ω_4) on the field at ω_1. The other terms represent wave coupling processes. Mixing processes are not always verified: their occur only in absence of phase mismatch between E_1 and P_1, governed by $\theta_+$and θ_-.

The term containing θ_+ accounts for a process in which three photons at frequencies ω_2, ω_3, ω_4 transfer energy to a photon at frequency $\omega_1 = \omega_2 + \omega_3 + \omega_4$ (three photons absorption). The other term containing θ_- instead represents the interaction in which two photons at frequencies ω_1 and ω_2 are annihilated with simultaneous creation of two photons at frequencies ω_3 and ω_4 such that:

$$\omega + \omega_2 = \omega_3 + \omega_4 \tag{3.1.4}$$

The phase matching condition for this process to occur is:

$$\Delta k = k_3 + k_4 - k_1 - k_2 = 0$$

This energy transfer can lead to amplification of waves at ω_3 and ω_4, if they are initially present, or lead to their generation if only the first two waves (at ω_1 and ω_2) are launched into the fiber. One of the most important case for wavelength conversion experiment is the degenerate case ($\omega_1 = \omega_2 = \omega$): if only one wave at ω (referred as pump-wave) is launched into the fiber, ω_3 and ω_4 can be generated from noise with a frequency shift $\Omega_s = \omega_1 - \omega_3 = \omega_4 - \omega_1$.

In an optical fiber, the coupled evolution of the four waves along the fiber is obtained by inserting eq. 3.1.2 into the propagation equations of the optical fiber already discussed in chapter 2, obtaining:

$$\begin{aligned}
\frac{dA_1}{dz} &= i\frac{\delta n \omega_1}{c}\left[\left(|A_1|^2 + 2\textstyle\sum_{k\neq 1}|A_k|^2\right)A_1 + 2A_2^* A_3 A_4 e^{i\Delta k z}\right] \\
\frac{dA_2}{dz} &= i\frac{\delta n \omega_2}{c}\left[\left(|A_2|^2 + 2\textstyle\sum_{k\neq 2}|A_k|^2\right)A_2 + 2A_1^* A_3 A_4 e^{i\Delta k z}\right] \\
\frac{dA_3}{dz} &= i\frac{\delta n \omega_3}{c}\left[\left(|A_3|^2 + 2\textstyle\sum_{k\neq 3}|A_k|^2\right)A_3 + 2A_1 A_2 A_4^* e^{-i\Delta k z}\right] \\
\frac{dA_4}{dz} &= i\frac{\delta n \omega_4}{c}\left[\left(|A_4|^2 + 2\textstyle\sum_{k\neq 4}|A_k|^2\right)A_4 + 2A_1 A_2 A_3^* e^{-i\Delta k z}\right]
\end{aligned} \tag{3.1.5}$$

where $\Delta k = (n_3\omega_3 + n_4\omega_4 - n_1\omega_1 - n_2\omega_2)/c$ is the wave vector mismatch, and δn is the non-linear parameter that couples the fields evolution[3]. Each equation contains the interaction terms corresponding to self-phase modulation, cross-phase modulation and wave mixing as discussed above.

It is possible to find general solutions for 3.1.5 on several textbooks [26], [1]. Here, it will be analyzed the case of FWM processes in degenerate case because the experiment treated in this chapter is based on this configuration.

In degenerate configuration only three waves are involved in the interaction; we rewrite the set of equation 3.1.5 with boundary conditions such that there are only two input waves, a pump wave at $\omega = \omega_1$ and a signal wave at ω_2(i.e. $A_3(0) = 0$). With the further assumption that the approximation of non-depleted pump is valid, it is possible to show that the evolution of the waves powers (or, equivalently of their intensities) is given by [27]:

$$\begin{aligned}
P_2(L) &= P_2(0)\left[1 + \left(1 + \tfrac{\kappa^2}{4g^2}\right) sinh^2(gL)\right] \\
P_3(L) &= P_2(0)\left(1 + \tfrac{\kappa^2}{4g^2}\right) sinh^2(gL)
\end{aligned} \tag{3.1.6}$$

In 3.1.6, L indicates the propagation length, $\kappa = \Delta k + \gamma(2P)$ the net phase-mismatch (accounting for chromatic dispersion and phase modulation induced by the non-linearity), $g = \sqrt{4\gamma^2 P^2 - \frac{\kappa^2}{4}}$ is the parametric

[3] Here δn indicates the optical Kerr effect coefficient that in chapter 2 was indicated as n_2. The notation change is used to avoid confusion with the wave indexes.

gain coefficient and P is the input pump signal power.

According to 3.1.6 the signal wave at ω_2 is amplified and a new wave at ω_3 (not present at the input) is generated by the FWM process. The generated wave is commonly referred as *idler.*

From 3.1.6 it is possible to extract 2 remarkable points:

1. *Instantaneous gain*
   A common feature of non-linearities in optical fibers, is that the response is very fast: typical life-times of excited virtual states are in the order of few fs [18]. This means that the idler wave follows instantaneously all the variations in the input signal. In other words, a modulation imprinted on the input signal, is transferred to the idler wave, except from an additive constant. Introducing the time dependency in 3.1.6, the evolution of signal and idler waves can be rewritten as:

$$\begin{aligned} P_2(L,t) &= P_2(0,t)\left[1+\left(1+\tfrac{\kappa^2}{4g^2}\right)sinh^2(gL)\right] \\ P_2(L,t) &= P_2(0,t)\left(1+\tfrac{\kappa^2}{4g^2}\right)sinh^2(gL) \end{aligned} \tag{3.1.7}$$

   This is the *core* idea of wavelength conversion using FWM: the idler wave follows the signal temporal variations, thus carrying all the information encoded in the signal. For the conversion process it is possible to define a conversion efficiency parameter as

$$\eta_c = \frac{P_3(L)}{P_2(0)} = \frac{4(\gamma P^2)^2}{g^2} sinh^2(gL) \tag{3.1.8}$$

   With the same principle, and same configuration (input made by a pump wave, plus an input modulated signal), FWM can be used to realize simple AND-type logic ports that can be used in several devices: the idler signal appears only when both the signal and pump waves have an *high* (in binary logic) *value* at fiber input.

2. *Bandwidth*
   FWM efficiency strongly depends on pump power, the fiber length, and the phase matching condition; fixed the input pump power level, and the fiber length, it is possible to determine the FWM efficiency bandwidth enclosed in item 3.1.8. This has been done by Stolen et al [27]: they defined the FWM efficiency bandwidth $\Delta\Omega_{FWM}$ the region in which the efficiency decreases by a factor of $\pi^2/4$: this results in a bandwidth slightly larger than the full-width half-maximum but greatly simplifies the bandwidth derivation.
   In the limit in which the phase mismatch is dominated by the material dispersion$\kappa \gg \gamma P$, it can be found that the parametric gain expressed as $P_3(L)/P_3(0)$ is given by [27]

$$G_p \simeq 1 + \gamma PL \frac{sin^2(\kappa L/2)}{(\kappa L/2)^2} \tag{3.1.9}$$

with a corresponding bandwidth equal to

$$\Delta\Omega_{FWM} = \frac{\pi}{\beta_2 \Omega_s L} \tag{3.1.10}$$

where β_2 is the chromatic dispersion coefficient, Ω_s is the signal-pump frequency detuning and L is the fiber length.
At higher pump power levels, the approximated expression item 3.1.9 is not valid anymore, and the bandwidth is given by:

$$\Delta\Omega_{FWM} = \frac{1}{|\beta_2|\,\Omega_s}\left[\left(\frac{\pi}{L}\right)^2 + (\gamma P L)^2\right]^{1/2} \tag{3.1.11}$$

that approximates item 3.1.10 in the limit $\kappa \gg \gamma P$.
The interaction bandwidth increase with the propagation distance, but decrease with pump-signal frequency detuning, while it can be enhanced operating near the zero-dispersion wavelength: in particular, in the spectral region in which β_2 approaches zero the bandwidth is determined by higher order dispersion parameters. This is why fibers with flat dispersion profiles have been developed [28], [29]: in such fibers, the *walk-off* tends to the infinite and the interaction efficiency is limited mainly by the fiber attenuation. The fiber lengths needed to observe FWM depend of course on a number of parameters, but it can be said that in typical experimental conditions fiber Lents of several kilometers are needed. Those lengths can be shortened using optimized fibers having huge non-linear coefficients [30], [31]. It was shown that many devices realized in the past with kilometers-long fiber spools have been realized with few meters long dedicated fibers (an example was given in [32]).

FWM can be observed also in SOAs, and can be described (from a phenomenological point of view) in the same way it has been done for an optical fiber: two photons are annihilated to generate two other photons at different frequencies satisfying 3.1.4. But FWM in SOA is driven by fundamentally different processes respect to the ones discussed for the fibers. A first important difference is that while the FWM in fibers is mediated exclusively by the non-linear refraction index modification, in an SOA the FWM is mediated both by refractive index and gain modulation. As in any optically active medium the gain provided by an SOA can be modified by an optical wave passing through it: this increases the coupling (and the interaction) between more waves that travel through the same SOA at the same time.

An SOA consists of a waveguide in which a semiconductor material (usually InGaAsP compounds) is electrically pumped in order to obtain a population inversion between material valence and conduction bands in order to provide light amplification at proper wavelengths. An SOA is much similar to a semiconductor laser: the SOA differs from the semiconductor laser because its facets are treated with anti-reflection coatings to avoid lasing condition. To further reduce undesired reflections some devices are realized with tilted facets. The electrical pumping is realized by embedding the active region in a p-n junction (thus acting as a diode). The active material is characterized by an higher refractive index than

the surrounding p-n junction; thus the active material acts like a waveguide. This kind of structure (also known as double hetero-structure) also helps in carriers confinement in the active region. In order to reduce the threshold electrical current needed to obtain population inversion (typical threshold values are around 20 mA at room temperature) the waveguide is realized so that it is possible to achieve also a lateral confinement. Lateral confinement can be achieved by gain or index guiding techniques, the latter being preferred because allow to obtain light amplification with lower threshold currents.

Light amplification inside an SOA can be represented by the formula [33]:

$$g(z) = \frac{\bar{g}}{1 + P(z)/P_s} [1 - \varepsilon P(z)] \tag{3.1.12}$$

in which z is the propagation length into the semiconductor, and $P(z)$ is the total wave power. In eq. 3.1.12, P_s is the saturation power. The saturation power depends on the bulk material and on the SOAs design; typical values are in the order of few mW. As expressed in eq. 3.1.12, the SOA gain can be modulated by the input power $P(z)$: this means that a probe signal can experience the gain modulation induced by a stronger pump signal (such phenomenon is known as Cross Gain Modulation and can be very useful for all-optical signal processing [34]).

The gain variations induced by a traveling wave are very fast, but do not follow instantaneously the traveling wave power excursions: indeed the eq. 3.1.12 is only an approximation as it does not contain the non-instantaneous response. The gain recovery is determined by several mechanism occurring into the semiconductor [35]. To explain the FWM process, 3 of those processes are particularly important. Those processes can be divided in two classes: *inter-band* (radiative and non-radiative decays) and *intra-band* processes.

- Inter-band processes are due to the carrier density modification via the usual absorption and emission processes induced by the light traveling into the SOA. While the light is amplified by stimulated emission transitions (thus reducing the carrier density in the conduction band), the population inversion is not kept constant: there is a recovery time in which the carriers are re-pumped again in conduction band to re-establish the population inversion (and consequently the gain condition). Beside radiative processes, there are also non-radiative decays process (Auger effect) that concur to those inter-band relaxation times.
  Inter-band process due to radiative decays are characterized by relaxation times on a range of $0.1 - 1\,\text{ns}$, while non-radiative decays occur on a time scale of $100\,\text{ps}$.

- Intra-band processes are related to carrier density redistribution inside the SOA energy bands after the interaction between the traveling wave and the SOA itself. Occurring in the same band, those processes are much faster and have recovery times on scales of hundreds of femtoseconds. The first process is the so called Spectral Hole Burning (SHB). This phenomenon accounts for an hole that is formed into the energy density spectrum after a stimulated process. Stimulated processes occur only for transition that correspond to traveling wave pulsation: this means that electrons in valence

band will be removed only in correspondence of well determined energy levels, creating a hole in the carrier distribution. Those holes are *filled* by carriers diffusion processes.
Another important intra-band process is related to the so called Carrier Heating effect: it can be found that the carriers temperature increases after stimulated transitions or two-photon absorption processes. The relaxation time associated with this process is typically in the order of few ps.

The non-linear contribution to the wave mixing can be treated in a similar way as it has been done for the optical fiber case by writing amplitude couple equations for the various fields that are involved in the wave mixing process. In the degenerate case (in which two fields have the same frequency), it is possible to write such equations in the form [36], [37], [38]:

$$\begin{aligned} \frac{dE_{p,q}(z)}{dz} &= \frac{1}{2}\left(g(z)-\alpha_l\right)E_{p.q}(z) \\ \frac{dE_s(z)}{dz} &= \frac{1}{2}\left(g(z)-\alpha_l\right)E_s(z) - \kappa(z)E_p^2E_q^*(z)e^{i\Delta kz} \end{aligned} \tag{3.1.13}$$

In eq. 3.1.13, $E_{p,q}$ represent respectively the electric fields associated to the pump and probe waves, while E_s is the signal wave (the converted signal); α_m represents internal losses of the SOA. As in the fiber coupled equations, $\Delta k = 2k_p - k_q - ks$ represents a phase mismatch factor and $\kappa(z)$ is the coupling factor. If the interaction between the pump and probe signal are neglected, $\kappa(z)$ can be expressed phenomenologically as:

$$\kappa(z) = \frac{1}{2}\frac{\bar{g}}{1+\frac{P(z)}{P_s}}\sum_{m=1}^{3}\frac{1-i\alpha_m}{1-i2\pi f\tau_m}\frac{1}{P_m} \tag{3.1.14}$$

Here, the summation over m takes in account the three processes that are determinant for FWM: $m = 1,2,3$ for carrier density modulation, carrier heating and SHB respectively; τ_m indicates the relaxation time, P_m the saturation power associated with the single mechanism, while α_m indicates the ratio between the real and imaginary parts of the refractive index change induced by the m-th mechanisms; f indicates the frequency detuning between the pump and the probe waves.

Using the boundary condition $E_s(z=0)=0$, it is possible to find the following expression for the signal at the output of the SOA:

$$E_s(l) = -\frac{E_p^2(l)E_q^*\kappa(l)e^{i\Delta kl}}{0.23G + i\Delta kl} \tag{3.1.15}$$

where $G \propto \int_0^l \left(g(z)-\alpha_l\right)dz$.

As for the fibers, it can be seen that in the degenerate case it is possible to generate a wavelength converted copy of the probe wave E_q conserving its amplitude and phase modulation characteristics. Also in SOA case the wavelength conversion process is coherent. It should be noted however that this expression does not take in account the gain recovery dynamics. A full description of such behavior can be found in [39], [33].

3.1.2 Multicast Conversion by means of a multi-pump configuration in SOAs and Optical Fibers

We have seen how in the *common* configuration (one strong pump at frequency Ω and one probe at $\Omega + \omega_0$), FWM interaction produces a signal at $\Omega - \omega_0$. In some cases, it is possible that the waves involved in this process interact, generating cascaded products; for example, the interaction between the pump and the signal can produce an idler wave, at $\Omega_i = \Omega + 2\omega_0$: in turn, the wave at Ω_i could interact with all the other waves at Ω, $\Omega + \omega_0$, ..., generating always new product. Of course, this process is strongly limited by the phase matching conditions and from the decreasing intensity of those higher-order products. Generally those *extra* produced waves, are characterized by very low intensity (and correspondingly by very low OSNRs). This means that of all the FWM products, only the firsts can be generally used as converted signals. Therefore, FWM based devices are not usually suitable to realize wavelength conversion to more than one wavelength simultaneously, i.e. multicast devices. However it has been shown that enhancing the FWM process with parametric amplification (for example Raman amplification, discussed in chapter 2), the generated components show high OSNR values also on higher harmonics, and there were suggestions to indicate that in this way FWM could be used to realize a multicast device [40] in which the information is transferred from the input signal to each higher order FWM product. However, this technique shows a fundamental limitation: the OSNR of the generated waves is not homogeneous (it decreases with the product order); this introduces system limitations.

To overcome those limitation, we realized a multicast device with a multi-pump configuration [41], [42], sch etched in Figure 3.1. The system is designed in order that distinct FWM processes (each for every pump) arises in a non-linear medium. Due to the phenomenological similarities between FWM in fibers and SOAs, the proposed scheme has been tested in both materials, comparing the differences in the quality of the converted channels. In the multi-pump configuration, each pump (indicated as $P1$, $P2$, $P3$ in the following) provides the generation of 2 converted channels.

In the scheme, the input signal s ($Ch4$), enters into the non-linear device (a fiber or an SOA, as discussed below), with the same state of polarization of the pump $P1$, thus producing the idler indicated as Ch3, via a degenerate FWM interaction. The pump $P1$ and the signal s are detuned so that the frequency spacing between $Ch3$ and $Ch4$ is 200 GHz, a value compatible with the ITU grids for standard WDM systems. Together with the pump $P1$, other two pumps, $P2$,and $P3$, are sent into the non-linear medium; $P2$ and $P3$ have an orthogonal polarization state respect to $P1$, (see Figure 3.1) thus avoiding an interaction with it.

In the fiber, the beating between $P1$ and s produces an index modulation that is transferred to the pumps $P2$ and $P3$, producing a side-band modulation on them and thus creating the copies $Ch1$, $Ch2$, $Ch5$ and $Ch6$.

Inside the SOAs, instead, the beating between $P1$ and s, is transferred to the pumps $P2$ and $P3$ by the effect of index modulation and gain modulation: this lead to two advantages. The first is that the set of channel $Ch1$, $Ch2$, $Ch5$ and $Ch6$ shows enhanced OSNRs respect to the one obtained when the fiber acts as non-linear medium; but most important the conversion efficiency of this set of channels is almost independent from the position of the two pumps, as long as the pumps are placed in the region in which

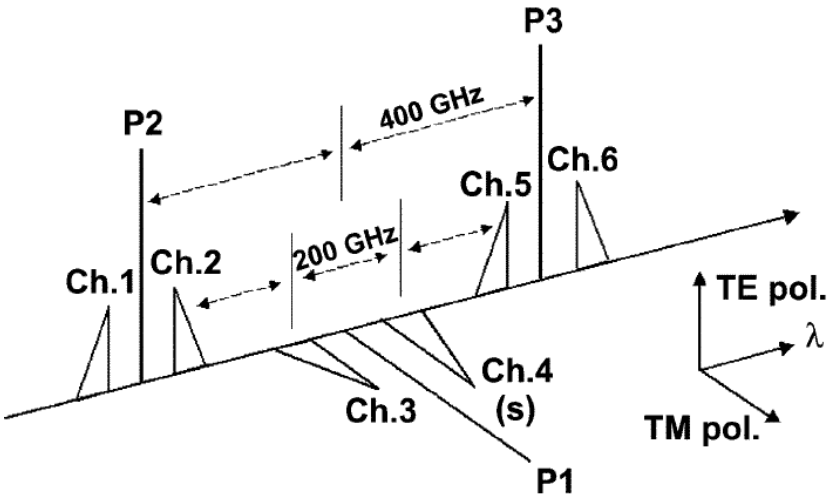

Figure 3.1: Scheme of the multi-pump configuration. The pumps P1, P2, P3 have a particular relative state of polarization, that allows to produce 5 copies of the input signal *s* (ch4) in the figure.

the SOA gain is flat [25]. This means that when the wavelengths of the pumps $P2$ or $P3$ is changed, the corresponding couple of multicasted signals are translated in frequency by the same amount. From a system point of view, this allows for flexible selection of output wavelengths.

The proposed device has been realized experimentally as described in Figure 3.2.

A DFB laser at $\lambda = 1554.3\,nm$ is modulated by a common $LiNbO_3$ Mach-Zender interferometer driven by a 10 Gb/s PRBS (Pseudo Random Bit Sequence) pattern generator to produce a set $2^{31}-1$ bits long pattern. The signal is amplified and then inserted into the multicast device. In the multicast device, the three pumps are injected into the SOA. The relative State of Polarization of the pumps ($P1$ orthogonal to $P2$ and $P3$) has been achieved with polarization controllers and a Polarization Beam Splitter: one port is used to inject the co-polarized pumps $P2$ and $P3$, while the other (that selects orthogonal polarization) is used for the modulated signal s and the pump $P1$ coupled together by means of a 3dB splitter. Fixed the wavelength of the incoming signal, the wavelength of the three pumps are selected in order that all the produced channels are 200 GHz spaced, as shown in Figure 3.1. The four waves (the 3 pumps and the modulated signal) are sent into the non-linear medium.

In the case of the SOA, we used a commercially available, pigtailed device with 25 dB small signal gain and 5 dBm saturation power. As non-linear fiber we used a $3.5km$ long Dispersion Shifted Fiber (DSF) with $\lambda_0 = 1555\,nm$ and dispersion slope of about $0.07\,ps/(nm^2\dot{km})$. The short length of the fiber permitted to relax the constraints imposed by the phase-matching conditions; this also allowed to obtain a flat conversion efficiency among the converted channels. The pump signals didn't need to be amplified, so that the overall complexity was reduced considerably, and the ASE noise contribution from the amplifiers was avoided.

The multicast channels have been extracted singularly by means of an AWG to be characterized with Bit-Error-Rates (BER) measurements.

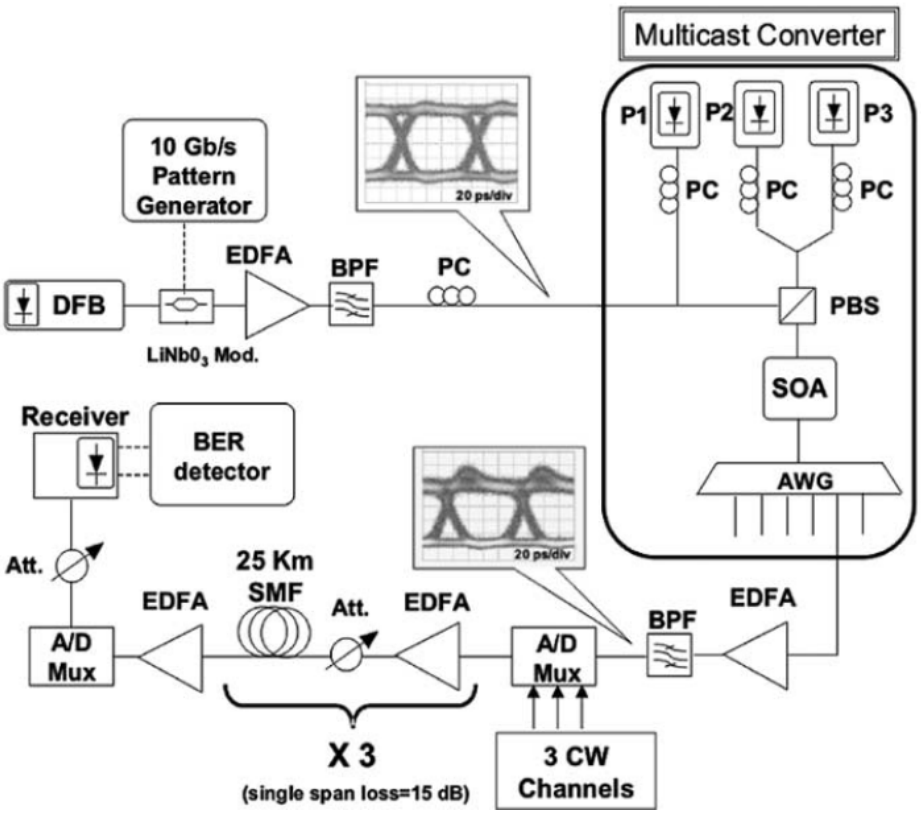

Figure 3.2: Experimental setup of the Multicast device. An input signal is realized by external modulation of a DFB laser. The multicast device is "grouped" into the figure. The input signal is co-polarized to the pump $P1$ (by means of a polarization controller) and then sent into the Non-Linear medium. The State of Polarization described in Figure 3.1 is obtained by means of a Polarization Beam Splitter (PBS). At the output of the multicast device each channel is separated by means of a $100GHz$ AWG and then sent into a 3×25 km transmission span. Through a Bit Error Rate tester each channels has been characterized in terms of power penalty, in order to measure the impact of the pattern effect induced during the conversion process (as discussed in the text). The insets show the eye-diagram of the input channel and typical eye diagram of the converted channels.

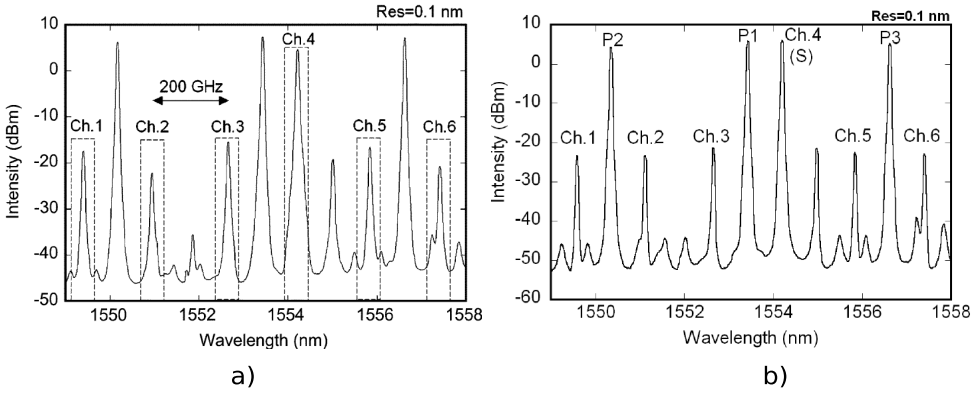

Figure 3.3: Comparison of the output spectra after the multiwavelength conversion. a) SOA; b) fiber

In Figure 3.3, the spectrum of the converted channels is shown both for SOA (a) and the fiber (b).

Detailed information about OSNR, power levels and conversion efficiency η of wavelength converted signals are reported in the table below:

		SOA				DS Fiber			
	$\lambda(nm)$	Input Power (dBm)	Output Power (dBm)	OSNR (dB)	η	Input Power (dBm)	Output Power (dBm)	OSNR (dB)	η
CH1	1549.5		-17.3	28	-24.3		-21.7	28	-31.4
P2	1550.3	9.3				8.2			
CH.2	1551.1		-22.5	23	-29.5		-21.6	27	-31.3
CH.3	1552.7		-15.4	30	-22.4		-19.9	29	-29.6
P1	1553.5	9.8				9.7			
CH.4 (S)	1554.3	7	3.7	48	-3.3	9.7	7.1	54	-2.6
CH.5	1555.9		-16.5	25	-23.5		-21.6	26	-31.3
P3	1556.7	8.9				8.1			
CH. 6	1557.5		-20.7	23	-27.7		-22.0	24	31.7

In both cases, the OSNR of the converted signal, is greater than $23\,dB$ and it is compatible with the value of $20\,dB$ required for 10 Gb/s modulated signals. Conversion efficiency is different in the two cases: in the SOA, the values are generally greater than about 7 dB in respect to the values obtained using the non-linear fiber; the fiber shows lower conversion efficiency but more homogeneous values among the channels (η is inside a range of 2 dB). The needed input power levels (for the incoming signal) are comparable for both media.

An important difference is given by the signal to pump power ratio. It could be noted that while in the SOA case the input signal power level has been kept $4\,dB$ under the pump $P1$, in the fiber case it was possible to keep the input signal and the pump with the same power level, thus increasing the conversion efficiency. This is due to a fundamental limitation of FWM in SOAs: if the input signal power is enough to induce strong gain modulations, those are imposed also on the pump. The beating between the $Ch.4$ and $P1$ is responsible for the generation of all the other channels, but it also can affect $Ch.3$ introducing Inter-Symbol-Interference (ISI) due to the gain modulation generated by the beating. The wavelength converted signal $Ch.3$ shows improved OSNR values when the signal power is increased, and this affects positively the signal quality. But over a *threshold value* of the signal to pump power ratio, while the OSNR can be still increased, pattern effects arise in the converted channel due to the gain modulation effect: as briefly discussed above, the gain modulation is not instantaneous but is affected by a recovery time (due to the carrier density modification). The gain recovery dynamics are strongly affected by the intensity pattern of the incoming signal[4]. Pattern effects introduce two main limitations: first of all, they introduce ISI, thus affecting the power penalty of the converted channels; second, they pose a limit on the possibility to use the converted channels in successive wavelength conversion operations. In an Optical Network environment, in which a single channel could be wavelength converted at each node, it is important that the penalties

[4]Pattern effect arises in particular when sudden power variations occurs

accumulated at each conversion are minimized, otherwise a channel couldn't be routed on more than few nodes. The pattern effects should be minimized to allow Cascaded Wavelength Conversions stages. The limit of the signal to pump power ratio in FWM in SOAs that allows to minimize pattern effects with limited conversion penalties, depends on a number of factor: the signal bit-rate, and the physical properties of the SOA in which the FWM takes place. The power levels of all the waves involved in the multicast device were experimentally optimized in order to find a trade-off condition minimizing the pattern effects and the power penalty on all the converted channels, while obtaining the best OSNR and conversion efficiency values. Typical values reported in literature show that optimal values of signal to pump power levels ratio should be around $-10\,\mathrm{dB}$; in our case, such ratio wouldn't be enough to generate all the channel copies. Indeed we found that a signal to pump power ratio around $-4\,\mathrm{dB}$ was necessary to obtain acceptable results for all the channels, introducing a slight signal distortion as shown in Figure 3.4.

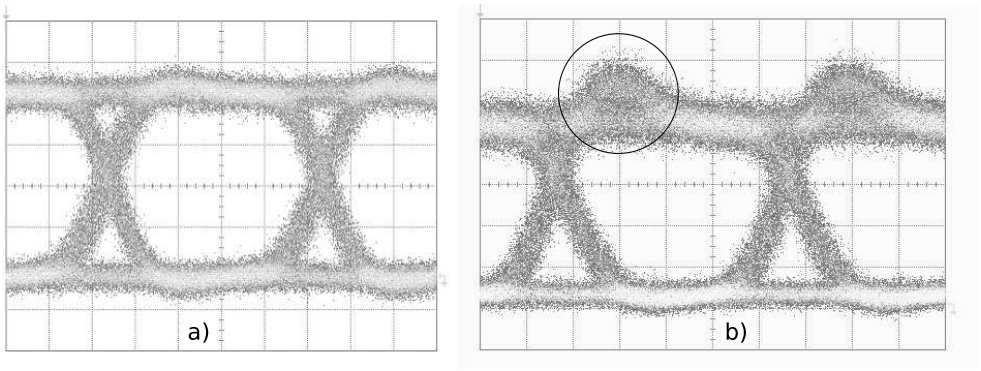

Figure 3.4: Input (a) and Converted (b) signals eye diagrams in the case of SOA. The converted eye diagram is taken just after the multicast device, before amplification. The induced pattern effect due to the high signal to pump power levels ratio (around $-3\,\mathrm{dB}$) is evidenced in a circle for better clarity. The eye diagrams are recorded with a 60 GHz photodiode. Time division scale is $20\,\mathrm{ps}/div$ on both images.

It should be noted that despite the pattern effect, the eye-diagram of the converted channels is still wide open.

To characterize the penalties introduced by this pattern effect, we performed a set of BER measurements. First we measured the power penalty of each channel just after the multicast device (in Back-to-Back configuration). The results are shown in Figure 3.5-a). This first serie of BER measurements shows the power penalty accumulated during the wavelength conversion process. We found a power penalty lower than $2.5\,\mathrm{dB}$ for all the converted channels at a BER reference value of 10^{-9}. It is worth to note that the worst BER values are associated to channels 2 and 6; these channels are characterized by the lowest OSNR values (further decreased after the output preamplifier, cfr. Figure 3.2). The other channels suffer from lower penalties that seem less directly related to OSNR, higher than 19 dB (the value required for having 10^{-9}BER with our receiver) on all the channels; the performance difference among the various channels might be due to some different XGM contribution and/or to some low in-band high-order FWM product (the channels are frequency equi-spaced, so high order FWM products due to one pump can fall in correspondence of channels generated by the conversion operated by other pumps).

As mentioned before, some of the channels (namely $Ch1, Ch3, Ch5$) are spectral inverted copies of the

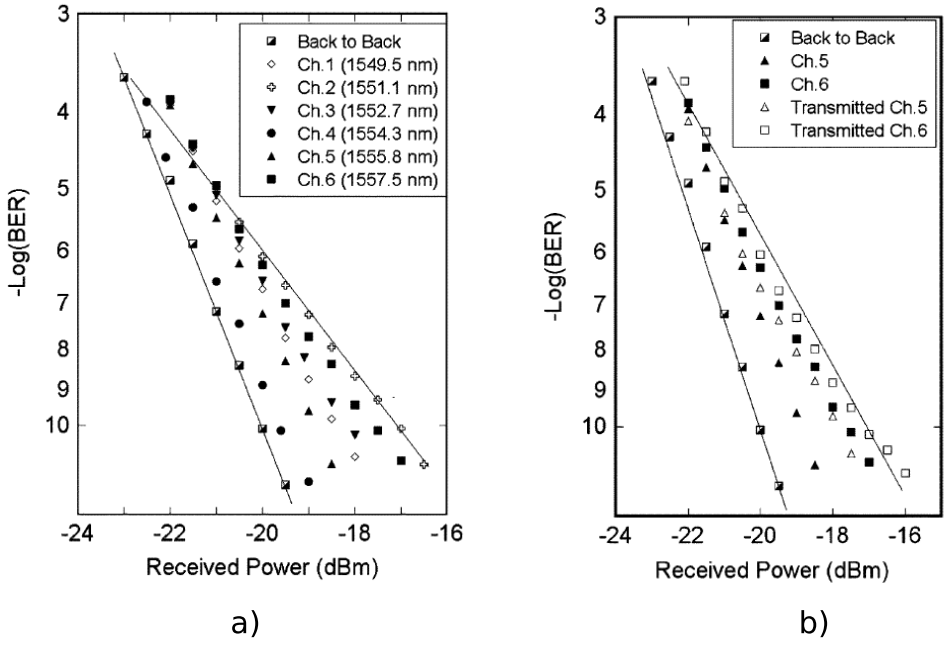

Figure 3.5: BER measurements to characterize power penalties of converted channels when SOA is used as Non-linear Medium. a) BER performed on each channel after AWG demodulation. b) BER of selected channels before and after 3x25km span transmission (cfr Figure 3.2). Back to back curve is reported on each graph for completeness.

input signal: to test how this property and the distortion effect due to XGM affect differently each channel during a transmission, some channels have been inserted in a metro-like system testbed that was available in the laboratory. This metro-like testbed is a ring network composed by 3 spans of Single Mode Fiber each one 25 km long. We sent one converted channel at time into the ring network to fully emulate a real system in which each channel is routed to its proper output port, multiplexed with other signals coming from other point of the network, and then transmitted. The test has been carried out with 2 channels, comparing the BER after the multicast device and after the transmission stage. The results are reported in Figure 3.5-b. After 75 *km* the accumulated power penalty due to the transmission is less than 1 dB at a BER of 10^{-9}.

In the case of the fiber (in which the FWM is mediated only by an index modulation that can be considered instantaneous) there are no pattern effects induced on the eye-diagram. Paying the price of a lower conversion efficiency, the channels show uniform OSNR values. Despite this, we still observe a similar amount of power penalty between the channels after the Multicast device (measured in Back-to-Back configuration at the output of the multicast device), as it is reported in Figure 3.6

In the case of a DS Fiber, we outline that an higher number of multicast channels could be generated in the same scheme by using additional pumps being mainly limited by the phase matching condition among the fields propagating in the fiber. Hence, the use of a shorter piece of properly optimized photonic crystal fiber with flat dispersion slope, together with additional pumps, could allow for an increased number of multicast signals, overcoming phase matching impairments and realizing a more compact device. When

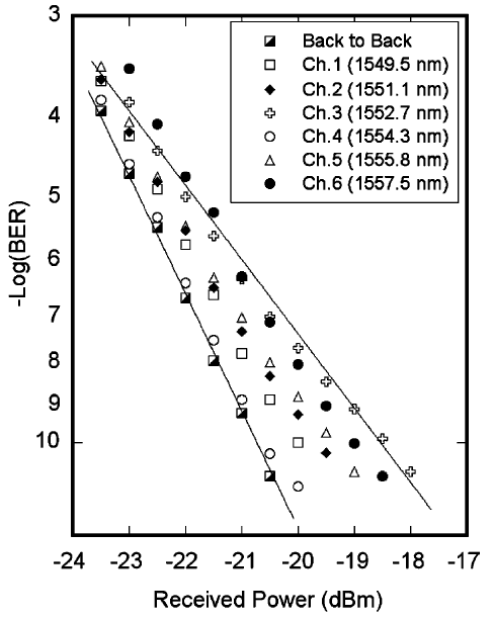

Figure 3.6: BER in Back-to-Back configuration for the converted channels when a DS Fiber has been used as a Nonlinear Medium.

using additional pumps however, a critical point could arise by the effect of the FWM interaction among adjacent co-polarized pumps on the orthogonal polarized signal *s*. Indeed, this process generates two CW signals at exactly the same wavelength as Ch. 2 and Ch. 6.

In principle, the same scheme could be used (both in a fiber or an SOA) with 100 GHz or 50 GHz grid spacing: this would allow for higher conversion efficiency, because of the lower *s* and *P*1 detuning, and hence better performance. In that case, however it should be noted that also the pumps would have a lower detuning. This means that to remove them at the device output, it is required to have filters with minimized cross-talk.

3.1.3 Conclusions

We realized a 1 to 6 WDM multicast device for 10 Gb/s signals based on a particular multi-pump FWM scheme that has been tested and compared in an SOA and a DS fiber, that, despite being based on different non-linearities show similar behaviors. The multicast device has been tested with OOK amplitude modulated signals, but it is expected to have good performance with constant envelope signals (such as phase modulated, DPSK encoded signals), due to the coherent nature of FWM. SOA-based device shows higher and wider conversion efficiency, while the DS-Fiber based device can guarantees uniform converted signals OSNR values. Flat conversion efficiency could be obtained with ad-hoc designed fibers. Both schemes show comparable power penalties on converted channels (less than 2.5 dB in both cases) and could be realized in principle with finer grid spacing.

3.2 Multiple Wavelength Conversion in SOAs by means of Nonlinear Polarization Rotation

The second Multicast implementation presented here is realized for signals at higher bit-rates (40 Gb/s). Apart from the different bit-rate operation, main differences with the previous scheme are:

1. Instead of FWM, we exploited the induced birefringence in an SOA by an input signal; this phenomenon is known as Nonlinear Polarization Rotation.
2. Conversion process is not coherent: this means that the input signal must be amplitude modulated (or converted to an amplitude modulation format before entering the multicast device).
3. There is no need for *pump signals:* it is only required that destination wavelengths must be locally available (in the previous scheme they were generated inside the multicast device itself).
4. Due to the different process the incoming signal requires lower power levels: this represents an improvement from the system point of view.

As in previous section, we first review the induced Non Linear Polarization Rotation process in SOAs, and then we describe the experimental realization of the device.

3.2.1 Nonlinear Polarization Switching in Semiconductor Optical Amplifiers.

Nonlinear Polarization Switching (NPS) in SOAs is based on the polarization rotation experienced by a probe beam traveling in a semiconductor traversed by a stronger pump beam. The pump beam change the gain provided by the SOA on its two principal axis. This behavior was characterized by Mishra et al. In [43] they measured the different gain experienced by an SOA on different principal axis vs the pump energy of a pump pulse. For this experiment they used 120 fs pulses from an Optical Parametric Oscillator at 1520 nm at low repetition rate (72 MHz). Their results are reported in Figure 3.7.

A typical experimental configuration used to observe this effect, is ditched in Figure 3.8. A probe signal is launched in the medium, with a linear polarization state oriented at 45° in respect to the principal axes of an SOA. At the other end of the SOA, a Polarization Controller is set in order that in absence of the pump signal the light is routed to one port of a Polarization Beam Splitter (PBS). When a pump signal is launched into the SOA with enough power to modify the SOA index ellipsoid, the polarization of the probe signal is rotated: if the index modification is enough to rotate the state of polarization of the probe signal by 90°, the light exit on the second PBS port, thus realizing the so called Nonlinear Polarization Switch (NPS).

The rotation mechanism can be understood considering that each component of the probe signal, propagates along the SOA principal axes independently. At the exit of the SOA, they collect a phase mismatch that is proportional to the index variation induced by the pump power. This effect is maximum when the

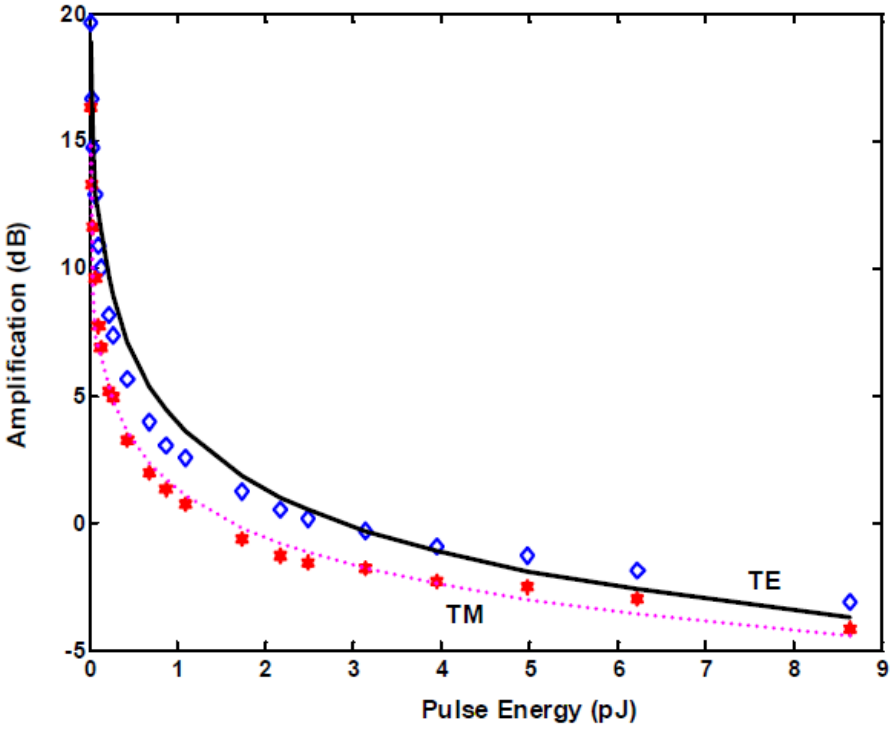

Figure 3.7: Experimental measurement of polarizations dependent gain for TE and TM modes in a SOA as a function of a pump pulse energy. (from [43]).

pump is aligned with one of the principal axis of the SOA[5]. This system is similar to a Mach-Zender interferometer in which the two arms are represented by the path corresponding to the two principal axes of the medium, and the relative delay is controlled by the pump signal.

The phase-mismatch between the two axes is transformed into an amplitude variation by means of a PBS. This allows to use NPS in SOA for wavelength conversion purposes if the probe signal is chosen to have a different wavelength of the pump. More in general, NPS in SOA allows to transfer a modulation information to any other wave acting as a probe in the SOA. NPS is related to SOA gain dynamics, and for this reason the converted channel can suffer from the pattern effects discussed in the previous section.

The NPS realized with an SOA can be compared to the so called Kerr-Shutters that can be realized with Kerr media. The Kerr Shutter is also based on the non-linear induced birefringence phenomenon. They are of course deeply different processes. For example, for Kerr media, the induced rotation is linearly proportional to the pump beam, while for the NPS this is not true (see Figure 3.7). Another important difference is found in the response times: while the relaxation times in a Kerr medium (like a fiber) are almost instantaneous, in a SOAs the polarization rotation is related the gain dynamics (that are in the order of hundreds of picoseconds as seen in the previous paragraph) and can pose a limitation on the highest operational speed that can be reached.

Another important difference between Kerr effect and SOAs dynamics is in the dependence between

[5]Refraction index modification is not critically dependent on the state of polarization of the pump.

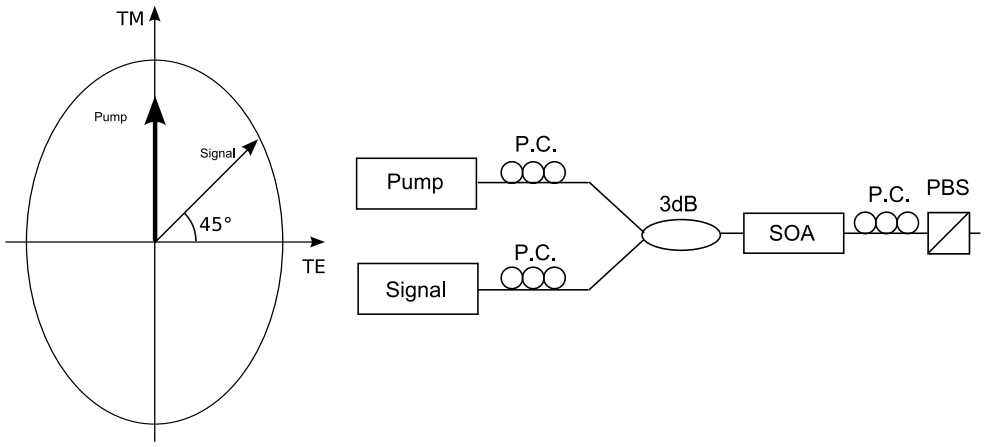

Figure 3.8: Principle of Induced birefringence in SOA by injection of a strong pump. A probe signal enter the SOA with a linear polarization state at 45° respect to the axes. The 2 probe components that propagate independently one from the other experience different gain and phase shift. Once recombined, at the end of the device the two components interfere (constructively or destructively) depending on the relative phase shift. On the right, it is shown a typical setup used to observe this effect. Two signals are coupled with proper polarization (achieved with the help of separate Polarization Controllers) into an SOA. At the output, a Polarization Beam Splitter, is used to select positive or negative interference states.

the principal axes on the induced birefringence. While in the fiber, the index modulation on one axis is independent from the other, in the case of a SOA the gain dynamics on the two principal axes are coupled by carrier dynamics. As a result, in the fiber the optical modes corresponding to the principal axes propagate independently, while in the SOA, the two modes have an indirect interaction mediated by the carriers density distribution.

A simple model that explains the characteristics of NPS in SOAs was given by Dorren et al. in [44]. The model starts by a *diagonalization* of the propagation equation along the SOA principal axes. The propagation equation is a generalization of 3.1.13 and it can be written as:

$$\left(\frac{\partial}{\partial t}+v_g^{TE(TM)}\frac{\partial}{\partial z}\right)A^{TE(TM)}(z,t)=\frac{1}{2}\left[\Gamma^{TE(TM)}\left(1+i\alpha^{TE(TM)}\right)g^{TE(TM)}(z,t)-\alpha_{int}^{TE(TM)}\right]A^{TE(TM)}(z,t) \tag{3.2.1}$$

here, $A(z,t)$ is the slowly varying complex envelope of the optical field, v_g is the group velocity, Γ is the confinement factor, $g(z,t)$ is the gain function, α is the phase-modulation parameter and α_{int} represent internal losses. The index $TE(TM)$ accounts for the different parameters corresponding to the two propagation modes. The slowly complex envelope can be expressed as:

$$A^{TE(TM)}(z,t)=\sqrt{S^{TE(TM)}(z,t)}e^{i\Phi^{TE(TM)}(z,t)} \tag{3.2.2}$$

where $S^{TE(TM)}(z,t)$ is the power carried by the field and $\phi^{TE(TM)}$ is its phase. Considering the geometrical properties of the waveguide inside an SOAs, it could be assumed with good approximation that TE and TM polarizations couple the electrons in the conduction band with two distinct reservoirs of holes.

Labeling the number of electrons in conduction band with $n_c(z,t)$ and the number of holes involved in x and y transitions with n_x and n_y respectively, it is possible to approximate the linearized gain for both polarization as

$$g^{TE(TM)}(z,t) = \xi^{TE(TM)}\left[n_c(z,t) + n_{x(y)}(z,t) - N_0\right] \tag{3.2.3}$$

where ξ denotes the gain coefficient and N_0 is the total number of electronic states involved in the transition. The gain factor can be corrected in case of strong intense beams to account for saturation due to the carrier heating effect:

$$\xi^{TE(TM)} = \frac{\xi_0^{TE(TM)}}{1+\varepsilon S^{TE(TM)}}$$

where ε has typical values around 10^{-7} per photon in the SOA. Assuming that the total number of holes is equal to the number of electrons, i.e.

$$n_c(z,t) = n_x(z,t) + n_y(z,t)$$

it is possible to obtain a system of coupled equations for the gain on the two polarization directions in the SOA:

$$\begin{aligned} g^{TE}(z,t) &= \xi^{TE}\left[2n_x(z,t) + n_y(z,t) - N_0\right] \\ g^{TM}(z,t) &= \xi^{TM}\left[2n_y(z,t) + n_x(z,t) - N_0\right] \end{aligned} \tag{3.2.4}$$

The final step of the model is obtained by specifying the rate equations for the carriers. For x polarization, it can be written as:

$$\frac{\partial n_x(z,t)}{\partial z} = -\frac{n_x(z,t) - \bar{n_x}}{T_1} - \frac{n_x(z,t) - f n_y(z,t)}{T_2} - g^{TE}(z,t)S^{TE}(z,t)$$

The two time constants T_1 and T_2 account for electro-hole recombination time (usually of the order of hundreds of picoseconds) and inter-hole relaxation times (in the order of femtoseconds). The factor f, known in literature as *imbalance factor*, is introduced phenomenologically to account for the tensile strain induced by the pump field, that enhances transitions on TM mode. In case of unstrained material, $f = 1$, while in the general case, TM gain will be larger than TE one, so that $f < 1$. Neglecting ultra-fast carriers related effects (T_2) it is possible to find an equilibrium condition

$$\bar{n_x} = \frac{\bar{n}f}{1+f} \quad \bar{n_x} = \frac{\bar{n}}{1+f}$$

where $\bar{n} = \frac{I}{e}T_1$, I is the electric pump current and e the electronic unit charge.

The phase difference accumulated during the propagation in the SOA between TE and TM modes, can be evaluated from the propagation equations 3.2.1:

$$\theta = \phi^{TE} - \phi^{TM} = \frac{1}{2}\left(\frac{\alpha^{TE}\Gamma^{TE}g^{TE}}{v_g^{TE}} - \frac{\alpha^{TM}\Gamma^{TM}g^{TM}}{v_g^{TM}}\right)L \tag{3.2.5}$$

where L represents the SOA length.

The two fields propagated along the different SOA axes interfere in the PBS ports following the expression:

$$S_{out} = S^{TE}(L) + S^{TM}(L) + \sqrt{S^{TE}(L)S^{TM}(L)}cos\theta \tag{3.2.6}$$

where

$$S^{TE(TM)} = S_{in}^{TE(TM)} e^{\left(\Gamma^{TE(TM)}g^{TE(TM)} - \alpha_{in}^{TE(TM)}\right)\frac{L}{v_g^{TE(TM)}}} \tag{3.2.7}$$

The output field given by 3.2.7 is obtained solving the gain equations for both modes.

Eq. 3.2.6, expresses the switching capabilities of NPS in SOAs. When the pump beam is present with a power level in order to induce a relative phase-shift of $\frac{\pi}{2}$ on the probe signal, the output reaches one PBS port, while, when this is not the case (there is no significant phase shift in absence of the pump), the output field is routed to the other PBS port.

The pump field can be separated from the signal beam in a couple of way: with a bandpass filter, if the pump and the probe have different wavelengths, or using a counter-propagating pump configuration in the SOA if the two signals have the same wavelengths.

3.2.2 Experimental Results

The non-linear switching process described above has been realized to perform single and multiple wavelength conversion experiments for a NRZ, 40 Gb/s amplitude modulated signal.

The setup is based on the scheme sketched in Figure 3.8, and is represented in detail in Figure 3.9.

The incoming data signal was obtained by using a common DFB, CW laser at $\lambda = 1556.5$ nm modulated by an Electro-Absorption Modulator driven by a 39.813 Gb/s pattern generator, set to generate a Pseudo Random Bit Sequence $2^{31} - 1$ bits long in NRZ format. A Polarization Controller was also used to maximize the extinction-ratio of the modulator (around 8 dB). This signal is sent into the multicast device after passing into a polarization controller used to set the right polarization state at the input of the SOA. A set of four CW lasers, 200 GHz spaced is also coupled into the SOA. These local channels have the same polarization state. They are coupled together by means of an AWG and pass through a polarization

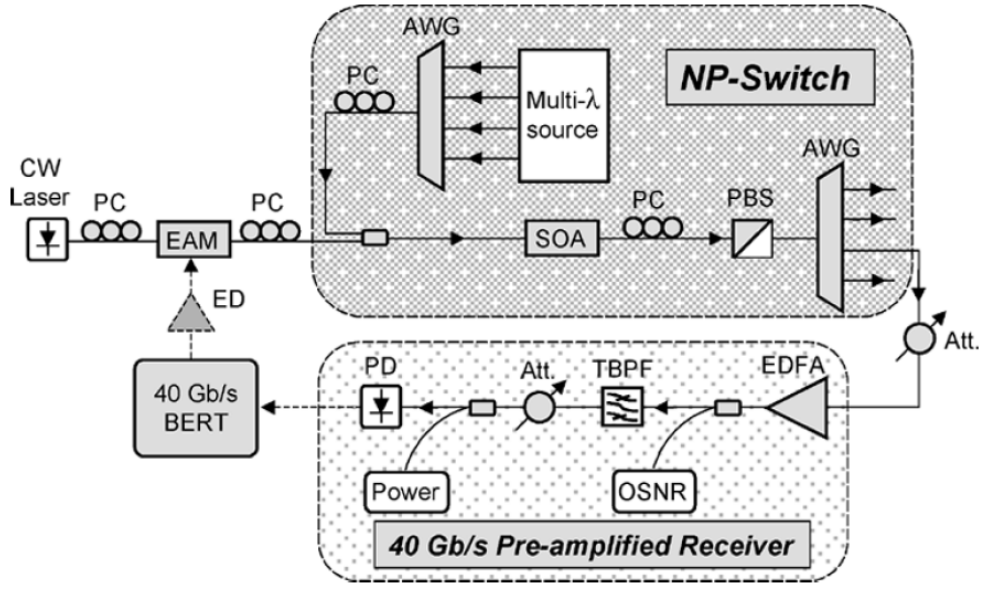

Figure 3.9: Experimental setup used to perform 40 Gb/s single and multiple wavelength conversion using nonlinear polarization switching in a SOA. In the picture, multicast device and the receiver used to perform the characterization are grouped in separate blocks. The same setup was used for single and multiple conversion; single conversion was realized by turning on only one of the channels of the Multi-λ source.

controller before being coupled into the SOA. The pump signal works as the pump wave, and induces the switching effect simultaneously on the local channels.

At the SOA input, the incoming signal enters with a power level of 13 dBm, while each CW signal is set to have 6.5 dBm power. The signals are carefully polarization-optimized. The local channels enter the SOA with a linear polarization state and polarization angle of 45°s in respect to the SOA axes (as discussed in the previous section). At the SOA output, by another Polarization Controller, the polarization of all these signals is rotated so that the transmission through the PBS output is zero when the co-injected pump signal is zero. The pump power is set so that in correspondence of optical ones on the pump signals, the local channels experience a polarization rotation and thus are transmitted through the selected PBS port. With the same polarization state of all the inverted signals, by exchanging the PBS port, the wavelength conversion can be realized in inverted logic-mode.

The SOA is a commercially available pigtailed device, with 31 dB small signal gain, 10 dBm output saturation power, and 1.5 dB polarization dependent gain. In this device, electron-hole recombination time is quite fast, and the gain is recovered at 60% in 12 ps. The PBS had an extinction-ratio between the ports of about 30 dB. At the output of the multicast device, an AWG was used to separate each converted channel.

For single conversion, we sent a CW probe signal 800 GHz detuned in respect to the incoming data signal. The eye-diagrams of input and converted signal are reported in Figure 3.10.

The converted signal eye-diagram shows a clear aperture. The spectrum of the converted channel is shown, together with a BER measurement, in Figure 3.11. It is possible to observe a residual FWM product, that in this case is not detrimental, because it is placed far away from the converted channel.

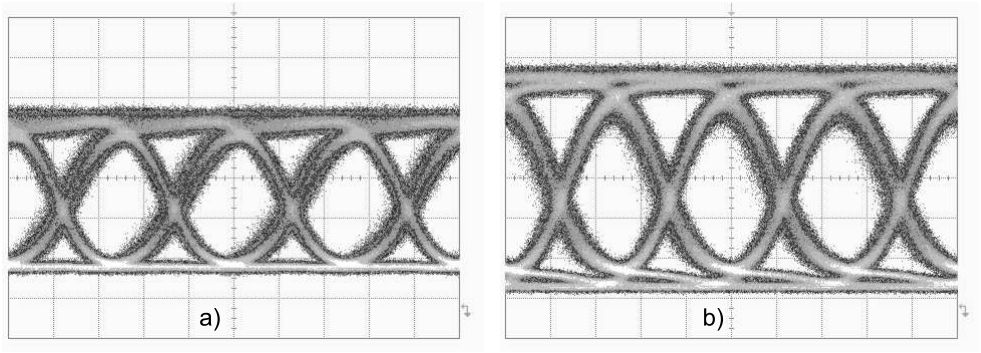

Figure 3.10: Comparison between input eye-diagram (a) and converted channel eye diagram. Traces are recorded with a 45 GHz bandwidth photodiode. In both figures time scale is 5 ps/div.

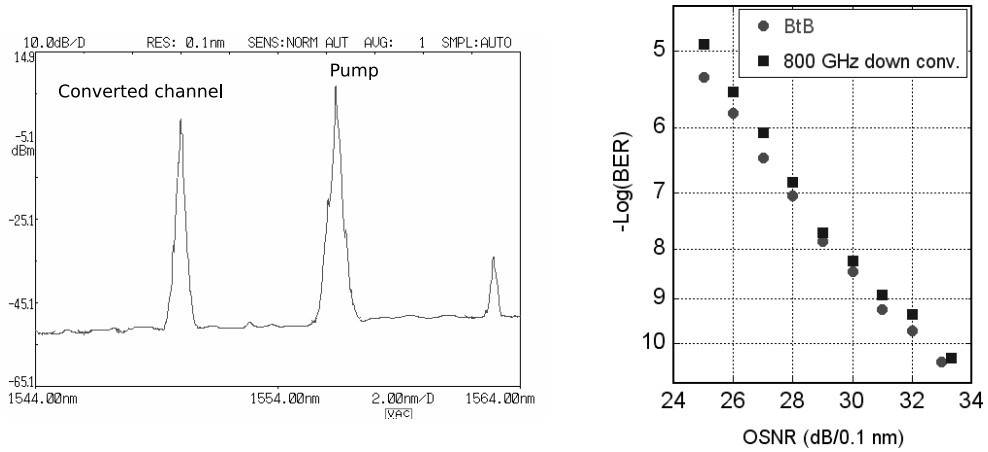

Figure 3.11: Left: spectrum of the pump and converted channel. It is possible to observe also a spurious FWM product. Right: BER measurement comparison for the incoming signal and the converted signal. Less than 1 dB penalty is produced during the conversion.

The BER measurement is realized using the setup illustrated in Figure 3.9. A variable attenuator and an high gain amplifier are used to vary the OSNR of the signal to be characterized, while a 1.2 nm Bandpass Filter (used to reject ASE noise from the amplifier) and another attenuator are used to keep at a constant level (-2 dBm) the power sent to the receiver. The OSNR measure was realized by using an Optical Spectrum Analyzer, with a spectral resolution of 0.1 nm. This is a different BER characterization, respect to the one made for the wavelength conversion device shown in the previous section: it guarantees that the BER measurements are not limited by the Photodiode Sensitivity.

The same characterization was made when all the four local CW channels were coupled together in the Nonlinear Polarization Switch.

The channels were 200 GHz spaced each other. The eye diagram of each channel, obtained by filtering with an AWG, are reported in fig Figure 3.12. Despite some noise on the mark level, all the channels show a clear eye opening. The intensity noise is probably due to the beating of the different FWM components that arise in the multi-mixing process in the SOA. Several FWM tones are unavoidably generated between the four co-polarized channels. Moreover, internal channels (two and three), jammed by more FWM

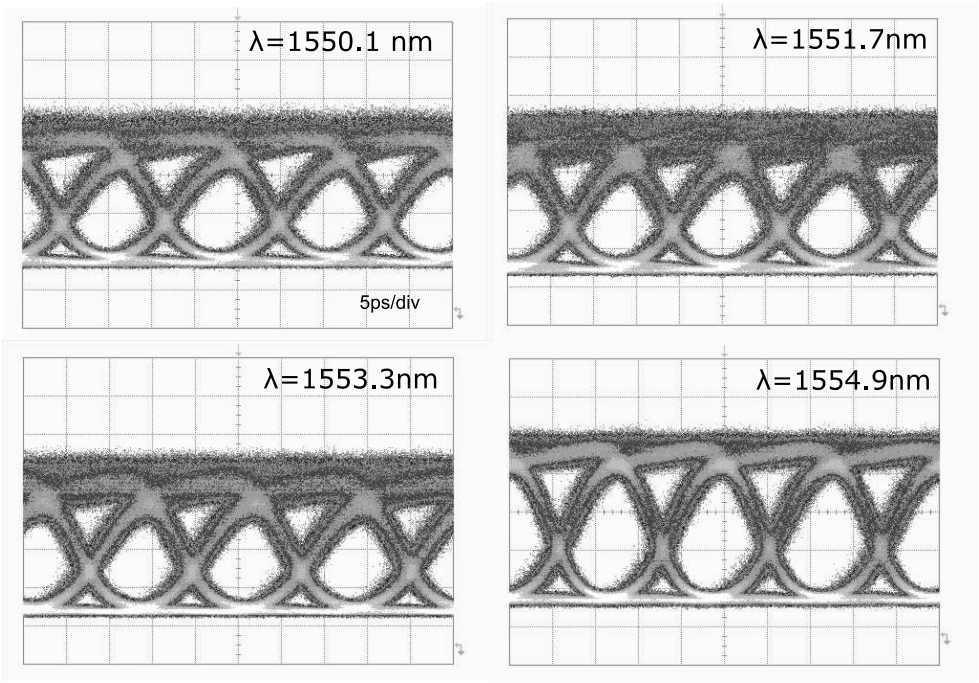

Figure 3.12: Eye diagram for each of the converted channels. Despite some noise on the high level, the eye opening is clear on all the channels.

components show higher intensity noise than aside channels (one and four). These contributes are clearly visible in the spectrum of the converted channels, reported in Figure 3.13.

While the maximum conversion efficiency is obtained for the CW signals with SOP at 45° with respect to the SOA axis, the switching process has a noncritical dependence on the SOP of the pump signal. This can be understood by noticing that the phase difference between the co-propagating modes in the SOA is proportional to differential gain between the two modes. In case of polarization insensitive devices, the differential saturated gain has only a slight dependence from the SOP of the saturating signal. Indeed we found limited variations at the SOA output in the case of limited changes of the incoming signal SOP. On the other hand, when we performed abrupt changes of the input signal SOP, a slight re-optimization of the polarization controller at the SOA output was required. This behavior is likely due to the residual PDG of the device. The intensity of the four converted channels at the AWG output is between 2 and 4 dBm, hence conversion efficiency of the switch for all the channels is in the range between 8.5 and 10.5 dB.

BER performance of the converted channels outside the multicast device are reported in Figure 3.14.

In this case, all the four CW channels are turned on (see spectrum in 2). The maximum OSNR penalty is around 3.2 dB for Channels 1 and 2. This penalty is related to the distortions in the mark level that are shown in Figure 3.12. Nevertheless, those penalty levels are significantly lower than those previously obtained at 40 Gb/s using an alternative technique [45].

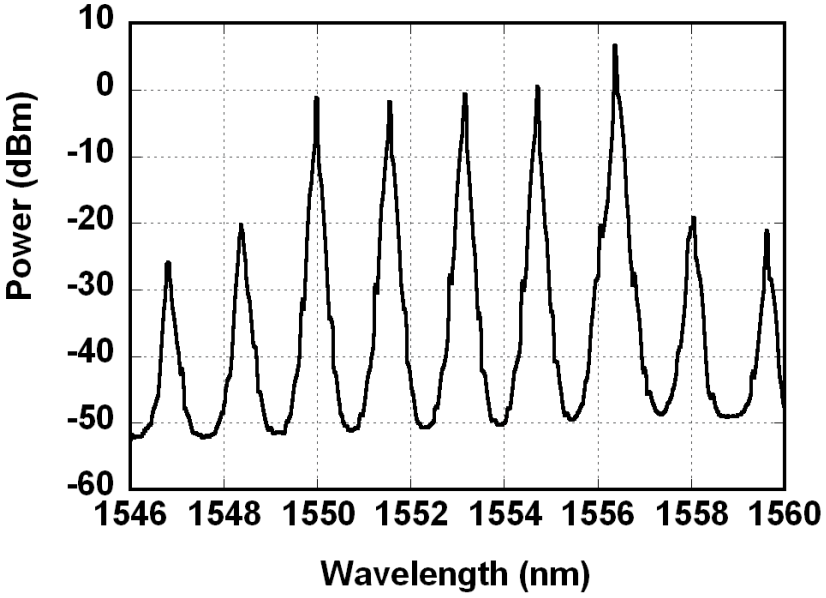

Figure 3.13: Spectrum of the output of the converted signals. FWM products are evident.

3.3 Conclusions

In this chapter, we reported two different techniques that enable the multicast operation for intensity modulated signals. The first technique, being based on a FWM process is transparent to the modulation format. In particular, the same experiment could be realized with constant envelope modulation formats for example Differential Shifted Phase Keying (DPSK). This choice would benefit the SOA operation with two main advantages: first of all the constant envelope ensures to avoid all the gain recovery dynamics related problems (the pattern effects evidenced in Figure 3.4). This enable higher bit-rate operations. It should be said using very high non-linear SOA devices in which gain recovering times can be shortened, makes possible to operate wavelength conversion at higher bit-rates also for amplitude modulated signals. However, the same bit-rate could be reached using constant envelope modulation formats with *slower* SOAs. Another big advantage offered by constant envelope formats is the possibility to use higher power probe signals. Indeed, as it was mentioned in subsection 3.1.1 in a degenerate FWM process the pump and the probe signal should not interact: in the case of constant envelope modulation formats, in which there is not gain modulation, it is possible to enhance the pump to probe power ratio, thus enhancing the conversion efficiency.

The second technique shown in this chapter, demonstrates that nonlinear polarization switching can be effectively used for multiwavelength conversion purposes for *NRZ* signals up to 40 Gb/s. Respect to other

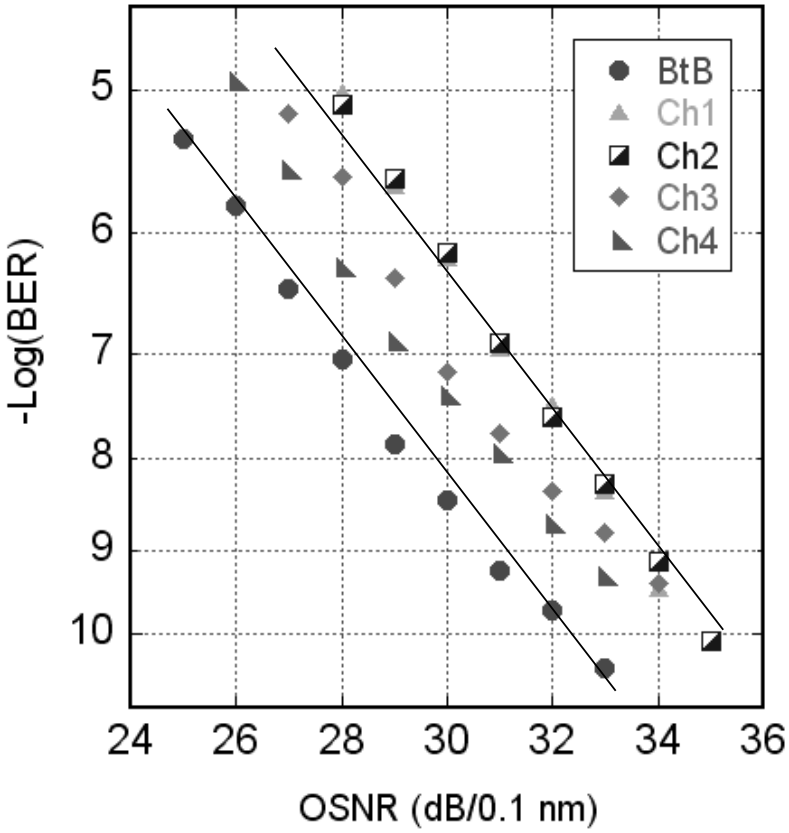

Figure 3.14: BER evaluation on all the selected channels

results reported in literature, we obtained better results on the penalty, reducing it almost to zero in the case of single wavelength conversion (against the 3 dBpenalty reported in [46]).

This technique is not modulation format transparent, but allows to obtain very high conversion efficiencies. In fact with this technique, it is possible to adjust polarization of the local CW channels in order to set to 0 the transmitted power in correspondence of 0-bit levels in the incoming data signal; at the same time, the average power on the ”1”-bits in the converted signals, are proportional both to the incoming data signal power and the local CW signals powers.

4 Optical Clock Recovery at 40 Gb/s

This chapter is dedicated to the discussion of the results obtained in the realization of all-optical clock recovery circuits. After a brief introduction on in which CR circuits will be reviewed by discussing their role in optical networks, their characteristics and requirements, an overview of typical all-optical clock recovery implementations will be given. Then the chapter will be focused on two techniques proposed to accomplish the clock recovery operation in optical domain. The first solution is based on periodic and sharp filtering of a modulated data signal; the second is based on the realization of a phase locked loop by means of a metal-semiconductor point contact diode.

4.1 Overview of common techniques used for all-optical Clock Recovery

In communication systems by means of Clock Recovery it is mean the task that allows to extract a synchronism information from an incoming modulated signal. The the recovered clock it is useful to further process the incoming signal itself (for example for regeneration at intermediate nodes) or to trigger other devices like a receiver at the end on the transmission link. Clock Recovery extraction is a fundamental operation in asynchronous systems. Typically clock signals extraction is accomplished by first converting the incoming optical signal to the electric domain, then performing the Clock Recovery in the electronic domain. This Optical/Electrical conversion process requires in principle low power levels: in fact, the first optical-electric conversion can be performed with very low optical power levels (down to $-40\,\mathrm{dBm}$). This is important, because the clock recovery operation has to be realized usually at the end of a transmission line, where the power is usually very low. The CR operation in the electrical domain has been proven to be a well established and affordable task. However, the O/E conversion poses several limitations: first of all it requires wide-band photodiodes to perform the O/E conversion and wide-band electronic components to perform the digital processing; but also appropriate high-frequency cables, and optionally electro-optical modulators, that are very expensive components. Even if the actual technology allows to achieve elaboration of high bit-rate electronic signals (up to $100\,\mathrm{GHz}$) it is not reasonable to think that this limit can be increased endlessly. Moreover, highest bandwidth photo-receivers reported in literature operate at frequencies up to $80\,\mathrm{GHz}$ thus, lower than the electrical processing speed limit.

Clock Recovery in optical domain, on the other end, does not suffer from this *speed* limitation; most important, as it will be shown in this chapter, all-optical CR can be realized with circuits made of few integrable optical components. In this case, as for may all-optical circuits, one of the major drawback is represented by the requirement on optical power levels required to accomplish the clock extraction: most

all-optical CR circuits are often based on non-linear optical effects, thus requiring proper input power levels.

The future Asynchronous Optical Packet Switched Networks will also benefit the use of all-optical CR circuits. It has been recently been shown that with the use of proper techniques (one of them is proposed in this thesis) it is possible to perform clock extraction after reading few bits of an incoming signal: this is an essential operation to achieve packet-by-packet clock recovery in asynchronous networks where packets arrive at random times to each node, and being able to perform data retiming (for regeneration purposes) or drive burst data receivers.

All-optical clock recovery circuits are designed and realized using the same principles of signals elaboration that are exploited to realize CR circuits in electrical domain. Respect to other class of functionalities that can be realized with coherent non-linear effects (for example wavelength conversion) Clock Recovery extraction it is not generally transparent to the modulation formats; it preserves however the advantage of high speed operation.

Several techniques were developed in the past to accomplish CR in optical domain. It can be said that they have a common feature. All the techniques are based on the *manipulation* of the optical spectrum of the input modulated signal; even if a signal is modulated, it always contains a *trace* of the periodicity fixed by the modulation bit-rate: any modulated signal spectrum contains *clock* lines at a frequency spacing equal to the bit-rate.

This can be derived directly by calculating the power spectrum of a digital amplitude modulated signal. We start by considering an amplitude modulated signal that contains a Random-Bit-Sequence. Such signal can be written as:

$$x(t) = \sum_k a_k p(t - kT_b)$$

where, a_k represents the k-th symbol in the sequence,

$$p(t) = \Pi\left(\frac{t}{\tau}\right) = \begin{cases} 1 & t \leq \tau \\ 0 & t > \tau \end{cases} \tag{4.1.1}$$

represents a squared pulse (that has value 1 into a bit and 0 outside it), and T_b is the bit duration (so that the bit-rate is defined as $r_b = \frac{1}{T_b}$).

The power spectrum for the signal $x(t)$ is given by:

$$G_x(f) = \frac{1}{T_b^2} |P(f)|^2 \sum_{n=-\infty}^{\infty} R_a(n) e^{-j2\pi n f T_b}$$

where f is the frequency, $P(f)$ is the Fourier Transform of the pulse signal and R_a is the auto-correlation function of the random pattern sequence a . The auto-correlation function, defined as $R_a(n) =< a_k * a_{k-n} >$, can be expressed as:

$$R_a(n) = \begin{cases} \sigma_a^2 + m_a^2 & n = 0 \\ m_a^2 & n \neq 0 \end{cases}$$

in case of a random bit sequence pattern ; $m_a$and σ_a are respectively the statistical mean and variance of the $a_k$distribution.

In the case of a NRZ signal with square pulses like in eq. 4.1.1, the single symbol spectrum is given by:

$$P(f) = \frac{1}{r_b} sinc\left(\frac{f}{r_b}\right) \tag{4.1.2}$$

For an RZ pulse (assuming a square shape similar to the one defined in eq. 4.1.1 but with half duration) the symbol spectrum is given by:

$$P(f) = \frac{1}{2r_b} sinc\left(\frac{1}{2r_b}\right) \tag{4.1.3}$$

where the *sinc* function is defined as $sinc(x) = \frac{sin(\pi x)}{\pi x}$. The origin of the factor $\frac{1}{2}$ in the RZ spectrum can be understood thinking that an RZ pulse has value "1" only for half the bit duration time (it has a 50% duty-cycle).

After some elaboration, the spectrum is found to be:

$$G_x(f) = \frac{\sigma_a^2}{T_b} |P(f)|^2 + \left(\frac{m_a}{T_{:b}}\right)^2 \sum_{n=-\infty}^{\infty} \left|P\left(\frac{n}{T_b}\right)\right|^2 \delta\left(f - \frac{n}{T_b}\right) \tag{4.1.4}$$

From eq. 4.1.4, it can be seen that the power spectrum of $x(t)$ is composed of lines positioned at the harmonics of the bit-rate $\frac{1}{T_b}$(unless $m_a = 0$ or $P(f) = 0$ for $f = 0$ and $f = \frac{n}{T_b}$ for all n). In the case of an ideal NRZ modulated signal the symbol spectrum is such that it is null in correspondence of all the clock lines: $P(f) = 0$ for $f = n/T_b$ at any $n \neq 0$. As a consequence the NRZ signal spectrum is a continuous sinc function without clock lines. In real applications, however, those lines are present (even if with very low intensities) also for NRZ signals. This is due to a series of *non-ideal* processes that happen in the signal generation, as it will be discussed in this chapter. The main cause of this the finite-bandwidth of the devices (both electronic and opto-electronic) used to produce NRZ data: it is impossible to achieve experimentally an *ideal* NRZ signal with perfect squared pulse as in eq. 4.1.1. The clock lines are present in the spectrum but are really weak (compared to he ones contained in ideal RZ signals spectra, that instead are characterized by the presence of strong clock lines). This make possible to realize clock recovery circuits using the same techniques used in RZ systems also for those modulation formats (as NRZ) that ideally do not contain clock lines: in those cases the signal is first elaborated to enhance the clock lines intensity, and then the clock recovery operation is performed.

Exploiting the presence of clock lines in the input signals spectra (or having enhanced the ones in NRZ signals), some all-optical clock recovery circuits use the input modulated signal to *seed* other systems

(either active or passive) that can resonate at multiple or sub-multiples of the clock frequency. Typical resonant systems used for this purposes are optical cavities (active or passive) with high merit factor and self-pulsating lasers. The basic idea is that the resonant device selects only the clock components and suppresses the spectral regions where the information is contained.

Another widely used scheme is the Phase Locked Loop: in this case, through a phase comparator, the incoming signal is mixed with a local oscillator (at the same clock frequency) whose phase is controlled by a feedback circuit in order to be synchronized to the input signal. Those circuits can be realized both in electrical and optical domain: relying on a feedback system, PLL are usually able to reach the lock conditions after time averaging operations, and therefore are not characterized by ultra-fast locking times.

A Clock Recovery circuit can be characterized by a number of parameters:

- Locking-Range: this parameter indicates the range of frequencies around the system bit-rate in which the clock recovery can be performed. The higher is the locking range, the more tolerant is the circuit in respect to possible small variations of the bit-rate.
- Capture Time: this parameter indicate how many bits must be received by the circuit before a clock signal is generated and synchronization occurs. This parameter should be as short as possible, in order to be able to follow all the deviations from the nominal clock.
- Holding Time: this parameter indicates the time during which the clock signal keeps to be emitted by the circuit when long sequences of constant '0' symbols are transmitted[1].

In Optical Time Division Multiplexed (OTDM) systems, it could be important to extract both the single channel clock (known as *pre-scaled clock*) or the aggregated stream clock: the needed clock depends on the application purposes. For example, pre-scaled clock could be useful for demultiplexing or add/drop operations.

A typical clock recovery circuit that exploit a *resonance* phenomenon, is based on injection locking of a properly tuned mode-locked cavity (either active or passive). If the cavity length matches the incoming data signal bit-rate, clock recovery occurs.

In Figure 4.1 it is shown an example of this technique proposed by Smith and Lucek [47]. In this case, the incoming data signal is coupled to the cavity by means of a Non-Linear Optical Modulator (NOM) so that the data signal is practically not affected. The signal is transferred to the cavity that starts lasing at the frequency $\frac{1}{T}$. In this case the clock signal is a stream of pulses. This scheme has been proposed in a huge number of variants, and it is possible to divide them in two main categories: circuits that are based on active or passive mode-locked cavities. In active cavities, the cavity gain is modulated by an electro-optical modulator inserted in the cavity itself and driven by an external local oscillator; in this case, the cavity is driven by two external forces: the incoming data signal and the gain modulation.

[1] It should be noted that while for RZ data streams long sequences of '1' symbols are beneficial for CR, in the case of NRZ streams long sequences of '1' symbols are detrimental (because for all the sequence the signal has no amplitude variations).

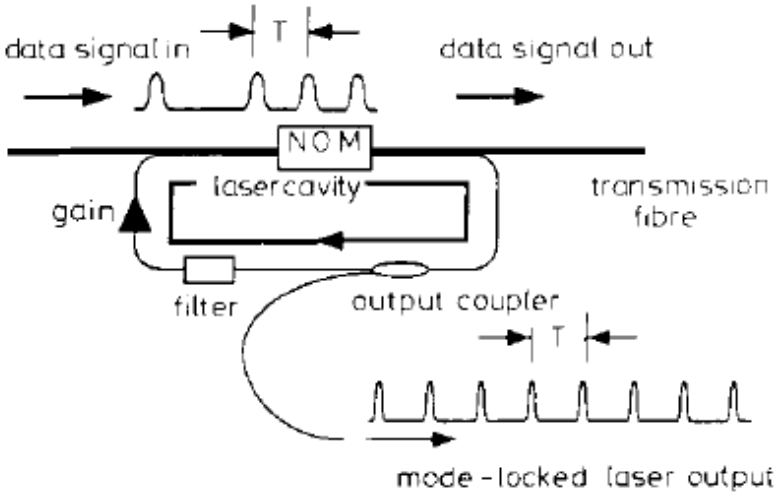

Figure 4.1: Clock Recovery circuit based on a mode-locked cavity. (After [47]). An incoming data signal, amplitude modulated, RZ, is partially coupled to a passive laser cavity tuned to resonate to the bit-rate.

This technique allows to obtain clock signals with very low timing jitter and enhanced mode-locking operations. However, those systems are not tolerant to frequency mismatch between the local oscillator and signal bit-rate: it is accepted that the two driving forces are only slightly detuned, otherwise the mode-lock cavity cannot lase. Therefore, with injection locking of active mode-locking laser it is possible to realize clock recovery circuits with a very limited locking range (few MHz). On the contrary, in passive cavities, the cavity gain is regulated by passive non-linear elements, such saturable absorbers [48], SOAs [49], fiber loops [50], that guarantee higher locking ranges (several hundreds of MHz). As drawback, those circuits require high input power levels, in order to generate the desired non-linearities into the cavity. In passive cavities, the resonance frequency is determined practically only by the cavity length itself: in active configurations instead, it is possible to drive the cavity in harmonic mode (i.e.: at frequencies that are multiples of the cavity fundamental).

It has been demonstrated that the same technique of injection locking can be achieved with the self-pulsating DFB lasers [51].

In this case the clock recovery is achieved by forcing the lasers self-pulsation to be synchronous to the incoming data signal. Using the self-pulsing DFB lasers, clock recovery can be performed in the incoherent or coherent mode [52]. In incoherent mode clock recovery is mediated by carrier modulations in the laser cavity induced by the intensity modulation associated to the data stream. The incoherent mode is wavelength (and potentially polarization) insensitive but suffers from low sensitivity and pattern-dependent timing jitter. Moreover, the sensitivity (minimum injection power) is bit-rate dependent and decreases exponentially with bit rate beyond the inverse of the carrier lifetime. In coherent mode instead, two optical spectral lines associated with the clock component in the data stream directly injection lock the two optical spectral lines associated with self-pulsation. The coherent mode has high sensitivity and virtually no speed limit but is both polarization and wavelength sensitive. An example of this technique is reported in Figure 4.2 (from [51]). In that case, the incoming data is first wavelength converted in order

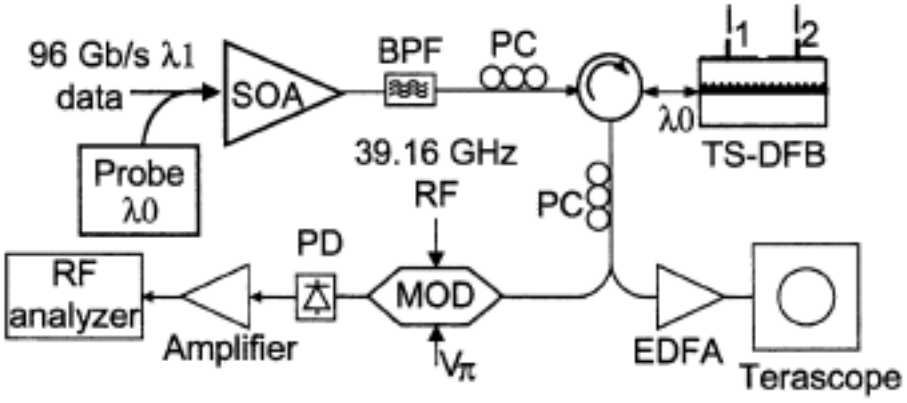

Figure 4.2: Scheme of (after [51]) clock recovery obtained using a self-pulsating laser. The incoming data signal modulates the self-pulsating laser forcing it to emit at the frequency corresponding to the incoming data signal bit-rate. In this particular case, the circuit has been made wavelength independent, by adding a wavelength converter *before* the clock recovery stage.

to obtain a copy of incoming data signal at a wavelength matching the free self-pulsating laser one (this is to make the clock recovery circuit wavelength and polarization independent), than sent to the CR circuit. The circuit itself is also polarization independent as long the wavelength converter itself is polarization independent.

Another class of Optical Clock Recovery Circuits is represented by the Optical Phase Locked Loops. In this case, through an optical phase comparator, an incoming signal is synchronized to a local oscillator, whose phase is controlled (by means of a feedback circuit) in order to match the incoming data signal one.

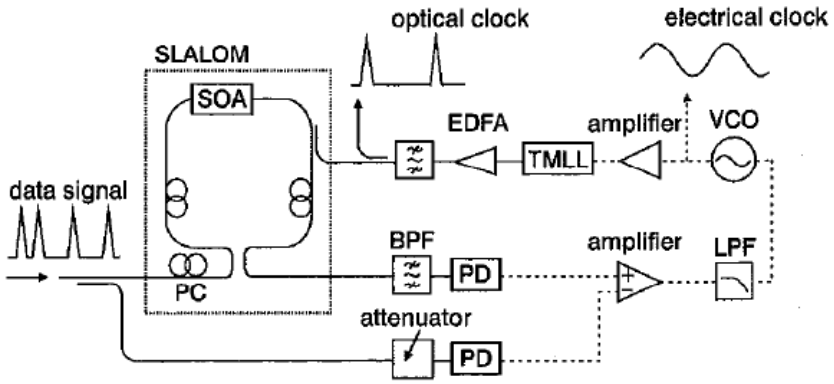

Figure 4.3: Example of Phase Locked Loop circuit (after [53]. The non-linear interferometer (SLALOM) is used to obtain an error signal that is proportional to the phase mismatch between the incoming data and local clock. The error signal is then used to correct the phase of the local oscillator.

The phase comparator is realized using an optical *mixer* that couples the local clock and the incoming data signal. Mixers exploiting non-linearities in SOAs [54], [7], [55] and Optical Fibers [56], [57] have been demonstrated. Most of the non-linear effects used to realize the mixing process can be defined, to some

extents bit-rate independent. This means that using Optical Phase Locked Loops it is possible to operate at very high bit-rate without adding too much complexity, if the mixer bandwidth is wide enough. On the other side, Optical Phase Locked Loops require an optical clock source, and this is not always compatible with design and low-cost constraints typical of modern Optical Systems.

4.2 Optical Tank Circuit

4.2.1 Theory

All the CR illustrated circuits are based on non-linear optics effects. The next class of CR circuits that that will be discussed do not rely on such non-linearities, and the operating principle on which they are based it is derived from the electronics world. They rely on an optical implementation of the so called Tank Circuit. This technique is based on a periodical and sharp filtering of the incoming data signal.

If we consider an RZ data signal, its spectrum will be composed of a set of clock lines, spaced at the signal bit-rate, plus a continuous spectrum with a shape depending on the pulse shape. This can be evinced by 4.1.4. Such spectrum is sketched in Figure 4.4. If an RZ modulated signal is sent through a periodic filter with the same periodicity of the clock lines in the spectrum (i.e. the periodicity corresponding to the signal's bit-rate), the resulting signal will be composed of the clock lines only; the filtering process removes the modulation information from the data signal. The filter should be also sharp enough in order to remove the more modulation information is possible.

To this aim, the best class of periodical filters is represented by Fabry-Perot cavities (a simple cavity with high reflectivity mirrors), or by a ring resonator (that provide the same transfer function). Both are characterized by a periodical frequency response. A periodical filter is characterized by equi-spaced power transmission peaks. Each transmission peak has the same functional form. The frequency separation between the peaks is known as *Free Spectral Range* (FSR), while the ratio between the FSR and the transmission line-width is known as *Finesse* (F) and indicates the filter selectivity. As known, the FSR of a Fabry-Peròt is given by its length L and refraction index n as from the relation:

$$FSR = \frac{c}{2nL} \tag{4.2.1}$$

The intensity of the transmitted light is given by:

$$I_T = \frac{(1-R)^2}{(1-R)^2 + 4Rsin^2(\frac{\pi f}{FSR})} I_I \tag{4.2.2}$$

where $I_I$is the input intensity and R is the mirrors reflectivity (the mirrors reflectivity is assumed to be the same for both the cavity mirrors). The Finesse, instead is given by:

$$F = \frac{\pi\sqrt{R}}{1-R} \tag{4.2.3}$$

In the limit $F \gg 1$ the Finesse is related to the FP filter line-width Δf by the relation $\Delta f = \frac{2\pi}{F}$.

Similar considerations, hold for ring resonator; in a ring resonator the cavity length should be related to the ring radius while the reflectivity with the ring input and coupling coefficient.

Three point are critical in the choice of the filter transfer function:

- The filter Free Spectral Range must match the bit-rate.
- The pass-band peaks of the filters must be superimposed to the clock lines contained in the spectrum.
- The line-width of the filter must be larger than the source line-width, but not too larger, to obtain the maximum modulation removal.

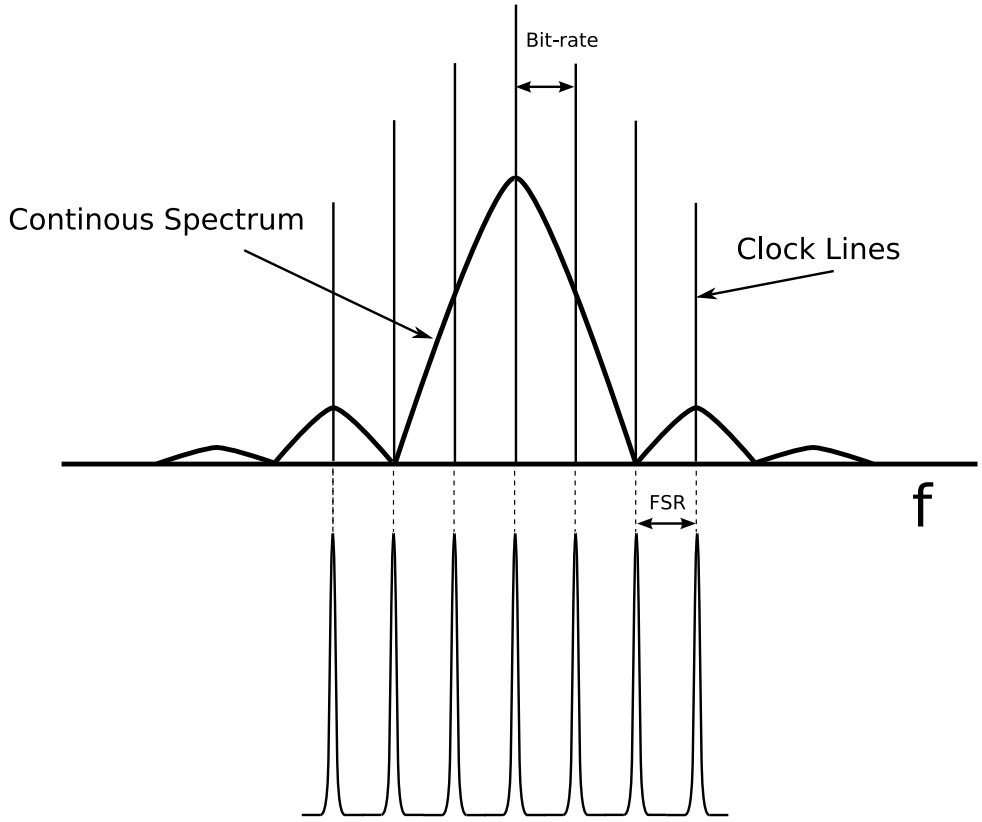

Figure 4.4: Working Principle of Fabry-Peròt filtering of an RZ data signal: the periodical filter extract only the clock lines, this transforming an input modulated signal in a periodic stream.

The clock recovery extraction can be also analyzed in the time domain: it is possible to think to a pulse of the sequence that enter the filter. It will start bouncing into the cavity, exiting with decaying energy at each round-trip. Moreover, the pulse train exiting from the cavity is spaced by a period T corresponding to $\frac{1}{FRS}$. Thus it can be said the the Fabry-Peròt cavity fills any bit slot with missing pulses (the '0' bits) with a pulse. However, this process is characterized by a decay time, fixed by the photon life-time into

the cavity $\tau = nL/c(1-R)$. The number of pulses extracted in the time τ is given by τB where B is the data bit-rate. Writing this product, it can be seen that the number of pulses exiting the cavity in the decay time is given by:

$$N \cong \frac{F}{2\pi} \tag{4.2.4}$$

The number N from eq. 4.2.4 shows that the tolerance to long '0' bits sequences depends on the FP filter Finesse. It should be said that, even if a long '0's sequence lasts for a time shorter than the decay time (so that the Tank Circuit can tolerate it), the output pulses will not have the same amplitude and the clock will not be amplitude equalized: this means that the extracted signal, even if semi-periodic[2], it is not suitable for direct use. it could be observed that increasing the Finesse it would be possible to extend endlessly the number of pulses in the decay time: this is a paradox that can be resolved including the losses in the FP filter description. Moreover, the Finesse cannot be increased arbitrarily: if on one end increasing the Finesse value benefits the holding time of the circuit, on the other end too high Finesse values can introduce other problems: if the source line-width (i.e. the line-width of the optical carrier) is larger than the FPF transmission band-width, the filtering effect can be detrimental. Moreover taking into account the finite line-width Δf_s of the signal laser source, it can be shown that the resonator Finesse is lowered by a factor:

$$F_{eff} = \frac{\Delta f_{res}}{\Delta f_{res} + \Delta f_s} F_{res} \tag{4.2.5}$$

where $\Delta f_{res}$and F_{res} are the resonator transmission peak line-width and Finesse respectively, and F_{eff} is the effective lowered Finesse. This relation poses a limitation to the highest source line-width that is compatible with the needed Finesse value (fixed by the required holding time of the circuit). An upper limit value for the source line-width can be found from 4.2.5:

$$\Delta f_s \leq B\left(\frac{1}{F_{eff}} - \frac{1}{F_{res}}\right) \tag{4.2.6}$$

Fortunately, this limitation is relaxed for high bit-rate systems: in fact, while the decay time τ is fixed by the cavity mirrors reflectivity, the number of bits contained in the decay time τ increase with the bit-rate. This means that standard DFB sources used in modern communication systems are compatible with this kind of clock recovery technique [58].

From these considerations it can be evinced that the all-optical Tank Circuit woks better at high bit-rates, with relevant advantages for the future optical networks.

There were some implementations of optical tank circuit to achieve all-optical clock recovery. A fundamental milestone was posed by Jinno [58], who realized this circuit at very low bit-rates (5 GHz). Several

[2]The signal exiting from the FP filter cannot be defined as periodic because of the amplitude modulation: still, the pulses emerging from the filters are equi-spaced in time

attempts were tested at higher bit-rates: in those implementations, however, the FP filtering was used as an *helper* mechanism for the CR circuit already illustrated in the previous section (mainly to seed other optical cavities [59],[60],[61],[62]). In the following instead we will demonstrate that a properly designed FP filter can act as the main CR circuit element even at high-bit rates (40Gb/s).

4.2.2 Experimental Realization and Results

The technique discussed above, will be shown experimentally with amplitude modulated data signals at 40 Gb/s (both NRZ and RZ). Due to important differences in the spectrum of RZ and NRZ signals, the circuit cannot be used in both cases. RZ implementation will be discussed first, and then the results will be extended to the case of NRZ input signals.

4.2.2.1 Clock Recovery from 40Gb/s RZ signals

The setup used to realize the clock recovery with RZ data is represented in Figure 4.5. It should be noted that the whole circuit is composed only by the two elements enclosed into the dashed box: the rest of the experimental setup regards the realization of the data stream and the diagnostic instrumentation (optical spectrum analyzer, electrical spectrum analyzer or optical sampling oscilloscope).

The incoming data signal is generated by external modulation of a DFB laser emitting at $\lambda = 1559.3\,\text{nm}$ with a low chirp electro-absorption modulator (EAM). This first modulation stage, it is used to produce a *pulse* sequence; we used this technique because the limited instrumentation in the laboratory didn't allow to build the soliton source described in chapter 2 for this experiment. This pulse train is not intended to be transmitted, and its spectrum is perfectly compatible with the requirements for this measures, so the lack of a soliton source is not a major limitation for the experiment purpose. The EAM is driven by a tunable RF generator, with frequency set to 39.97 GHz. This value was chosen in order to match the FSR of the available Fabry-Peròt filter. The Fabry-Peròt filter was a commercial device, with fiber pigtails characterized by an high Finesse value (270) and 4 dB insertion loss. The device can be temperature controlled by means of a fine Peltier cell in order to shift the transmittance spectrum. We found that temperature variations do not introduce sensible FSR changes with wavelength shifting. Moreover, as it will be discussed later, until the Finesse is kept constant against temperature fluctuations, the FSR it is not a crucial parameter in this circuit: it turned out that this system can provide locking ranges in the order of hundreds of MHz.

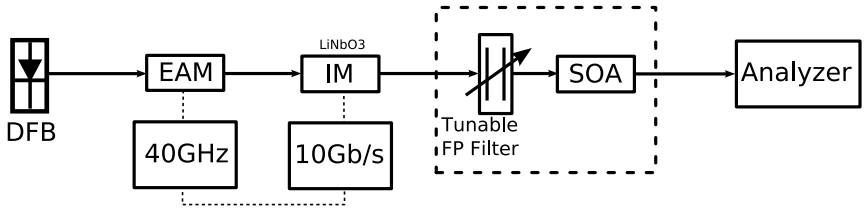

Figure 4.5: Experimental setup realized for 40Gb/s Clock Recovery from an RZ modulated signal

The filter capabilities do not strictly depend on the polarization state of the incoming signal, so that the whole circuit is also polarization independent. The pulses train has been encoded with a second modulation stage in which a Mach-Zender LiNbO3 modulator was employed. Due to the lack of a 40 Gb/s pattern generator, we modulated the pulses train imposing over it a 9.9925 Gb/s data stream, composed of a $2^{31}-1$ long Pseudo Random Sequence (PRBS). We modulated the RZ pulses train with a PRBS at exactly a quarter of the pulse frequency. The pattern and the RF generator are synchronized by a common reference signal at $10MHz$. With this technique we overcome the lack of a 40 Gb/s pattern generator, producing a sequence of pulses modulated four at a time. This data signal is not actually pseudo-random but shows, compared to a 10 Gb/s PRBS, four times longer sequences of zero symbols (i.e, the longest sequence is $31x4 = 124$ bits long). This means that this technique allows a better testing and stressing of the CR circuit.

The modulation trace can be seen in Figure 4.6 (left). The eye diagram is affected by a poor extinction ratio offered by the EAM in the pulses formation stage, and on the long rise and fall response time of the 10 Gb/s Mach-Zender modulator. From the point of view of the clock extraction this is not a problem: after all, clock recovery circuits are positioned at the end of a line when the signals are often distorted, and not in optimal shape. The spectrum of the input signal is also plotted in Figure 4.6 (right): in the spectrum (recorded with a resolution of 0.1 nm) the clock lines and the modulation superimposed are clearly visible.

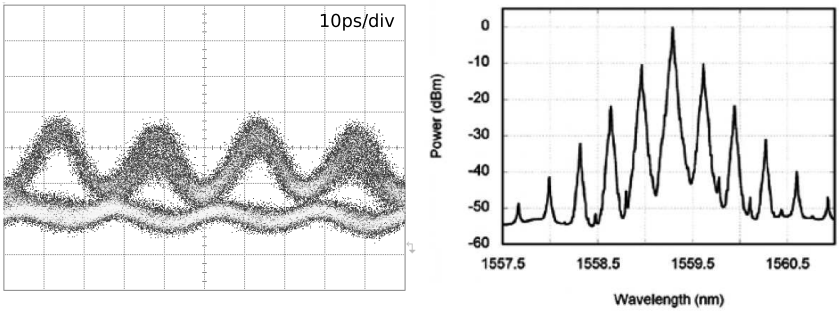

Figure 4.6: Eye diagram of the modulated pulses at 40 Gb/s. On the right the optical spectrum is plotted (recorded with a 0.1 nm resolution).

The modulated signal, is directly injected into the Fabry-Peròt filter. The signal at the output, and its spectrum are plotted in Figure 4.7. As it can be seen, the zero symbols are completely removed, and the original periodicity is recovered. However, the pulse sequence still shows a strong low-frequency modulation. The origin of this residual modulation is understood by thinking to the time response of the FP filter. As discussed in the previous section, the pulses exit from the cavity with a decaying intensity.

With the Finesse value provided by the FP (270), from 4.2.4 it can be seen that the number of pulses in the decay time is of about 43. With our modulation scheme, as indicated before, we have '0's sequences long up to 124 bits: this explain the residual low amplitude modulation. The CR signal is thus pattern dependent and not suitable to be used as a clock signal for further incoming signal processing.

The residual modulation was removed by simple further processing. To this aim, we exploited the high-pass filter property of saturated Semiconductor Optical Amplifiers (SOA). A detailed description of SOAs

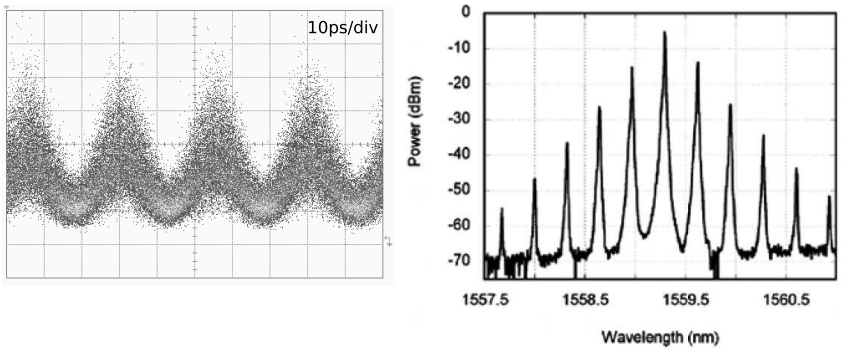

Figure 4.7: Eye diagram (left) and optical spectrum (right) of the signal extracted at the output of the Fabry-Peròt.

is well beyond the purposes of this thesis so that the following statements will be not discussed deeply, but it can be shown that a SOA have a transfer function given by:

$$X(\omega) = G_{CW} \frac{1 + \frac{\ln(\frac{G_0}{G_{CW}})}{G_{CW}-1} - i\omega\tau_c}{1 + G_{CW}\frac{\ln(\frac{G_0}{G_{CW}})}{G_{CW}-1} - i\omega\tau_c} \tag{4.2.7}$$

where ω is the modulation frequency, G_{CW} is CW amplifier gain and G_0 is the unsaturated amplifier gain (the linear, or small signal gain). The CW amplifier gain, can be found from the closed equation:

$$G_{CW} = G_0 e^{-(G_{CW}-1)\frac{P_{in}}{P_s}}$$

where P_{in} is the SOA input power and P_s is the SOA saturated power. The frequency response is expressed by $|X(\omega)|^2$; a schematic diagram of the frequency response is shown in Figure 4.8. As it can be seen, at high frequency, the response is flat, and proportional to the CW power gain, and the modulation depth is conserved at high frequencies.

Typical commercially available SOAs have cut frequencies around 1 GHz : these considerations lead us to employ an SOA to remove the low modulation content of the FP extracted signal, thus amplitude equalizing the clock.

This effect it is clearly shown in Figure 4.9.

The clock signal extracted from the circuit, shows no amplitude modulation, but it is clearly affected by a low modulation depth. This can be justified looking at the input signal, that it characterized by a non perfect extinction ratio: in fact, a very long sequence of '1' bits should be not practically affected by this circuit, thus preserving also the poor extinction ratio.

We also studied the radio frequency spectra of the recovered clock to realize a measurement of the timing jitter of the extracted clock.

The radio frequency (RF) spectra of the signals as detected by a 50-GHz photodiode and a 40-GHz electrical spectrum analyzer (ESA) are reported in Figure 4.10. In Figure 4.10 we report on the left the

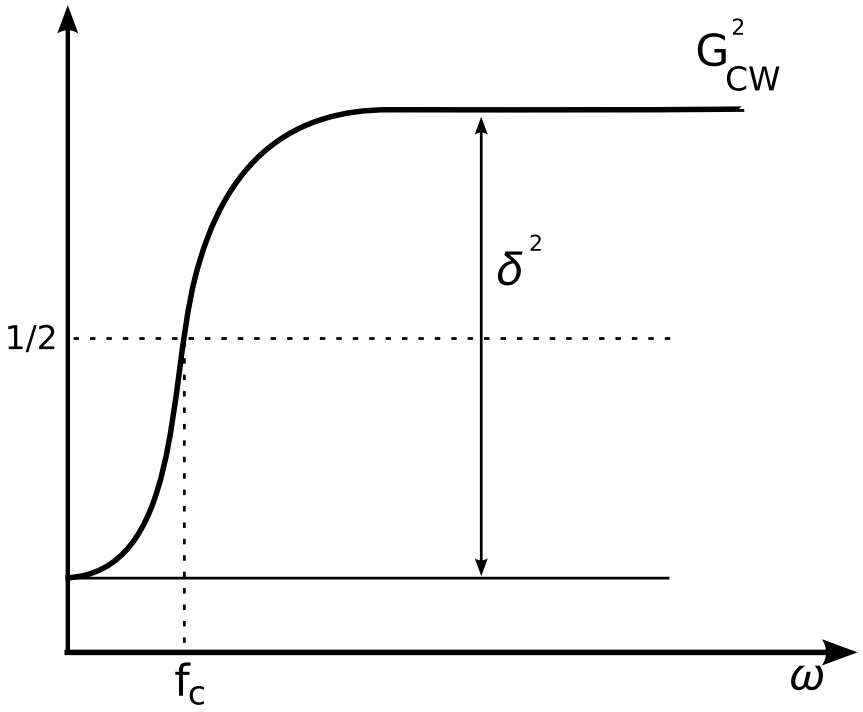

Figure 4.8: Schematic diagram of the frequency response of an SOA. δ is the modulation depth.

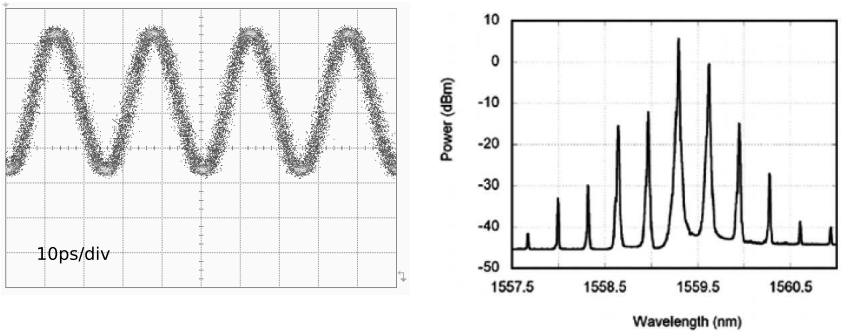

Figure 4.9: Clock signal after SOA equalization. On the left it is shown the eye-diagram of the clock. The effect of low frequency amplitude modulation (compared to Figure 4.7 is clear). On the right the optical spectrum of the clock is reported.

RF spectrum of the input modulated signal, while in Figure 4.10 on the right it is reported the RF spectrum of the clock recovered signal. The modulated signal exhibits continuous spectral components around the carrier and around the 40-GHz clock line together with 10 GHz and multiple clock lines, which are due to the particular modulation scheme previously described. From the spectra it is clearly possible to see how the clock extraction circuit removes all the spectral components but the carrier and the 40-GHz line. In this way, the spectrum of the recovered clock results quite similar to the one obtained for the original 40-GHz train. We measured 60-dB side-mode suppression, with 3-kHz resolution bandwidth for the 40-GHz clock line.

To further assess our scheme, we first measured the relative standard deviation (RSTD) of the 40-GHz

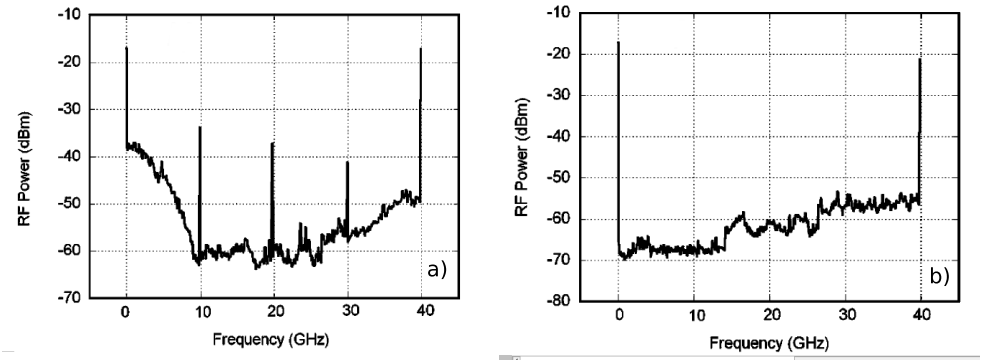

Figure 4.10: RF spectra of input modulated signal (left) and clock recovered signal (right). The input spectrum shows 10GHz spaced lines, due to the particular modulation scheme (see the text). The removal of modulation in the region $0 - 40$ GHz is evident. On the left figure, it is possible to observe 3 *steps* corresponding to three different sensitivity regions of the available Electrical Spectrum Analyzer.

recovered signal. The RSTD is defined as the ratio between the standard deviation and the mean value of the amplitude taken with the oscilloscope. We found that the amplitude stability suffers from a very limited degradation, i.e., from 0.4% RSTD of the input signal to 0.5% RSTD of the recovered clock, although we had very long zero sequences at the input. Time jitter characterization of the clock signal is then obtained from the single sideband (SSB) phase noise spectrum.

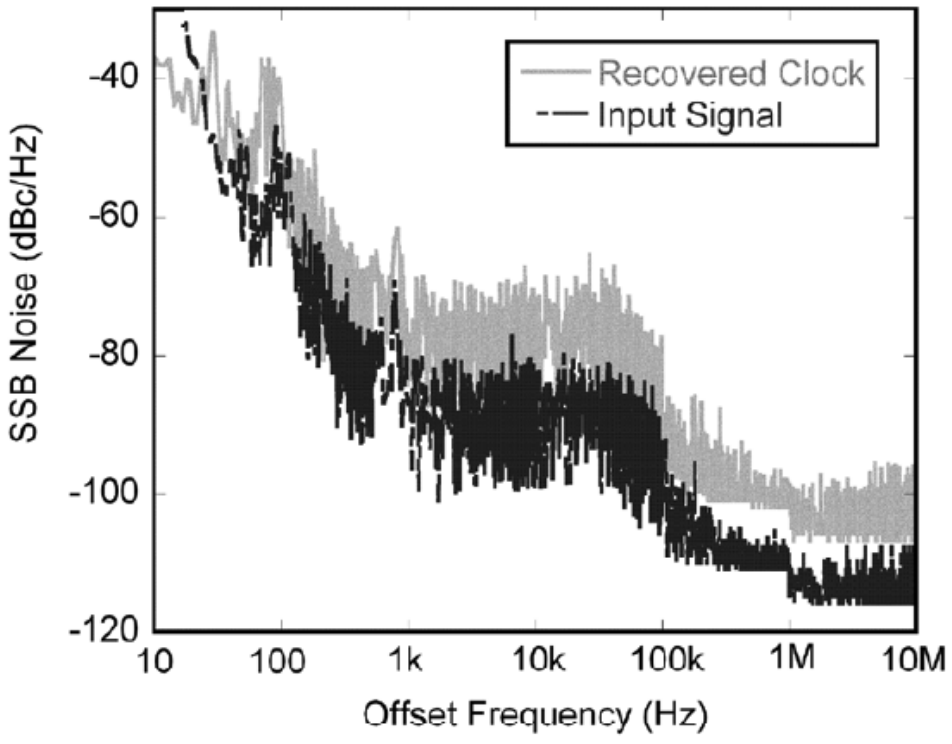

Figure 4.11: Single Side Band noise spectra of the input 40 GHz pulse train and of the clock recovered signal.

Figure 4.11 shows the SSB noise spectra of the original 40-GHz pulse train and of the recovered clock

signal. The spectrum is normalized to the resolution bandwidth of the ESA. Numerical integration of this spectrum on the tail of the clock frequency component results in an upper limit for the root mean square (rms) of the time jitter σ_{jitter}. As known, the jitter can be estimated by [63], [64]

$$\sigma_{jitter} \leq \frac{T}{2\pi}\sqrt{2\int_{f_1}^{f_2} L(f)df} \tag{4.2.8}$$

where T is the pulse repetition rate (here 25 ps) and $L(f)$ is the Single Side Band (SSB) noise spectrum. We numerically integrated $L(f)$ from the off-set frequency $f_1 = 50Hz$ up to $f_2 = 10MHz$ (note that $L(f)$ cannot be accurately measured in the limited very low-frequency region $f < f_1$, but the corresponding error can be neglected). Thus, we obtain 87 and $497fs$ as upper limits for σ_{jitter} of the input and the clock recovered signal, respectively. Even considering this upper bond value ($\simeq 0.5$ ps), the recovered clock jitter is comparable with values generally reported in literature and well within the specified limits for the current optical transmission systems (around 10% of the bit rate). By changing the bit rate of the input signal, we found that the locking range is around $150MHz$. This value is quite larger than usually reported, and it is directly determined by the FWHM of the periodic FPF transmission (and hence, by the Finesse). Even when the signal and the transmittance peak of the FPF are detuned by $75MHz$ and the signal attenuation is 3 dB higher than when they are exactly wavelength matched, we still obtain a good quality recovered signal.

4.2.2.2 Clock Recovery from 40Gb/s NRZ signals

The same circuit was also tested with NRZ signals. Even if the clock recovery extraction principle is the same of the RZ signal, there is an important difference: a pure NRZ signal (in which the unit symbol is a perfectly rectangular shaped function) does not carry clock lines in its spectrum. This can be seen evaluating the 4.1.4 for the signal

$$x(t) = \sum_k u_k p(t - kT)$$

where

$$p(t) = \Pi\left(\frac{t}{T}\right) = \begin{cases} A & |t| < T/2 \\ 0 & |t| > T/2 \end{cases} \tag{4.2.9}$$

and T is the signal period. As known, the Fourier Transform of the rect function is the $sinc(x) = \frac{sin(\pi x)}{\pi x}$, so that $P(f) = sinc(f)$ with the symbols of 4.1.4 .

If the sequence is completely random, we have:

$$\sigma_a^2 = \tfrac{A^2}{4} \quad m_a^2 = \tfrac{A^2}{4} \tag{4.2.10}$$

Inserting 4.2.10 into 4.1.4 we have:

$$G_x(f) = \frac{A^2}{4r_b} sinc^2 \frac{f}{r_b} + \frac{A^2}{16} \sum_{n=-\infty}^{\infty} sinc^2(n)\delta(f - nr_b) = \frac{A^2}{4r_b} sinc^2 \frac{f}{r_b} \tag{4.2.11}$$

In 4.2.11 all the clock lines (represented by the δ functions) vanish because in correspondence of the lines, the $sinc()$ approaches zero: thus the spectrum of an ideal NRZ data stream does not show clock lines, but only a continuous distribution around the zero frequency.

In the practice, however, the signal cannot be represented by a rect function: it is impossible to obtain instantaneous transactions between the high and zero level. So, in the practice it is possible to have signals whose spectra do not have zeros in correspondence of the clock lines, and then it is possible to observe optical spectra with clock lines, even if with very low intensities. Usually, those lines have so low intensities that it is not possible to apply directly the filtering process to extract a clock: the incoming data signal has to be pre-processed, to enhance interested lines in the spectrum.

The presence of these clock lines is derived to the finite bandwidth frequency response of the apparatus that encode the signal (pattern generator and electro-optical modulators). This means that, fixed the cut-off frequency of the data encoders f_c and electro-optical modulators that forms the modulated optical signal, the clock lines in the spectrum can be more intense as the bit-rate r_b increases. As result, the optical processing for clock recovery extraction from NRZ signals seems more suitable than electronic clock recovery and it is expected to work more efficiently at higher bit-rates.

The pre-processing stage can be realized in several ways. We used a simple pre-processor, made by an SOA and a tunable bandpass filter (Figure 4.12).

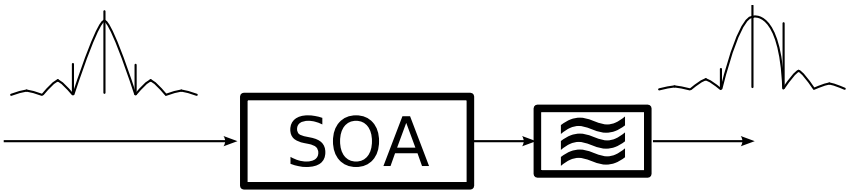

Figure 4.12: Schematic representation of the pre-processor: a combined action of SOA non-linear effects and filtering reshape the signal spectrum to enhance on of the weak clock lines.

When the NRZ signal enters in the SOA, the spectrum is red-shifted, and a corresponding overshoot is observed in correspondence of the leading edge of the signal. This overshoot is selected by means of the tunable filter. The spectrum is then strongly distorted toward longer wavelengths, and correspondingly the clock lines on the “higher wavelength side” of the spectrum, are enhanced.

The overshoot effect, can be observed in Figure 4.13. The tunable filter can be optimized in order to maximize the overshoot. In the frequency domain, this is equivalent to select the spectrum region where the clock lines are located. Signals processed with this technique are often known in literature as Pseudo-RZ signals.

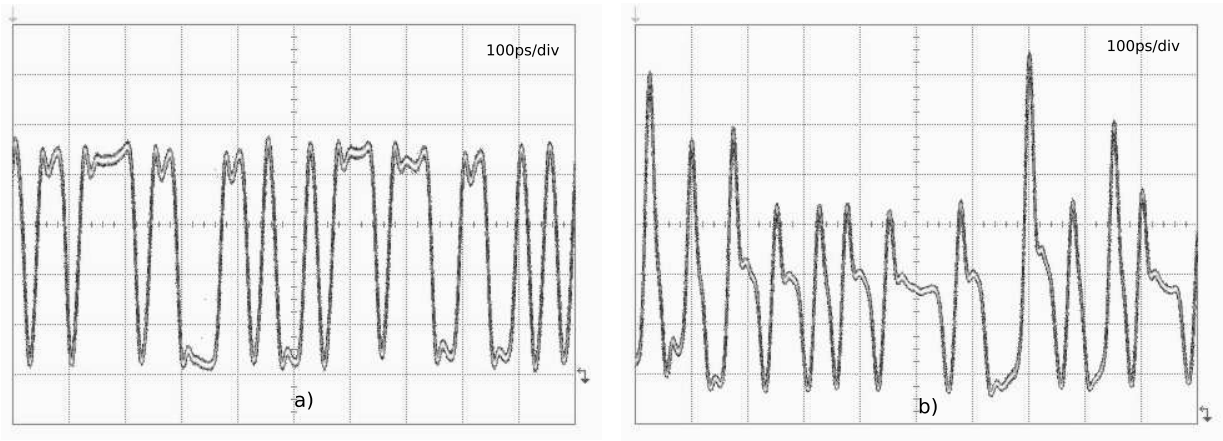

Figure 4.13: Effect of the pre-processor. a) input data stream b) signal output after the pre-processor. In correspondence of the leading edge, an overshoot can be observed.

The experimental spectrum distortion can be observed in Figure 4.14. In the input spectrum (dashed curve), the clock lines are weak (about 23 dB under the carrier). After the pre-processing, the clock to carrier ratio is enhanced of about 15 dB. It can be noted that even if enhanced, the line seems to *disappear* into the spectrum. This is not a problem in our case, because we operate a sharp filtering.

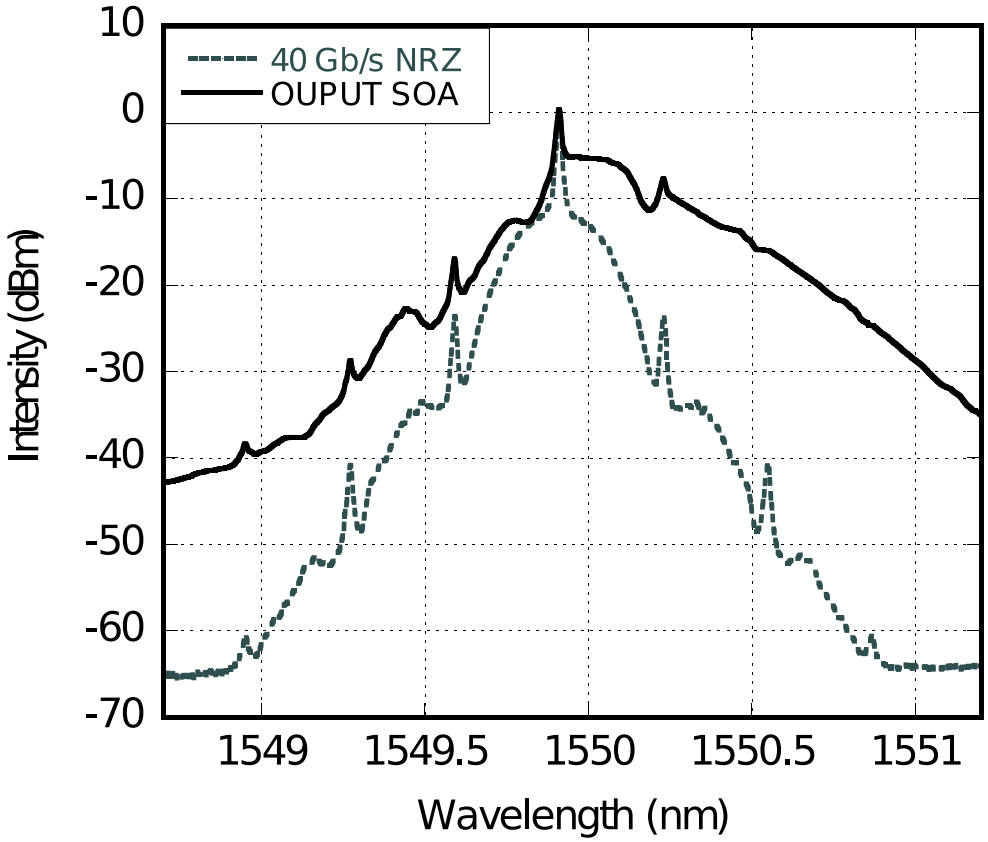

Figure 4.14: Induced spectrum distortion in the pre-processor. The tunable bandpass filter has a 0.8 nm bandwidth.

This signal is now suitable to be processed with the same circuit shown before. The complete experimental setup is drawn in Figure 4.15.

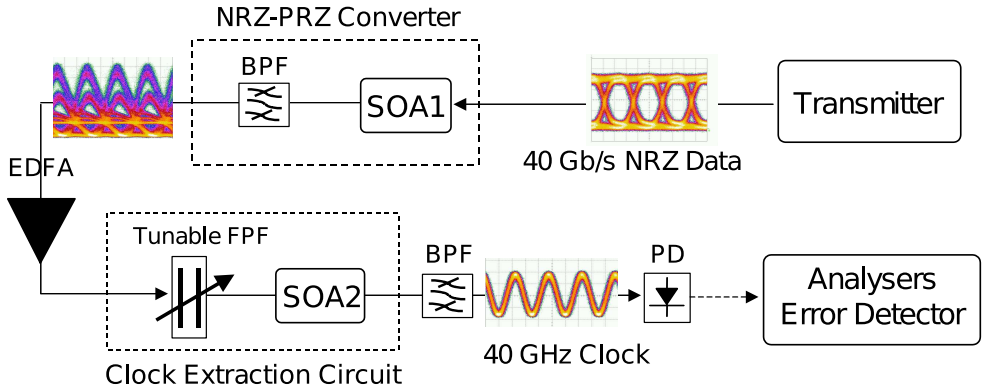

Figure 4.15: Complete setup of 40Gb/s NRZ Clock Recovery. The inset show the eye diagram of the signal at various stages: input, after the pre-processor and the extracted clock.

The modulation is realized by a DFB laser emitting at $\lambda = 1549.9\,\text{nm}$ externally modulated by a Mach-Zender $LiNbO_3$ based modulator, driven by a $2^{31}-1$ long PRBS.

The signal enter the pre-processor with an input power of about 6 dBm. After the first SOA, the signal is passed through a tunable bandpass filter with 0.8 nm bandwidth. The preprocessed signal (Pseudo RZ signal) is then inserted into the clock-recovery circuit, realized with the same components used in the RZ case. While in the RZ experiment the clock signal at the output of the FP filter was affected by a strong low frequency amplitude modulation, due to the presence of the long '0' bit sequences (up to 124 '0' bit) due particular modulation scheme, in this case, the longest '0' bit sequence lasts for *only* 31bits. In this case, we still expect a low frequency amplitude modulation, but with lower modulation depth.

This can be seen in the eye-diagram of the clock signal extracted at the output of the FP filter (Figure 4.16-a). As in RZ case (Figure 4.7) the zero level is completely removed, but there is still a trace of amplitude modulation. The comparison shows also a net reduction of the amplitude fluctuation due to the shorter length of the '0' bit sequences. Some of the noise in the output of the FP filter could be also attributed to the amplified spontaneous emission accumulated in the amplifiers in the pre-processor stage and before the clock recovered signal. The EDFA in the setup is needed to guarantee that the clock signal enters the equalizing SOA (SOA2 in Figure 4.15) with a power level that can bring it in saturation regime: if SOA2 it is not saturated, the equalizing effect it is not observed.

Both SOAs are polarization independent devices with 28 dBm small signal gain and 5 dBm output saturation power.

The spectra of the clock recovered signal is reported and compared to the spectrum of preprocessed signal (Figure 4.17). As it can be seen, the double red-shifting effect (experienced in second SOA) further increases the clock to carrier ratio, taking it to $-3\,\text{dB}$ about: the overall increase is then estimated to be around 22 dB.

This enhancement is more evident in the RF spectrum (Figure 4.18). The spectra are recorded with a

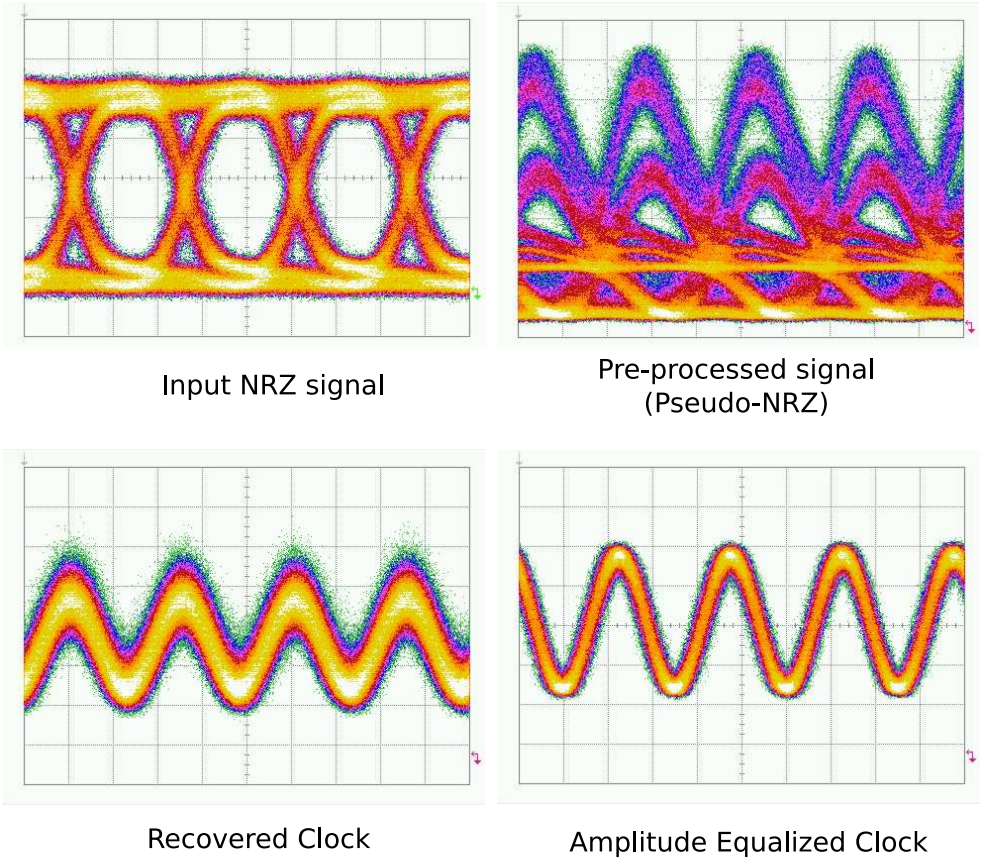

Figure 4.16: Detail of signal evolution at every stage of clock recovery circuit. All figures are recorded with a 55 GHz photodiode and a sampling oscilloscope in eye-mask mode. All images have time scale set to 10 ps/div.

50 GHz photo-detector and a 40 GHz spectrum analyzer set to a Resolution Band Width (RBW) of $3MHz$. As it can be seen, the modulation components are all removed and the clock line is strongly enhanced (more than 30 dB).

Integrating the SSB RF spectrum as in 2.1.7, we found a upper value for the timing jitter of 0.2 ps, slightly lower than the one obtained in the RZ case. This can be explained with the presence (in the case of RZ signal) of a stronger modulation at the output of the FP filter: as an SOA induce a phase shift on the signal that it is proportional to the gain; in that case, the pulses with different input power experience different gains, and then different phase-shifting, thus increasing the overall timing jitter.

At the moment of the realization of this experiment, a 40 Gb/s Bit-Error-Rate measurement system was available, and the extracted optical clock was used to synchronize the receiver: we obtained error-free operation in back-to-back configuration, thus demonstrating the validity of the circuit.

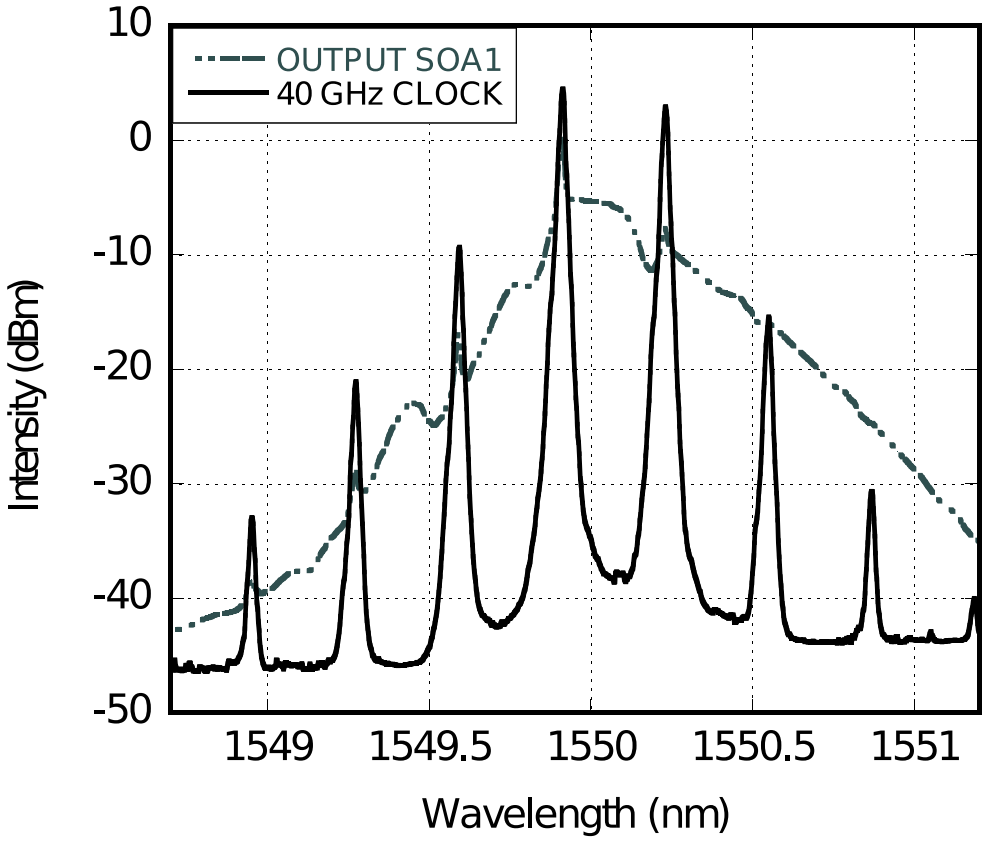

Figure 4.17: Effect of FP filter (continuous line) on the preprocessed signal (dashed line)

4.3 Optical Phase Comparator with Point Contact Diodes

As discussed at the beginning of this chapter, another technique used to obtain a clock-recovery signal, consists in the use of a Phase-Locked-Loop circuit that minimizes the phase delay between a local oscillator and the incoming signal. Usually, the phase extraction is based on non-linear response of a medium, that is generated only when both the local and incoming signals are temporary superimposed in the medium itself: the intensity of the non-linear signal produced by the interaction is taken as a measure of the relative phase delay of the signal. We tested this scheme using as non-linear medium a Point-Contact-Diode.

4.3.1 Metal-Semiconductor Point Contact Diodes

Metal-Semiconductor Point Contact Diodes are systems composed by a contact between a fine metal wire and a (p or n doped) crystal. Many types of point contact diodes have been developed during the last 50 years: Metal-Insulator-Metal, Schotky diodes have been widely used in microwaves applications. PCD have been also used as mixer in metrology applications, exploiting their wide detection spectrum. Depending on the crystal used, they can detect radiation with wavelengths from visible to infrared: this allows to perform mixing between waves that are very far in the electromagnetic spectrum, leading to the

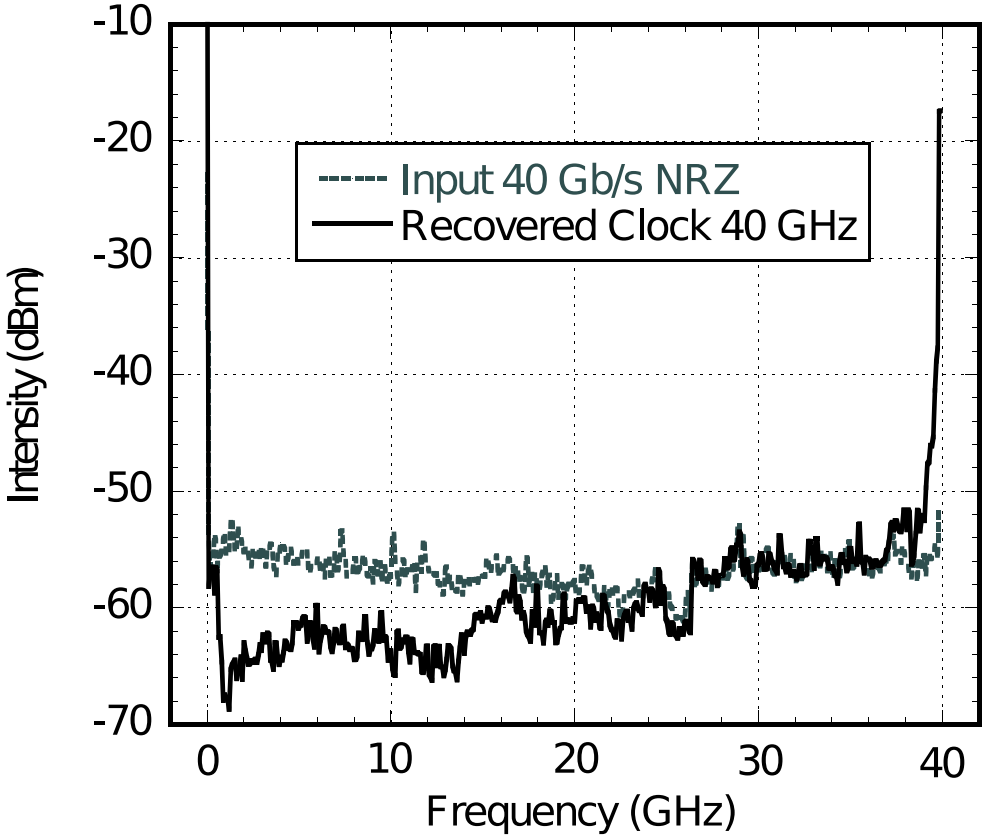

Figure 4.18: Comparison between the input and clock-recovered signals RF spectra. The clock line is strongly enhanced (more than 30 dB).

possibility of direct high precision measurement of laser frequencies. Beside this peculiarity, as the response time is the reciprocal of the difference between the signals frequencies, those device are extremely fast.

A schematic representation of this diodes is reported in Figure 4.19

The wire, also known in literature as *cat whisker* can be hook-shaped, in order to ensure a pressure against the crystal. Unlike other kind of junctions (the *p-n* junction, for example) its properties depend on the wire pressure against the crystal: by varying it, it is possible to vary the contact resistance, thus its performance. The pressure of the contact can be controlled by means of a translation stage, as shown in Figure 4.19-a). During the construction of the diode, an high current is usually let flow across the contact, in order to generate a polarized zone (around the contact) thus forming a *p-n* junction. This process, represented in Figure 4.19, is known as *electroforming.*

The diode is used by sending different signals over the contact region and then analyzing the produced signals at its edges, usually with a electrical spectrum analyzer, in order to study the mixing products.

Several different processes concur to the generation of the signal. One of them, is the tunneling effect, typical of Schottky diodes. Several papers reported the evidence of another process, probably of thermal nature, that could be responsible for the different responsivity of the diode respect to different mixing

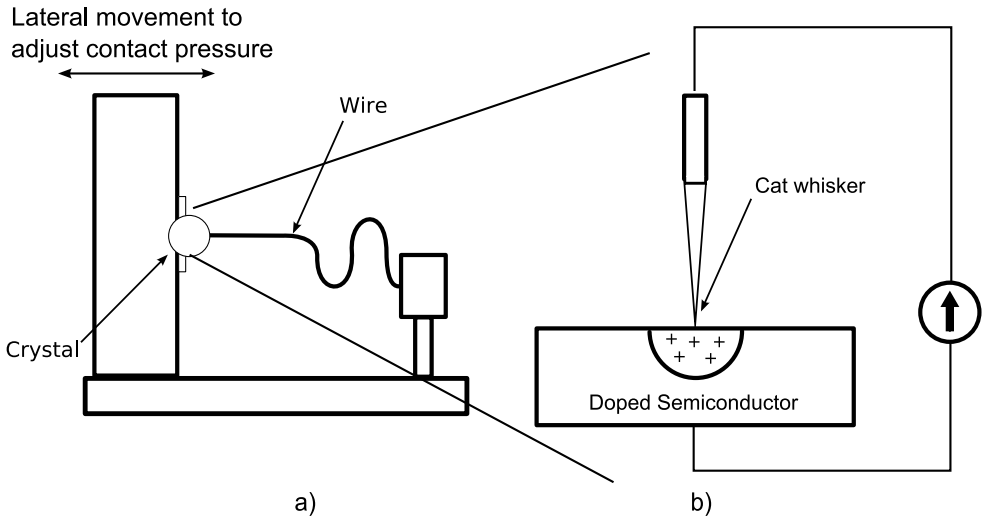

Figure 4.19: Schematic representation of a point contact diode. a) The wire can be hook-shaped in order to guarantee a good pressure on the contact. b) After a current injection through the contact, the region around the contact become polarized, thus forming a pn junction.

orders. However, there is still not a complete theory that describe those device [65].

As crystal, several sample were tested. The best performance were obtained with a *GaSb* sample *n*-doped with *Te* and a carriers concentration of $6-8x10^{17}cm^{-3}$.

The choice of *GaSb* crystal is also important to use the PCD with infrared radiation (around the spectral region of interest for Optics Communication), because, *GaSb* has an absorption peak around $1550\,nm$. In practice, *GaSb* acts as a *photodiode* while the whisker acts like an *antenna* to detect the RF radiation.

The tip radius, as well as the whisker diameter, are not expected to be critical parameters for the detection and mixing properties of the PCD [65]. Small tips radius offer faster response and higher mixing bandwidth; but at the same time, too small tips radius (under hundreds nanometers) can lead to very delicate and short lived contacts. A good compromise between contact *smallness* and *stability* has been found by Carelli and co-workers using tungsten wires, with $127\mu m$ diameter and a tip electrochemically etched to the desired radius (typically 100 nm) by immerging it into a $2N-HaOH$ solution.

PCD could be used inn Optics Communications for various application. Among them, PCD could be employed for timing-jitter measurement for high repetition rate sources. Timing Jitter of a periodic pulse train can be determined by analyzing it spectrum. Assuming that the individual pulse shape is specified by a function $f(t)$, and the repetition rate is $1/T$ if the train is affected both by amplitude modulation and timing jitter, its power spectrum can be expressed as:

$$P(\omega)=\left(\frac{2\pi}{T}\right)^2\left|\tilde{f}(\omega)\right|\left[\delta(\omega_n)+P_A(\omega_n)+(2\pi n)^2P_J(\omega_n)\right] \tag{4.3.1}$$

where $\tilde{f}$ is the Fourier Transform of pulse intensity temporal profile, ω is the optical frequency, and $P_A(\omega)$ and $P_J(\omega)$ are the power spectrum of amplitude modulation and timing jitter respectively. In 4.3.1,

n indicates the nth harmonic in the spectrum.

Of course the various harmonics are equi-spaced by an amount equal to $\frac{1}{T}$ as from the relation:

$$\omega_n = \omega_0 \pm \frac{n}{T} = 2\pi(f_0 \pm n f_r)$$

where $\omega_0$is the pulse train carrier and f_r is the pulse train repetition rate. It can be seen how the amplitude noise modulation is distributed with the same weight over all the harmonics, while the timing jitter contribution scales as n^2 and thus is more evident on higher harmonics. To isolate the timing jitter contribution in the spectrum, it is necessary to measure the line-width of two harmonics in the spectrum: one at low n and another with high n. Then comparing their line-width, it is possible to measure the timing jitter contribution, and hence, to derive information about the deviation on the repetition rate of pulse train under test.

This procedure, is commonly applied to low repetition rate pulse source; for a source operating at few MHz repetition rate, it is possible, with an adequate electrical spectrum analyzer, to study harmonics up order 50. For higher repetition rate pulse train, this is more difficult, due to the limited bandwidth of available instrumentation. If we consider the source presented in chapter 2, it is impossible to study harmonics at higher order than the first (40 GHz) because the widest bandwidth photodiodes have a pass-band of about 60 GHz: in this case, it is impossible to retrieve timing jitter information with direct detection. The PCD presented in this section, can help in doing a down conversion with high frequency Microwave generators, due to its wide range of detection. In principle, mixing the optical pulse source and a microwave reference (with known stability) it is possible to observe higher harmonics, and hence to extract information about the optical source stability. This kind of test as been performed with a couple of microwave source. Preliminary results about mixing between the source reported in chapter 2 can be observed here. Those measurements, are still in progress and the reported results are intended to be only demonstrative. The mixing between the optical pulse source and an external microwave generator is given by a series of beating. The generic beating is given by:

$$f_{beat} = |M(f_{n1} - f_{n2}) - N f_{MW}| \tag{4.3.2}$$

where $f_{n1}$and f_{n2} are two harmonic of the optical signal and f_{MW} is the microwave source frequency. N and M indicate the mixing order.

The relation 4.3.2 has been verified for first-order mixing ($N = 1$,$M = 1$). To this aim, we produced an optical sine-modulated wave by using a external modulation of a CW laser at 1550 nm.The CW wave was modulated with a continuously tunable RF source (between 0 and 40 GHz) driving a Mach-Zender modulator biased at null point (in order to double the modulation frequency).

The obtained wave was then mixed onto the PCD together with a Microwave oscillator emitting at a frequency around 72 GHz. The microwave oscillator is coupled to a Gunn waveguide that is placed close to the PCD whisker that act like an antenna. The optimal positioning is determined by maximizing the

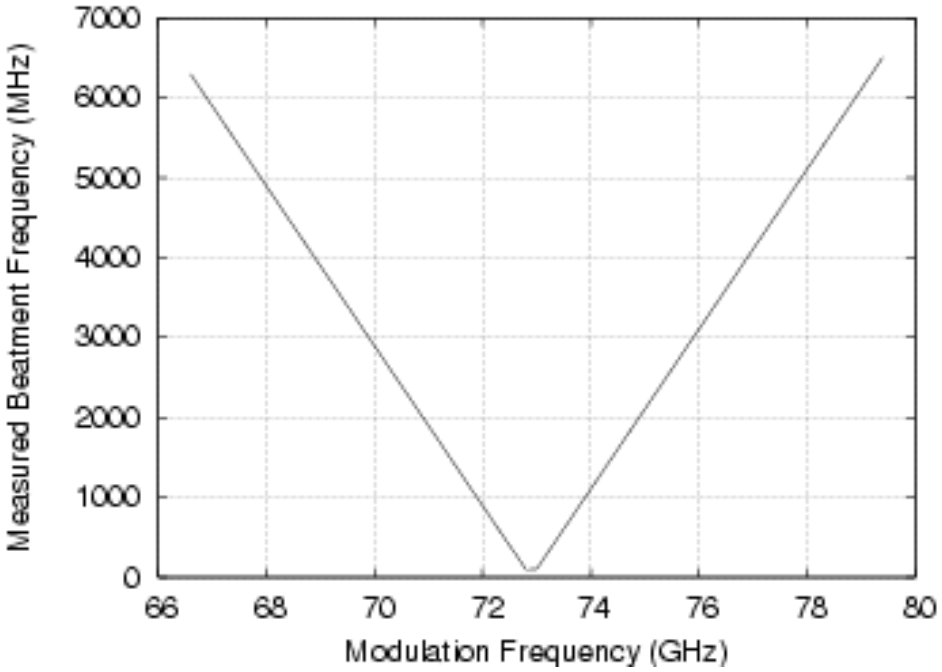

Figure 4.20: Experimental confirmation of the relation 4.3.2, obtained by coupling a microwave oscillator emitting at 72 GHz with a optical sine-like wave at a variable frequency between 66 and 80 GHz.

detected signal. The output power of the Gunn oscillator was 10 mW. The coupling of the pulsed source on the PCD was realized by putting the fiber output of the optical source in close contact with the PCD's crystal. While varying the modulation frequency, we recorded the frequency of the obtained beating. The result is plotted in Figure 4.20.

An example of second order beating is reported in Figure 4.21. It is possible to observe a screen image of a beat note at 8 GHz obtained by irradiating the PCD with the pulse source and a Microwave oscillator emitting at a frequency around 72 GHz. This beat note, is the result of the mixing with $N = 2$ and $M = 1$(referring to eq.4.3.2).

As indicated before, a typical application of this mixing experiment, could be found in the noise characterization of high repetition rate optical signals, provided that the microwave reference is stable enough. Conversely, this method can be used to characterize microwave signals considering the optical signal as a stable reference.

A second class of operation that can be performed with PCD regards the clock recovery. In the following, it will be shown how the PCD can act as a Phase Comparator to lock an incoming signal to a local oscillator. It should be noted that the reported results are similar to those that can be obtained with a PIN photodiode, since down-conversion using the Gunn MW it is not needed. This is because both the local oscillator and the signal we used have a repetition rate that is in the bandwidth of common photodiodes. However, by using a down-conversion process as described before, it should be possible to fully take the advantage of the high-bandwidth response offered by the PCD.

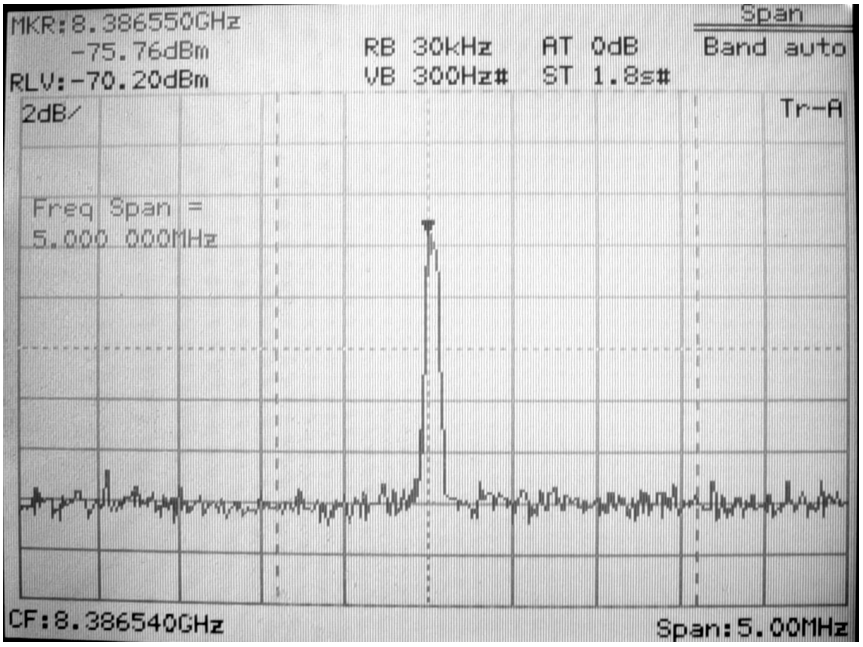

Figure 4.21: Beat note of a mixing experiment between a Gumn oscillator emitting around 72 GHz and an optical pulse source at 40 GHz repetition rate.. The reported beat note is at 8GHz ($40 \times 2 - 72$ GHz).

To show how the PCD can be effectively used as delay detector between two pulse trains, we realized the experimental setup shown in Figure 4.22.

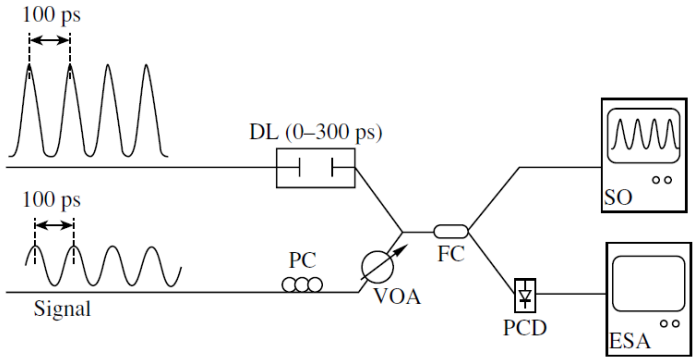

Figure 4.22: Experimental setup to measure the phase delay between two periodic signals. A single RF generator at 10 GHz is used to produce a sine-modulated wave and a pulse train, by means of an electro-optic Mach-Zender modulator. The two streams are delayed each other and then are combined over the PCD. Both a Sampling Oscilloscope and a electrical spectrum analyzer are used to measure the delay.

We first produce two sine-modulated waves by modulating a CW laser at 1555 *nm* with a common Mach-Zender modulator, driven by an RF generator at 10 GHz. One of the sine-like wave is then compressed in a Single Mode Fiber (exploiting the modulation instability phenomenon illustrated in chapter 2) to obtain a stream of 20 *ps* pulses. One of the two stream is passed into a piezo-electrical delay-line that can be tuned to set a delay in a range of ± 300 *ps*. In the other arm, a polarization controller and a Variable Optical Attenuator (VOA) are used to ensure that the two streams are coupled onto the PCD

with comparable power and identical polarization, in order to maximize the mixing effect. One sampling oscilloscope is used to position the relative delays to the desired values, and the usual Electrical Spectrum Analyzer is used to monitor the PCD response. The basic principle on which this phase comparator is used is the following. The mixing between spectral lines of the two pulse trains leads to the generation of some components in the low-frequency noise spectrum at the output of the PCD. Those components are maximum when the pulses are time-overlapped and decrease when they are out of phase. Hence, by integrating the beating noise spectrum in the low-frequency region, it is possible to extract an error signal that depends on the relative time delay between the pulse trains.

The result of the experiment is plotted in Figure 4.23

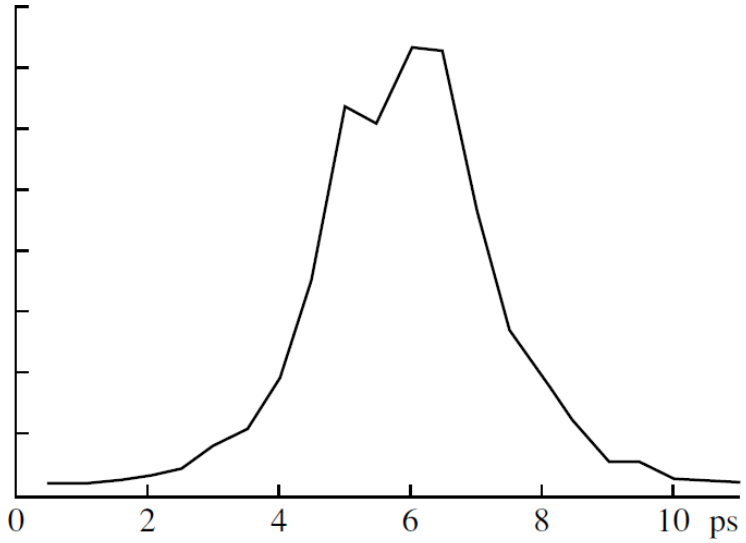

Figure 4.23: Error signal. The error signal is maximum when the two streams are superimposed. It is possible to measure an extinction ratio of about 15 dB.

This error signals has been recovered by numerically integrating the low frequency spectrum. In principle, it could be retrieved by realizing an electronic circuit that perform the integration in *real time*. Such error signal can be set to drive a dedicated delay line that can maintain the two streams in a synchronous state, thus realizing a phase locked loop.

4.4 Conclusions

In this chapter, we presented 2 different setup to obtain clock-recovery. The first one, is all-optical, and it has been demonstrated to work for RZ and NRZ (with the help of a pre-processing stage) data streams at $40\,Gb/s$. The method is based on a periodic and sharp filtering of the incoming data signal. The second method, instead, is based on the ultra-fast response properties of a Metal-Semiconductor Point Contact Diode. The second method was not fully investigated, but the preliminarily results shown that there is the possibility to build a phase comparator based on this peculiar technology. On this side, there is still much

to do: in particular the PCD can be a very useful instrument to determine the timing jitter properties of the soliton source analyzed in chapter 2.

The all-optical clock recovery scheme shown in this chapter, was demonstrated for amplitude modulated signal. It can be shown (experiments are being carried out at the time of writing) that with proper adaptations, it could be operated also with constant envelope modulation formats (such Differential Phase Shift key for example). The major improvement outlined in this research work is that the FP can be the true optical element that allows to perform the CR from a modulated signal, while in the past it has always been considered as an element able to improve the CR characteristics of already assested complex CR circuits.

Despite of its simplicity, there is still some perspective work on all-optical clock recovery experiments that can be done in the future, mainly in three directions; first, due to the intrinsic simple design, the clock recovery setup is a good candidate to be integrated on a small-scale photonic chip. FP filters, can be for example realized by means of micro-rings or integrated waveguides. Among the benefits that could come from the integration process, it is worth to mention the net reduction of the power needed by the circuit to work properly. The SOA used in the experiments are devices closed into butterfly packages that show significant coupling losses. The other direction in which those clock recovery experiments can be extended, is the test of the device in a real transmission line. It is not simple to predict how the filtering process behave at the end of a transmission line, where noise and distortions are superimposed to the signal. However, some steps are already moved in this direction by [66]. They shown that the circuit proposed in this thesis has been used in a $1.250.000\,km$ transmission: in particular, the clock recovery circuit has been used at each regeneration stage (every $60\,km$).

Another promising feature of the proposed CR circuit is the short capture time offered by the FP capabilities. The CR circuit, is a good candidate (also because its high degree of integrability) to be implemented in optical burst receivers. This was already demonstrated in [67], and other works are being carried on at the moment of writing.

5 Conclusions and outlook

This work has focused on several experimental realizations of subsystems and devices that can be successfully used in next generation Optical Communication Systems, and more in general in Optical Transparent Networks that are expected to be realized in the next decades. Optics Communications is a continuously growing field, feeded by the always increasing bandwidth demand both from network service providers and end-users. One of the main motivations behind this work was to find solutions and develop subsystems for Optical Systems with a special regard for design simplicity. Simplicity is not only a requirement inspired by the "low-cost" paradigm; the simplicity requirement was also a key-point to demonstrate that, even if Electronics can offers arbitrary circuits with capabilities and functionalities that we still lack in Optical domain (also due to the longer experience maturated in the field), it is possible to develop simple all-optical circuits providing functionalities that can replace and overcome the performance offered by the Electronic counter-part. Moreover some of the developed devices are potentially integrable[1], adding an important value to the research developed.

The devices developed in the thesis cover many functionalities needed in optics communication systems; the main results can be summarized in the following point.

- *A soliton pulse source*

  The source is capable to produce pulses at a 40 GHz repetition rate, and the produced pulse train is suitable to frequency upgrades up to 160 GHz
  The source is based on Adiabatic Compression (AC) in a dispersion shifted fiber: while AC is a known phenomenon and it was already used to demonstrate pulse generation, in this thesis it has been demonstrated how the AC can be enhanced (by counter-propagating Raman amplification) to form a regular, pedestal free, high power (100 mW), wavelength tunable pulse train. The source has been engineered in a box and provides tunability of central emitting wavelength over a range of more than 20 nm, and pulse-width over a range between 4 and 2 ps.
  The source is designed to have an internal *free-running* clock reference but also accept external precision reference clock to be used in real transmission systems.

- *Multi-wavelength converters*

[1] Unfortunately due to the lack of proper instrumentation, it was not possible to realize the integration of the proposed solutions.

We shown the possibility to realize multi-wavelength converters, based on non-linear effects in SOAs. SOAs are actually the most promising non-linear optical element to perform optical processing, and are the true candidates to realize the integration of a big number of functionalities on a single chip. We shown 2 non-linear effects in which it is possible to obtain simultaneous wavelength conversion to multiple destination wavelengths, at 10 and 40 Gb/s.
This functionality will be important in particular in Access Networks to deliver traffic associated to multimedia stream applications.
Both devices are easily integrable and realized using a single SOA, thus representing an advance in multi-wavelength converters technology.

- *Clock Recovery Circuit*

CR was demonstrated at $40Gb/s$ both for NRZ and RZ encoded signals by using a Fabry-Peròt filter as a key element in the device. Here, the main advance in respect to what was previously reported in literature is represented by the demonstration that a FP filter with adequate finesse can be effectively used as the main component to achieve CR extraction at bit-rates up to $40Gb/s$: in the past it was always used as a *preprocessor* for CR circuits. Due to the passiveness of this technique we expect that for a proper scaled finesse value the CR using a FP filter should work also at higher bit-rates.
The tank circuit proposed in this work has been already used by other research group to demonstrate all-optical clock recovery from burst data traffic [66], [68], [67], showing a good acceptance of the results reported. Integration of a variant of the proposed circuit (in which the equalizing SOA has been replaced by an integrated SOA-based Mach-Zender interferometer) has also been demonstrated recently [69] to realize a 3R burst receiver.

- Outlooks

Several possible research lines could be started from the results reported in the thesis. The pulse source still needs further work in order to fully characterize its noise properties: this is a necessary step to understand if it could be used as frequency reference in high-precision mixing experiments. Both noise characterization and mixing experiments can be carried out with Point Contact Diodes . Preliminary measurements in this directions have been performed, and are still under evaluation.
The Non-linear Polarization Switch used to realize the multiwavelength converter, has been proved to be effective also to other means: for example, we have encouraging results showing the possibility for this switch to have regenerative properties.
In general, it could be said that each *block* realized in the thesis can be further developed to be used with other modulation formats. For example, the pulse source, can be used to realize novel experiments on the transmission of RZ signals encoded with a Differential Phase Shift Keying (DPSK) modulation. This particular modulation scheme is, among other things, compatible with the pro-

posed CR scheme.
At the moment of writing, we are also testing the CR circuit on NRZ-DPSK signals, that due to the constant envelope, are characterized by stronger resilience to transmission impairments. The circuit has been tested also on packets data traffic: preliminary results, shown that due to the short capture time of the circuit it is possible to perform packet-by-packet CR, obtaining clock streams with the same length of the incoming packets, that is an important step toward the realization of an asynchronous packets receiver.

List of Figures

List of Tables

Bibliography

[1] G. P. Agrawal, *Nonlinear Fiber Optics*. San Diego: Academic Press, 1989.

[2] Y.R. Shen, *Principles of Nonlinear Optics*. 1984.

[3] M. Asobe, K. Suzuki, and T. Kanamori, "Nonlinear refractive index measurement in chalcogenide-glass fibers by self-phase modulation," *Appl. Phys. Lett.*, vol. 60, 9 Apr. 1992.

[4] J. T. Gopinath, H. M. Shen, I. Sotobayashi, E. Ippen, T. Nagashima, and N. Sugimoto, "Highly nonlinear bismuth-oxide fiber for smooth supercontinuum generation at 1.5 μm," *Optics Express*, vol. 12, p. 5697, Oct. 2005.

[5] S. V. Chernikov, E. M. Dianov, D. J. Richardson, and D. N. Payne, "Soliton pulse compression in dispersion-decreasing fiber," *Optics Letters*, vol. 18, pp. 476–478, Apr. 1993.

[6] K. N. Suzuki, Ken-Ichi; Iwatsuki, "160 Gb/s sub-picosecond transform-limited pulse signal generation utilizing adiabatic soliton compression and optical time-division multiplexing," *IEEE Photon. Tech. Lett.*, vol. 6, pp. 352–354, Mar. 1994.

[7] K. Mori, H. Takara, and S. Kawanishi, "Analysis and design of supercontinuum pulse generation in a single-mode optical fiber," *J. Opt. Soc. Am. B*, vol. 18, pp. 1780–1792, 2001.

[8] S. V. Chernikov and P. V. Mamyshev, "Femtosecond soliton propagation in fibers with slowly decreasing dispersion," *J. Opt. Soc. Am. B*, vol. 8, p. 1633, 1991.

[9] A. Hasegawa and M. Matsumoto, *Optical Solitons in Fibers*.

[10] A. Hasegawa and Y. Kodama, "Amplification and reshaping of optical solitons in a glass fiber - I," *Opt. Lett.*, vol. 7, p. 285, 1982.

[11] M. D. Pelusi and H. F. Liu, "Higher Order Soliton Pulse Compression in Dispersion-Decreasing Optical Fibers," *IEEE J. Quantum Elect.*, vol. 33, no. 8, pp. 1430–1439, 1997.

[12] J. Bromage, "Raman Amplification for Fiber Communications Systems," *J. Ligthwave Tech.*, vol. 2004, no. 22, pp. 79–93, 2004.

[13] T. Okuno, T. Tsuzaki, and T. Nishimura, "Novel Optical Hybrid Line Configuration for Quasi-Lossless Transmission by Distributed Raman Amplification," *IEEE Phot. Techn. Lett.*, vol. 13, pp. 806–808, 2001.

[14] K. J. Blow, N. J. Doran, and J. Wood, "Generation and stabilization of short soliton pulses in the amplified nonlinear Schroedinger equation," *J. Opt. Soc. of Am. B*, vol. 5, pp. 381–391, Feb. 1988.

[15] M. Artiglia, E. Ciaramella, and M. Gallina, "Demonstration of CW soliton trains at 10, 40 and 160 GHz by means of induced Modulation Instability," *CSELT TECHNICAL REPORTS*, vol. 25, no. 2, pp. 319–324, 1997.

[16] K. Tai, A. Hasegawa, and A. Tomita, "Observation of modulational instability in optical fibers," *Phys. Rev. Lett.*, vol. 56, pp. 135–138, 12 Jan. 1986.

[17] Y. Chen, "Four-wave mixing in optical fibers: exact solution," *J. Opt. Soc. Am. B*, vol. 6, p. 1986, 1989.

[18] R.H. Stolen, J.P. Gordon, W. J. Tomlinson, and H.A. Haus, "Raman response function of silica-core fibers," *J. Opt. Soc. Am. B.*, vol. 6, p. 1159, June 1989.

[19] C. R. S. Fludger, V. Handerek, and R. J. Mears, "Pump to Signal RIN Transfer in Raman Fiber Amplifier," *J. Lightwave Tech.*, vol. 19, Oct. 2001.

[20] S.V. Chernikov, D. J. Richardson, E. M. Dianov, and D. N. Payne, "Picosecond soliton pulse compressor based on dispersion decreasing fiber," *Electron. Lett.*, vol. 7, pp. 662–664, 2000.

[21] P.C. Reeves-Hall, S. A. Lewis, S. V. Chernikov, and J. R. Taylor, "Picosecond soliton pulse-duration-selectable source based on adiabatic compression in Raman amplifier," *IEEE Photon. Technol. Lett.*, vol. 14, pp. 1424–1426, Oct. 2002.

[22] E. A. Swanson and S. R. Chinn, "40-GHz Pulse Train Generation Using Soliton Compression of a Mach-Zehnder Modulator Output," *IEEE Photon. Tech. Lett.*, vol. 7, no. 1, p. 114, 1995.

[23] R. Jungerman, L. Lee, and O. Buccafusca, "1-THz Bandwidth C- and L-Band Optical Sampling With a Bit Rate Agile Timebase," *IEEE Phot. Tech. Lett.*, vol. 14, no. 8, pp. 1148–1150, 2002.

[24] Kjell J. Gåsvik, *Optical Metrology*. 1996.

[25] G. Contestabile, F. Martelli, and A. Mecozzi, "Efficiency flattening and equalization of frequency up- and down-conversion using four-wave mixing in semiconductor optical amplifiers," *IEEE Photon. Technol. Lett.*, vol. 10, pp. 1398–1401, Oct. 1998.

[26] G. P. Agrawal, *Fiber-Optic Communication Systems*. New York: Wiley, 1997.

[27] R.H. Stolen and J.E.Bjorkholm, "Parametric Amplification and Frequency Conversion in Optical Fibers," *IEEE J. Quantum Electron.*, vol. QE-18, pp. 1062–1073, July 1982.

[28] T. Frank, P. B. Hansen, T. N. Nielsen, and L. Eskildsen, "Novel duobinary transmitter," in *Proc. ECOC'97*, vol. 1, pp. 67–70, 1997.

[29] A. Ferrando, E. Silvestre, and J. J. Miret, "Nearly zero ultraflattened dispersion in photonic crystal fibers," *Opt. Lett.*, vol. 25, pp. 790–792, June 2000.

[30] K. P. Hansen, "Dispersion flattened hybrid-core nonlinear photonic crystal fiber," *Optics Express*, vol. 11, pp. 1503–1510, June 2003.

[31] K. P. Hansen, J. R. Jensen, and C. Jacobsen, "Highly Nonlinear Photonic Crystal Fiber with Zero-Dispersion at 1.55mum," in *Proc. Optical Fiber Communication Conf.*, p. PDFA9.

[32] J. H. Lee, W. Belardi, and K. Furusawa, "Four-Wave Mixing Based 10-Gb/s Tunable Wavelength Conversion Using a Holey Fiber With a High SBS Threshold," *IEEE Photon. Technol. Lett.*, vol. 15, pp. 440–442, Mar. 2003.

[33] A. Mecozzi, "Analytical theory of four-wave mixing in semiconductor amplifiers," *Opt. Lett.*, vol. 19, no. 12, pp. 892–894, 1994.

[34] K. E. Stubkjaer, "Semiconductor Optical Amplifier-Basd All-Optical Gates for High-Speed Optical Processing," *IEEE J. on Selected Topics in Quantum Electronics*, vol. 6, pp. 1428–1433, Nov. 2000.

[35] K. Hall, E. Ippen, and E. Thoen, *NONLINEAR OPTICS IN SEMICONDUCTORS II, 59, chap3. Nonlinearities in Active Media*. Elsevier, 1999.

[36] J. Zhou, N. Park, and J. Dawson, "Efficiency of Broadband Four-Wave mixing Wavelength Conversion Using Semiconductor Traveling-Wave Amplifiers," *IEEE Photon. Tech. Lett.*, vol. 6, pp. 50–52, Jan. 1994.

[37] G. P. Agrawal, "Population pulsations and nondegenerate four-wave mixing in semiconductor lasers and amplifiers," *J. opt. Soc. Am. B*, vol. 5, pp. 147–158, 1988.

[38] J. P. R. Lacey, M. A. Summerfield, and S. J. Madden, "Tunability of Polarization-Insensitive Wavelength Converters Based on Four-Wave Mixing in Semiconductor Optical Amplifiers," *J. Lightwave Technol.*, vol. 16, pp. 2419–2427, Dec. 1998.

[39] A. Mecozzi, S. Scotti, and A. D'Ottavi, "Four-Wave Mixing in Traveling-Wave Semiconductor Amplifier," *IEEE J, Quantum Electron.*, vol. 31, pp. 689–699, Apr. 1995.

[40] F. Curti, F. Matera, and G. M. Tosi-Beleffi, "All Optical Wavelength Converter-Reshaper Based on Multi-Wavelengths Spectral Components Generation,"

[41] G. Contestabile, M. Presi, and E. Ciaramella, "Multiple Wavelength Conversion for WDM Multicasting by FWM in an SOA," *IEEE Photon. Technol. Lett.*, vol. 16, pp. 1775–1778, July 2004.

[42] G. Contestabile, M. Presi, and E. Ciaramella, "A fiber-based 1:6 WDM multicast converter at 10 Gbit/s," *Optics Communications*, vol. 241, pp. 499–502, Nov. 2004.

[43] A.K. Mishraa, X. Yanga, and D. Lenstraa, "Ultrafast all-optical wavelength conversion using nonlinear polarization rotation in a semiconductor optical amplifier," in *ICTON 2004*, 2004.

[44] H.J.S. Dorren, D. Lenstra, Y. Liu; M.T.Hill, and G.D. Khoe, "Nonlinear Polarization Rotation in Semiconductor Optical Amplifiers: Theory and Application to All-Optical Flip-Flop Memories," *IEEE J. Quantum Electron.*, vol. 39, p. 141, Jan. 2003.

[45] L. Jeppesen, N. Chi, K. Yvind, L.J. Christiansen, L. K. Oxenlewe, J. Merk, and P Hanberg, "8x40 Gb/s RZ all-optical broadcasting utilizing an electroabsorption modulator," in *Proc. OFC 2004*,, vol. 1, pp. 23–27, Feb. 2004.

[46] N. Calabretta, Y. Liu, F. M. Huijskens, M. T. Hill, H. de Waardt, G. D. Khoe, and H. J. S. Dorren., "Optical signal processing based on self-induced polarization rotation in a semiconductor optical amplifier," *J. Lightw. Technol.*, vol. 22, pp. 372–381, Feb. 2004.

[47] K. Smith and K. J. Lucek, "All-optical clock recovery using a mode-locked laser," *Electron. Lett.*, vol. 28, pp. 1814 – 1816, 10 Sept. 1992.

[48] B. K. Mathason and P. J. Delfyett, "Pulsed injection locking dynamics of passively mode-locked external-cavity semiconductor laser systems for all-optical clock recovery," *IEEE J. Lightwave Technol.*, vol. 18, pp. 1111–1120, Aug. 2000.

[49] B. A. Yu, D. H. Kim, and J. C. Jo, "Wavelength tunable all-optical clock recovery using a semiconductor fiber ring laser," in *Proc. Cleo 2000*, p. cMY2, 2000.

[50] L. E. Adams, E. S. Kintzer, and J. G. Fujimoto, "All-optical clock recovery using a mode-locked figure eight laser with a semiconductor nonlinearity," *Electron. Lett.*, vol. 30, pp. 1696–1697, Sept. 1994.

[51] Yuhua Li, Cheolhwan Kim, Guifang Li, Y. Kaneko, R. L. Jungerman, and O.Buccafusca, "Wavelength and polarization insensitive all-optical clock recovery from 96-Gb/s data by using a two-section gain-coupled DFB laser," *IEEE Photon. Technol. Lett.*, vol. 15, pp. 590 – 592, 4 Apr. 2003.

[52] W. Mao, Y. Li, M. Al-Mumin, and G.Li, "All-Optical Clock Recovery for both RZ and NRZ Data," *IEEE Photon. Technol. Lett.*, vol. 14, pp. 873–875, June 2002.

[53] T. Yamamoto, L. K. Oxenlowe, and J. Schmidt, "Clock recovery from 160 Gbit/s data signals using phase-locked loop with interferometric optical switch based on semiconductor optical amplifier," *Electron. Lett.*, vol. 37, pp. 509 – 510, 12 Apr. 2001.

[54] O. Kamatani and S. Kawanishi, "Ultra-high-speed PLL-type clock recovery with phase lock loop based on four-wave-mixing in a travelling-wave laser diode amplifier," *IEEE J. Lightwave Technol.*, vol. 14, pp. 1757–1766, Aug. 1996.

[55] E. S. Awad, C. J. K. Richardson, and P. S. Cho, "Optical clock recovery using SOA for relative timing extraction between counterpropagating short picosecond pulses," *IEEE Photon. Technol. Lett.*, vol. 14, pp. 396–399, Mar. 2002.

[56] T. Saito, Y. Yano, and N. Henni, "Optical TDM 20 Gb/s-105 km transmission employing newly proposed optical PLL timing extraction," *IEEE Phot. Technol. Lett.*, vol. 6, pp. 555–557, Apr. 1994.

[57] T. Yamamoto, L.K. Oxenlowe, and C. Schmidt, "Clock recovery from 160 Gbit/s data signals using phase-locked loop with interferometric optical switch based on semiconductor optical amplifier," *Electron. Lett.*, vol. 37, 2001.

[58] M. Jinno and T. Matsumoto, "Optical tank circuits used for all-optical timing recovery," *IEEE Journal of Quantum Electronics*, vol. 28, pp. 895–900, Apr. 1992.

[59] G. M. Tosi-Beleffi, D. M. Forin, and F. Curti, "3R All Optical Regeneration," in *Transparent Optical Networks, 2004. Proceedings of 2004 6th International Conference on*, vol. 2, pp. 55–58, 4 July 2004.

[60] X. Zhou, C. Lu, and P. Shum, "A performance analysis of an all-optical clock extraction circuit based on Fabry-Perot filter," *J. Lightwave Technol.*, vol. 19, pp. 603–613, May 2001.

[61] C. Bintjas, K. Yiannopoulos, and N. Pleros, "Clock Recovery Circuit for Optical Packets," *IEEE Photon. Technol. Lett.*, vol. 14, pp. 1363–1365, Sept. 2002.

[62] T.Wang, C. Lou, and L. Huo, "Combination of comblike filter and SOA for preprocessing to reduce the patten effect in the clock recovery„" *IEEE Photon. Technol. Lett.*, vol. 16, pp. 614–616, Feb. 2004.

[63] E. Danny, A. S. Randal, and A. Yariv, "Noise characterization of a pulse train generated by actively mode-locked lasers," *J. Opt. Soc. Am. B*, vol. 13, pp. 1619–1626, July 1996.

[64] D. von der Linde, "Characterization of the noise in continuously operating mode-locked lasers," *Appl. Phys. B*, vol. 39, pp. 201–207, 1986.

[65] K.M. Evenson, M. Inguscio, and D.A. Jennings, "Point contact diode at laser frequencies," *J. Appl. Phys*, vol. 57, pp. 956–958, 1 Feb. 1985.

[66] Z Zhu, M. Funabashi, Z. Pan, and S. J. B. Yoo, "10 000-Hop Cascaded In-Line All-Optical 3R Regeneration to Achieve 1 250 000-km 10-Gb/s Transmission," *IEEE Photon. Technol. Lett.*, vol. 18, pp. 718–720, Mar. 2006.

[67] M. Funabashi, Z. Zhu, Z. Pan, and S. J. B. Yoo, "Packet-by-packet all-optical burst-mode 3R regeneration in an optical-label switching router," in *Optical Fiber Communication Conference and Exposition and The National Fiber Optic Engineers Conference on CD-ROM*, no. OFJ1, (Washington, DC), Opical Society of America, 2006.

[68] M. Funabashi, Z. Zhu, Z. Pan, and S.J. B. Yoo, "All-optical 3R regeneration in monolithic SOA-MZI to achieve 0.4 million km fiber transmission," in *Lasers and Electro-Optics Society, 2005. LEOS 2005. The 18th Annual Meeting of the IEEE*, pp. 137–138, 23 Oct. 2005.

[69] D. Petrantonakis, G. T. Kanellos, and P. Zakynthinos, “a 40Gb/s 3R Burst Mode Receiver with 4 integrated MZI switches,” in *OFC Postdeadlines Parers*, vol. PDP25, 9 Apr. 2006.

List Of Publications

Journals

Photonics Technology Letters *(Published monthly by IEEE Lasers and Electro-Optics Society, 445 Hoes Lane, P.O. Box 1331, Psicataway, NJ 08855-1331)*

1. Title: "**SINGLE AND MULTICAST WAVELENGHT CONVERSION AT 40 GB/S BY MEANS OF FAST NONLINEAR POLARIZATION CONVERSION SWITCHING IN AN SOA"**
   Authors: G. Contestabile, N.Calabretta, M. Presi, E. Ciaramella
   Volume 17, Number 12, December 2005 Pages 2652-2654

2. Title: "**EFFECTIVE SUPPRESSION OF TRANSIENT-INDUCED IMPAIRMENTS IN TRANSPARENT OPTICAL NETWORKS"**
   Autori: E. Ciaramella, M. Presi, L. Giorgi, A. D'Errico, J-P. Elbers, S. Herbst,
   Volume 17, Number 11, November 2005 Pages: 2487 - 2489

3. Title: "**40-GHZ ALL-OPTICAL CLOCK EXTRACTION USING A SEMICONDUCTOR-ASSISTED FABRY-PERÒT FILTER**"
   Authors: G. Contestabile, A. D'Errico, M. Presi, E. Ciaramella,
   Volume 16, Number 11, November 2004 Pages: 2523 - 2525

4. Title: "**MULTIPLE WAVELENGTH CONVERSION FOR WDM MULTICASTING BY FWM IN SOA**"
   Authors: G. Contestabile, M. Presi, E. Ciaramella
   Volume 16, Number 7, July 2004 Pages.1775 - 1777

5. Title: "**HIGH POWER WIDELY TUNABLE 40 GHZ PULSE SOURCE FOR 160 GB/S OTDM SYSTEMS BASED ON NONLINEAR FIBER EFFECTS**"
   E.Ciaramella, G.Contestabile, A.D'Errico, C.Loiacono, M.Presi
   Volume 16, Number 3, March 2004, Pages. 753-755

Electronics Letters *(Published monthly by IEE, PO Box 96 Stevenage Herts, SG1 2SD UNITED KINGDOM)*

1. Title: "**ALL-OPTICAL CLOCK RECOVERY FROM 40 GBIT/S NRZ SIGNAL BASED ON CLOCK LINE ENHANCEMENT AND SHARP PERIODIC FILTERING**"
   Authors: G. Contestabile, M. Presi, N. Calabretta, E. Ciaramella
   Volume 40, Number 21, 14 October. 2004 Pages.1361 - 1362

2. Title: "**COMPACT HEADER PROCESSING CIRCUIT FOR OPTICAL DPSK PACKETS**"
   Authors: N. Calabretta, M. Presi, G. Contestabile, E. Ciaramella
   Volume 42, Number 15, 20 July 2006 Pages 871 - 872

Optics Letters *(Published Optics Society of America 2010 Massachusetts Avenue, N.W. Washington D.C., 20036-1023).*

1. Title: "**STABLE OSCILLATING NONLINEAR BEAMS IN SQUARE-WAVE-BIASED PHOTOREFRACTIVES**"
   G.M. Tosi-Beleffi, M. Presi, C. Palma, D. Boschi, E. Del Re, A.J. Agranat
   Optics Letters, 25 1538 (2000)

Optics Communications *Publicazione quindicinale della Elsevier Science B.V. (P.O. Box 211, 1000 AE Amsterdam, The Netherlands)*

1. Title: "**A FIBER-BASED 1:6 WDM MULTICAST CONVERTER AT 10 GBIT/S** "
   G. Contestabile, M. Presi and E. Ciaramella
   Volume 241 Number 4-6, 16 November 2004, Pages. 499-502

2. Title: **"HIGH POWER, MULTIWAVELENGTH 40GHZ PULSE SOURCE FOR WDM-OTDM APPLICATIONS**"
   M. Presi, A. D'Errico, G. Contestabile and E. Ciaramella
   Volume 233, Number 4-6, 1 April 2004, Pages. 359-362

Laser Physics *(International Publication by MAIK NAUKA/INTERPERIODICA PUBLISHING, Profsouznaya St. 90, Moscow, 117997, Russia)*

1. Title: "**CHARACTERIZATION OF METAL-SEMICONDUCTOR POINT-CONTACT DIODES AROUND 1.55** μm**FOR OPTICALFIBER COMMUNICATIONS** "
   N. Beverini, G. Carelli, E. Ciaramella, G. Contestabile, A. DeMichele, M.Presi
   Volume 15 Number 9, 2005, Pages. 1334-1337

Conferences proceedings

1. Title: "**Simultaneous DAta Demodulation and All-optical Clock Extraction from Pure DPSK Packets**"
   Authors: M. Presi, N. Calabretta, G. Contestabile and E. Ciaramella.
   Conference: LEOS 2006, Th.3.5.5 (oral presentation)

2. Title: "**Versatile All-Optical Clock Recovery Circuit for OOK and DPSK Modulated Data Traffic**"
   Authors: M. Presi, N. Calabretta, G. Contestabile and E. Ciaramella.
   Conference: Photonic in Switching 2006, Mon.1.4 (oral presentation)

3. Title: "**A simple scheme to suppress Transient-Induced Degragations in Transparent Optical Networks**"
   Authors: E. Ciaramella, M. Presi, L. Giorgi, A. D'Errico, S. Herbst, J-P Elbers.
   Conference: Ecoc 2005, Th.3.5.5 (oral presentation)

4. Title: "**Experimental characterization of impairments induced by link-control-channels in DWDM systems**"
   Authors: Presi, M.; Giorgi, L.; Contestabile, G.; Herbst, S.; Ciaramella, E.;
   Conference: Transparent Optical Networks, 2005, Proceedings of 2005 7th International Conference Volume 2, July 3-7, 2005 Page(s):58 - 61

5. Title: "**Recupero del sincronismo ottico a 40Gb/s basato sul filtraggio selettivo dello spettro**"
   Authors: G. Contestabile, A. D'Errico, N. Calabretta, E. Ciaramella, M. Presi
   Conference: Fotonica, Trani, 30 Maggio-1 Giugno 2005

6. Title: "**Realizzazione ed ingegnerizzazione di una sorgente di impulsi a 40GHz basata su effetti nonlineari in fibra per sistemi OTDM a 160Gb/s**"
   Authors: M. Presi, R. Proietti, A. D'Errico, G. Contestabile, L. Giorgi, E.Ciaramella
   Conference: Fotonica, Trani, 30 Maggio-1 Giugno 2005

7. Title:"**WDM Multicast su 6 canali mediante Four Wave Mixing in Amplificatore Ottico a Semiconduttore** "
   Authors: M. Presi, G. Contestabile, E. Ciaramella
   Conference: Fotonica, Trani, 30 Maggio-1 Giugno 2005

8. Title: "**Multiple Wavelength Conversion for WDM Multicasting By Means of NonLinear Effetcs in SOAs**"
   Authors: G. Contestabile, M. Presi, E. Ciaramella
   Conference: OpNeTec, Pisa, Italy, 18-20 Ottobre 2004

9. Title:"**6x 10 Gbit/s WDM multicast by means of FWM in DS fiber**"
   Authors: Presi, M.; Contestabile, G.; Ciaramella, E.;
   Conference: Lasers and Electro-Optics, 2004. (CLEO). Conference on Volume 1, 16-21 May 2004 Page(s):2 pp. vol.1

10. Title: "**Widely Tunable 40GHz Pulse Suorce for 160Gb/s OTDM by Simultaneous Soliton Generation and Compression**"
    Authors: A. D'Errico, C. Loiacono, M. Presi, G. Contestabile, E. Ciaramella
    Conference: Ecoc 2003, We2.6.5 (oral presentation)

11. Title: "**Multiwavelength 40GHz Pulse Source Based on Parametric Effects in a Raman-Pumped Dispersion Shifted Fiber**"
    Authors: A. D'Errico, M. Presi, G. Contestabile, E. Ciaramella
    Conference: Ecoc 2003 We4.P11, (poster)

12. Title: "**Esperimento di trasmissione WDM a 80Gb/s (8x10Gb/s) con conversione di lunghezza d'onda in linea e ritrasmissione**"
    Authors: A. D'Errico, G. Contestabile, C. Loiacono, M. Presi e E. Ciaramella
    Conference: Fotonica 2003 (oral presentation)

13. Title: "**Stable oscillating nonlinear beams in square-wave-biased-photorefractives**"
    Authors: Tosi-Beleffi, G.M.; Presi, M.; DelRe, E.; Boschi, D.; Palma, C.;
    Conference: Lasers and Electro-Optics, 2001. CLEO '01. Technical Digest. Summaries of papers presented at the Conference on 6-11 May 2001 Page(s):429 - 431

Acknowledgements

Did you **really** think that this marvelous work (you were thinking it's marvelous, isn't it?) has been carried out by myself only? Oh, well. Let's be serious.. the real applause must go to the fabolous people that supported me along this research. Dear all, now it's your turn: I want you to join me here on the stage, for your own Moment of Glory. So let's turn the lights on.

The first to the stage is... (drums rolling.., suspence,...) **Irene**! She joined the adventure very early, just few months after the PhD course began and was taking care of myself constantly over all these years. Fortunately, it seems that I succeded to convince her to continue to play the game for the rest of our life.. so, please clap your hands loudely!

Then it's the time of the OpSys people: OpSys is the Optical Systems research group at the Scuola Superiore S.Anna. Let's start with prof. E. Ciaramella, the Opsys leader. He gave me the opportunity to start this adventure and I am grateful to him for this. Being his first PhD student, in some sense I was a guinea pig in an experiment of how to handle a PhD student. After all, we can say the experiment was quite good. His patience was consolidated and so was my knowledge of photonics. Jokes apart, Thanks for everything, Ernesto.

After our captain, I would like to have all the ligths pointing to Dr. Contestabile. A step forward, please. Now you see him with short hair.. but we all know he's still as wild as before! In four years I shared with him much more than the house and the work. Some people say he behaves like my second mum (hey Mamma don't worry, there's a place also for you on the stage!!), some asked us if we were brothers.. It's not easy at all to say about ourselves. He is undoubtedly a master of life and photonics, I am always wondering if I was able to left something to him. He provided most of the ideas developed in the thesis. Saying thanks to him is probably not sufficient. Let's try with some good wine at the end of the party!

And now, ladies and gentleman, please stand up for Dr. Calabretta. He is the real Diego Armando Calabretta: the unbridled genius. Almost impossible to find him without his smile, almost impossible trying to understand him while he tries to explain his latest brilliant idea... Thanks for teaching me that everything is simple. A special applause and our Best Whishes to him and his wife Suzanne for their little Anna.

Let's go on with the incarnation of our team.. the man that is able to transmit every kind of signal on every fiber, no matter how difficult it is. His secret? He just talks to the components. He's the Ing. D'Errico. It was later than midnight, four years ago, when we saw together our first 160 GHz pulse train. He is a model for every one in Opsys, for his dedication to the experiments and his *very* high human touch.

As every respected team, Opsys likes music. "Let's rock" is the perfect definition for the big boy: a star of the Heavy Metal. Ladies and Gentleman, let' tear off our hair for Ing. Proietti. He's the guy that with a lot of patience helped me to design and build the pulse source in a box. Thanks dude.

Still drums rolling.... it's a great moment because Ing. Giorgi is reaching the stage. He's the king of Marconi systems: he opens, re-assembly, change, modify them, invent new circuits. He really made possible to realize the node protection scheme for the Nobel project. Thanks for all your support.

In the last months our team grown, and three new researchers joined us: lights on Valentina, Emma and Stefano. Good luck to all of you.

Then, I would like to invite here on the stage prof. Beverini, from the Physics Department. I am grateful

to him fo his support and his patience. He has been always available to satisfy every my request, even if we didn't work strictly together. From Physiscs department I would like to have here also Dr. De Michele: he's the master of the gunn oscillators. Thanks for your help and for staying in the lab in August!! I also would like to have an applause prof. Pegoraro, president of the PhD course, for his encouragements.

Unfortunately most of the people I would like to have here on the stage, lives too far.. but I would like an applause also for them. We are talking about the Research Laboratory of Electronics at MIT, in particular to prof. Ippen and his group. Among them Ali Motamedi took care of me for all my staying at MIT: we had a great project, but unfortunately that laser didn't cooperate at all.. damn. And then Pete, Jason, Marcus, Johnatan, Milos, Robert, Donna,.. Let's clap our hands so loudly that they can here us.
Ing. Herbst (of Marconi-Ondata) lives in Germany so it's easier for him to hear our applause: he supported us within the Nobel project (within a great experiment), in beer tasting and during the Football World Championship... Stefan, we really appreciated your "Alè Italia" in the semi-final..
Another "foreign" is from Perugia, but he has come here today: it is Dr. Frigeri, my preferred example of determination. Thanks for insisting to teach me to follow my way.

The next group of people, is too big.. I am not sure if there's a place for you on the stage. So, let's move the stage, and let's point the lights on the audience.. there we will find all the people that made these four years really fantastic. Yes, I see Ing. Porzi. No matter how many movies you watched: he watched more. He is the one that knock the door at any time (day, night, ..): but I like it, because every time you bring your hirony, your songs and your hunger. Ehm.. is there someone that can give him a ride to the railway station? Then I see Mr. Parducci: the greatest lover in Pisa. If he went in St. Moritz, he would be the perfect actor for a re-make of "Berlinguer ti voglio bene" by R. Benigni. He's also a great old-fashion photographer. I am still waiting to learn from him how to develop films in the darkroom. We will find time also for this.

I would ask Gabriele to take a picture with all the other that make the life in the lab so nice: Nicola and Alessio that started with me the PhD adventure, Stefano and Gabriele, Marco (sor cannone) because he doesn't give up and continues to use Debian, Filo because he gave up and started to appreciate Debian and for (not so) many beers, and then Disu, Francesco (for the yogurt recipe), Francesco for his weekly "pagellone ragionato", Isabella, Gianluca, Sambo, Veronica, Fabio, Barbara. Hey, hey I want to be sure that also Cujo, Paolino, Luca and Antonella will fit in the picture!! "Oh mannaggia" I was forgotting Luca V.!!

A special applause must go also to the professors at the CEIRC labs: prof. Castoldi, prof. Di Pasquale, prof. Forestieri and prof. Prati. Their lectures have been very helpful to enrich my knowledge.

There is another picture to take, Gabriele: it is for all my friends in Roma. Francesco, that in the meantime becomed an important manager in ENI, Davide, that in the meantime become a physician, Stefano that in the meantime is becoming a great professional designer. Ok, ok, I am your black ship :).

Then, it's time for the free software guys: the hacknighters (bigpaul, xdatap, eowin, sama) for providing creativity, all the Debian people for providing the software, Linus for providing Linux.

Among all of you, I perfectly see the Morrona's guys: Mirna e Jimmy, Ricca Giada Miriam and Zoe, Sapu Cri and Tommy, the Fiori Family, Mario Jessica Sara and Benedetta, Giacomo and Mara, Filippo and Elisa, Filippo and Michela, Simona, Marco e Veronica, Marcello, the "Circolo i Lecci": thanks thanks thanks, every one of you knows why.

The party is going toward the end. Before leaving, I would like to thanks my families. Irene's family (Antonio, Daniela, Gianluca, Lidia, Iva, Roberta, Claudio, Tommy, Azzurra) for having adopted me; you know how I appreciated this. Thanks for making my staying in Pisa wormer. A special thanks to my syster Silvia and his husband Emmanuele: we really should try to be more in contact!! Then let's call also my grandmothers: Rosa and Pina, that are so proud of me. But the greater applause, ladies and gentlemans, must go to my parents. Too few times I asked such applause for them. So this is for them: my Mother (that I know has suffered my departure) and to my Father (that has always few words, but I know his feelings better than he thinks, or than I say to him). Let's make this applause strong!.